The effect of the Leu33Pro polymorphism on platelets phenotype

Inaugural dissertation

for the attainment of the title of doctor
in the Faculty of Mathematics and Natural Sciences
at the Heinrich Heine University Düsseldorf

presented by

Joana Patrícia Ventura Pereira

from Coimbra (Portugal)

Düsseldorf, December 2017

From the Department of General-, Visceral- and Pediatric Surgery
at the Heinrich Heine University Düsseldorf

Published by permission of the
Faculty of Mathematics and Natural Sciences at
Heinrich Heine University Düsseldorf

Supervisor: Prof. Dr. med. Nikolas H. Stöcklein
Mentor: Prof. Dr. William F. Martin

Date of the oral examination: 15.02.2018

Index

ZUSAMMENFASSUNG **1**

SUMMARY **2**

1 – INTRODUCTION **3**

1.1 – THE PLATELETS FORMATION AND FUNCTION 3

1.2 – THE INTEGRIN AIIBB3 4

1.2.1 – Structure and importance for platelet function *4*

1.2.2 – Activation of αIIbβ3: inside-out and outside-in *6*

1.2.2 – The Leu33Pro polymorphism of β3 ..... *8*

1.2.2.1 – Clinical and epidemiological studies 9

1.2.2.2 – Functional in-vitro studies 10

1.3 –TECHNOLOGIES AVAILABLE TO STUDY THE STRUCTURE AND FUNCTION OF AIIBB3 11

1.3.1 – Fluorescence Resonance Energy Transfer by the acceptor photobleaching method (FRET-APB) *11*

1.3.1 – Single-cell force spectroscopy (SCFS) *13*

2 – OBJECTIVES **15**

3 - MATERIALS AND METHODS **16**

3.1 – MATERIALS 16

3.1.1 – cDNA *16*

3.1.2 – Plasmids *16*

3.1.3 – Cell lines *16*

3.1.4 – Bacteria, enzymes, reagents, kits and antibodies *16*

3.1.5 – Equipment and plasticware *17*

3.2 – METHODS 18

3.2.1 – Plasmid preparation for expression of αIIbβ3 integrin receptor *18*

3.2.1.1 – Plasmid construction 18

3.2.1.2 – Bacterial transformation, bacterial growth and isolation of plasmids 18

3.2.2 – Expression of αIIbβ3 integrin receptor in HEK293 cells *19*

3.2.2.1 – Cell culture 19

3.2.2.2 – Cell transfection 19

3.2.3 – Detection of the integrin αIIbβ3 expression in HEK293 cells *21*

3.2.3.1 – Life-cell fluorescence microscopy 21

3.2.3.2 – Protein analysis 21

3.2.3.2.1 – Crued cell extracts 22

3.2.3.2.2 – SDS-PAGE 23

3.2.3.2.3 – Sample preparation 23

3.2.3.2.4 – Western blot 23

3.2.3.2.5 – Imunnodetection 24

3.2.3.3 – Flow cytometry 24
3.2.4 – Structural and functional studies of αIIbβ3 expressed in HEK293 cells 25
3.2.4.1 – Förster/Fluorescence Energy Transfer using acceptor-photobleaching (FRET-APB) 25
3.2.4.2 – Single-cell force spectroscopy (SCFS) using AFM technology 26
3.2.5 – Statistical Analysis 28

4 – RESULTS 29

4.1 – DESIGN AND CONSTRUCTION OF PLASMIDS 29
4.2 – EXPRESSION OF INTEGRIN AIIBB3 IN HEK293 CELLS 32
4.3 – STRUCTURAL AND FUNCTIONAL STUDIES OF AIIBB3 EXPRESSED IN HEK293 CELLS 36
4.3.1 – Spatial rearrangements of the cytoplasmic tails of αIIbβ3 upon Leu33Pro substitution 36
4.3.2 – Force involved in the interaction of both variants of αIIbβ with fibrinogen 43

5 – DISCUSSION 50

5.1 – EXPERIMENTAL MODEL FOR STUDIES WITH THE INTEGRIN AIIBB3 50
5.2 – LEU33PRO EXCHANGE IMPOSES MODIFICATIONS IN THE GLOBAL STRUCTURE OF THE AIIBB3 RECEPTOR 52
5.3 – LEU33PRO EXCHANGE INCREASES THE STRENGTH OF THE INTERACTION WITH IMMOBILIZED FIBRINOGEN 55
5.4 – GENERAL DISCUSSION 58

6 – CONCLUSIONS AND PERSPECTIVES 60

7 – LIST OF ABBREVIATIONS 62

8 – LITERATURE 64

APPENDIX 1 – CLONING STRATEGY FOR PLASMID PRODUCTION 76

APPENDIX 2 - SOLUTIONS 79

APPENDIX 3 - MANUSCRIPT SUBMITTED (REF. JBC/2017/000558 FROM 21/10/2017) 81

ACKNOWLEDGEMENTS 113

ZUSAMMENFASSUNG

Das Rezeptorintegrin αIIbβ3 spielt eine Schlüsselrolle in der Plättchenkoagulation und Hämostase. In Position 33 der β3 Untereinheit sind zwei Varianten - Leu33 (HPA-1a) und Pro33 (HPA1b) – bekannt. Klinische epidemiologische Studien deuten auf eine Assoziation zwischen der HPA-1b-Variante und einem erhöhten Risiko für einen Myokardinfarkt bei Patienten mit koronarer Herzkrankheit hin. Das Postulat eines prothrombotischen Charakters der HPA-1b-Variante wird durch diverse Funktionsstudien gestützt. Es fehlt jedoch an Wissen zu den Unterschieden in der Struktur-Funktionsbeziehung zwischen beiden Varianten des Leu33Pro-Polymorphismus. Speziell die Wechselwirkungen zwischen den Liganden des polymorphen αIIbβ3-Rezeptor sind weitest gehend unklar.

Das Ziel der vorliegenden Arbeit war, diese Lücken zu füllen. Es sollte eine Verbindung zwischen den publizierten Funktionsstudien und den beschriebenen klinischen epidemiologischen Studien gefunden werden. Für die Untersuchungen wurde ein Modell auf der Grundlage der transienten Expression des Integrins αIIbβ3 als fluoreszierende Fusionsproteine in HEK293-Zellen aufgebaut. Durch den Förster(Fluoreszenz)-Resonanz-Energie-Transfer und in Verbindung mit dem Akzeptor Photobleaching (FRET-APB) konnte mit diesem Modell gezeigt werden, dass bereits im ruhenden Rezeptorzustand die zytoplasmatischen Domänen („Beine“) der α- und β-Untereinheiten in der Pro33-Variante weiter voneinander entfernt sind als in der Leu33-Variante. Eine Bestättigung dieses Befunds lieferte eine unabhängige Studie mittels digitaler Strukturberechnungen. Somit wurde deutlich, dass das dynamische Konformationsgleichgewicht des αIIbβ3-Integrins hin zu einer offeneren Konformation in der Pro33-Variante begünstigt wird und die weitgespreizten zytoplasmatischen „Beine“ dem aktiven Rezeptorzustand näher kommen als in der Leu33-Konformation. Der Polymorphismus in der Ektodomäne entfaltet somit eine allosterische Wirkung auf die zytoplasmatischen „Beine“. Die zellulären Konsequenzen zu diesen Befunden wurden mittels Einzelzell-Kraftspektroskopie (SCFS) betrachtet, da Zellen der Pro33-Variante stärker und stabiler an immobilisiertes Fibrinogen binden als Zellen der Leu33-Variante.

Zusammenfassend zeigen die Strukturanalysen, dass die Pro33-Variante der β-Untereinheit (HPA-1b) Einfluß auf die Struktur des Integrins hat, der die Merkmale einer Rezeptorvoraktivierung trägt und somit auf einen prothrombotischen Charakter hindeuten. Gestützt wird diese Beobachtung, durch das Struktur-Funktion-Korrelat einer gesteigerten Avidität der Pro33-Rezeptorvariante zu seinem prominentesten Liganden - dem Fibrinogen.

SUMMARY

The receptor integrin αIIbβ3 expressed in platelets plays a key role in physiological processes as coagulation and haemostasis. The β3 subunit of the receptor has two diferent isoforms differing in the amino acid residue at position 33, on the human platelet antigen 1 (HPA-1). The isoform containing a Leucine (HPA-1a) is considered the wild type while the isoform containing a Proline (HPA-1b) has been associated with increased risk of myocardial infarction in patients with coronary disease. Dispersed functional studies support the prothrombotic character of HPA-1b, however there is still a lack of knowledge on the impact of the Leu33Pro polymorphism in αIIbβ3 receptor´s structure and function, namely in its capacity to interact with ligands. The aim of the present work was to fill these gaps and find a relation between the functional and the clinical epidemiological observations available.

We have constituted a model based on the transient expression of the two isoforms of integrin αIIbβ3 in HEK293 cells, in which the tails of both subunits were fused to fluorescent proteins. We have used Förster/Fluorescence Resonance Energy Transfer by the acceptor photobleaching (FRET-APB) to study the distances between the subunits and we could observe that in the resting state the cytoplasmic tails of α and β subunits are more separated in the Pro33 variant. Using Single-cell Force Spectroscopy (SCFS), we could observe that cells expressing the Pro33 variant bind more strongly and stably to immobilized fibrinogen, the main natural ligand of αIIbβ3 integrin.

Collectively, the results show that the Leu33Pro polymorphism, despite situated in the ectodomain, has an allosteric effect resulting in global structural changes. Our results suggest that these changes favor ligand binding in a way that can promote the outside-in signalling pathway necessary for platelet spreading, aggregation and thrombi formation. These results complement all-atom Molecular Dynamic (MD) simulations showing that the Pro33variant of αIIbβ3 shifts the dynamic conformational equilibrium of αIIbβ3 integrin towards a more open and extended state, resembling more the active state. In conclusion, the results of this work provide new mechanistic insights and a new basis for understanding the prothrombotic character of the αIIbβ3Pro33 receptor reported in previous functional and clinical studies.

1 – INTRODUCTION

1.1 – The platelets formation and function

The conclusive identification/discovery of platelets, also called thrombocytes, is attributed to Bizzozzero in the 19th century (Bizzozzero, 1882), despite previous works reporting the observation of "blood particles" thought to be originated from leucocytes or erythrocytes (Donné, 1842; Hewson, 1771; Hewson, 1780; Leewenhoeck, 1675; Schultze, 1865).

In healthy adult individuals, platelets are the second most abundant type of cells being present at a concentration ranging between 150 and $400x10^6$/ml of blood (Brecher et al., 1953), and their lifespan in circulation is between 8 and 9 days (Cohen and Leeksma, 1956). Platelets are the smallest type of cell in circulation with an approximate diameter of only 3 μm and a thickness of 0.5 μm, and they are generated from bone marrow megakaryocytes (MKs) (Wright, 1906).

As anucleated cells, platelets lack nuclear genetic material and therefore their multiple physiologic functions are not dependent on any internal dynamic (epi)genetic program, but are rather facilitated by components inherited from the precursor MK. In fact, all the major components necessary to platelet function seem formed already during MKs maturation (Italiano et al., 1999). Of utmost importance for platelet function are 2 types of granules included in the cytoplasmic package that these cells inherit from MKs,: (i) the α granules that store glicoprotein receptors (as integrins αIIbβ3 (Pabla et al., 1999) and αvβ3), adhesive proteins (as fibrinogen, fibronectin, and Von Willebrand Factor), and coagulation factors (as factor V and factor VIII); (ii) the dense granules that contain cations, phosphates, ADP and ATP compounds (Reviewed by (Fukami and Salganicoff, 1977).

In the resting state the platelets circulate free and have a round/oval shape, however in consequence of an injury in a vessel wall, platelets are attracted to the damaged area and undergo morphological changes involving cytoskeletal rearrangement and acquisition of filopodia (extensions of their cellular membrane) that allow them to attach (Figure 1) (Nachmias, 1983).

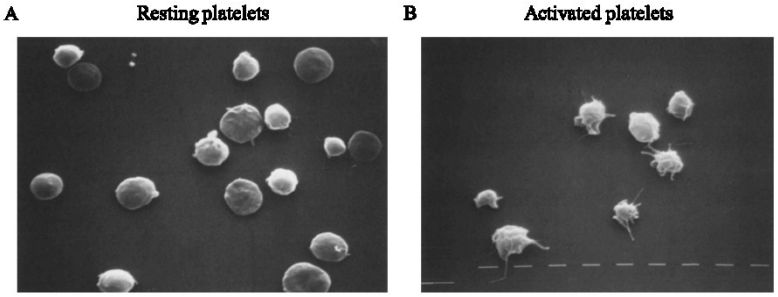

Figure 1 – Scanning electron micrographs of platelets. (A) Platelets in resting state presenting a discoid morfology. (B) Platelets after activation with ADP with the consequent formation of filopodia (x5000). Figure reproduced from (Zucker and Nachmias, 1985).

Platelets arrive to damaged areas very quickly as consequence of their high abundance and their positioning in the outer edge of the blood flow which results from their small size (Bizzozzero, 1882). First-arriving platelets release adhesive proteins present in their α-granules directly at injury sites (Wang et al., 2014), and this promotes the sequential recruitment of multiple circulating proteins (e.g. coagulation factor VIIIa (Mosher and Schad, 1979; Wang et al., 2014)) which lead to the adhesion, activation and aggregation of additional platelets. Aggregated platelets promote thrombin production, which in its turn is responsible for the conversion of fibrinogen into fibrin that together with fibrin-fibronectin complexes constitute the hemostatic plugs, a solid phase thrombus, the final clot that stop bleeding (Bevers et al., 1983; Mann et al., 1991; Zwaal and Bevers, 1983).

1.2 – The integrin αIIbβ3

1.2.1 – Structure and importance for platelet function

Platelet aggregation involves multiple platelet-platelet- and platelet--matrix interactions which are mediated by numerous membrane proteins and in which members of the integrin family play a central role. Integrins are a familly of transmembrane adhesion receptors that are ubiquitously expressed and mediate cell-cell and cell-extracellular matrix (ECM) interactions (Hynes, 1987). They bridge extracellular ligands and intracellular pathways through signalling, triggering diverse physiological responses. All integrins, consist of an heterodimer composed by one α and one β subunit non-covalently linked to each other and assembled as a cation-dependent complex (Fujimura and Phillips, 1983). There are 24 different integrins, each of it with a specific function, distinct from the others. Platelets

express six of them (α2β1, α5β1, α6β1, αIIbβ3, αvβ3 and αLβ2), belonging to three integrin sub-families, β1, β2 and β3, a classification based on evolutionary relationships and ligand specificity (Reviewed by (Hynes, 2002). The integrin αIIbβ3, also called as GPIIbIIIa, is by far the most expressed one in platelets. Notably, there are between 60000 and 80000 αIIbβ3 receptor copies per platelet (Wagner et al., 1996) that represent 18% of the total proteins present in the membrane of this cell type (Fujimura and Phillips, 1983). The two other most frequent integrins α2β1 and α5β1, are present only at 2000-4000 (Staatz et al., 1989) and 2000-3000 (Piotrowicz et al., 1988) receptor copies per cell, respectively. The genes encoding integrin subunit αIIb (ITGA2B, 30 exons spannig c. 17 kb) and subunit β3 (ITGB3, 15 exons spannig c. 46 kb) are both located on chromosome 17q21 and are separated by a distance of ≥ 365kb (Thornton et al., 1999). The αIIb subunit is translated as a preprotein composed by 1008 amino acids which is subsequently processed proteolytically to generate one heavy and one light chain that associate via disulfide bonds (Poncz et al., 1987). The β3 subunit is composed by 762 amino acids on a single chain (Fitzgerald et al., 1987; Zimrin et al., 1990).

Structurally, both subunits have a long N-terminal extracellular domain, a transmembrane domain and a short C-terminal cytoplasmic tail (Fitzgerald et al., 1987; Xiao et al., 2004; Xiong et al., 2001; Zimrin et al., 1990) (Figure 2). In the N-terminal extracellular fraction of both subunits, the most distal domains (β-propeller domain in the αIIb subunit, and βA-domain in the β3 subunit) form a globular "head" that provides the ligand binding site (Xiong et al., 2001). The remaining thigh, genu, calf-1 and calf-2 domains of the αIIb subunit, and hybrid, plexin, semaphorin and integrin (PSI), genu, epidermal growth factor (EGF) and membrane proximal β tail (βTD) domains of the β3 subunit form two long legs. Between the head and legs, the genu domains of both subunits, provide a region of interdomain flexibility.

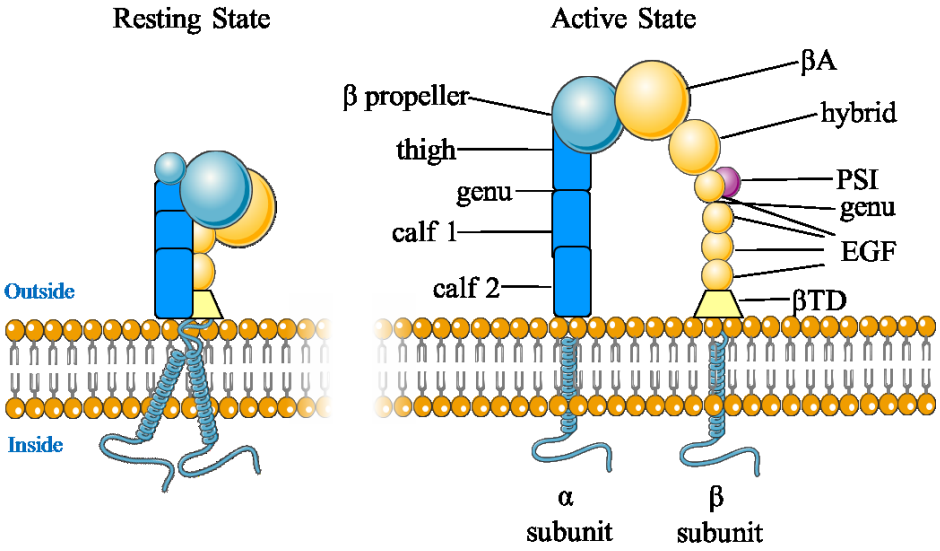

Figure 2 – Schematic representation of the structure of the αIIbβ3 integrin receptor in its resting and activated forms with its different domains. Figure based on (Moser et al., 2009b).

The cytoplasmic tails of αIIb and β3 integrin subunits are approximately 20-70 residues long (Bennett, 1996; Hynes, 1992; Schwartz et al., 1995) and their amino acid content, especially in the membrane proximal region is very similar. In the resting state αIIb and β3 subunits cytoplasmic domains interact with each other forming a clasp-like structure kept through hydrophobic and electrostactic interactions and a salt bridge between the R amino acid in the GFFKR motif of αIIb, and the D amino acid in the HDRRE motif of β3 (Muir et al., 1994; Vinogradova et al., 2000; Vinogradova et al., 2002). Disruption of these interactions is of key importance for receptor and platelet activation.

1.2.2 – Activation of αIIbβ3: inside-out and outside-in

The function of αIIbβ3 is mediated by binding of extracellular ligands (outside-in signalling). However, when platelets are in the resting state, the affinity of the αIIbβ3 receptor for its ligands is low, and the binding is minimal (Reviewed by (Topol et al., 1999) due to a bent or "closed" conformation in which the head is very close from the plasma membrane (Figure 3).

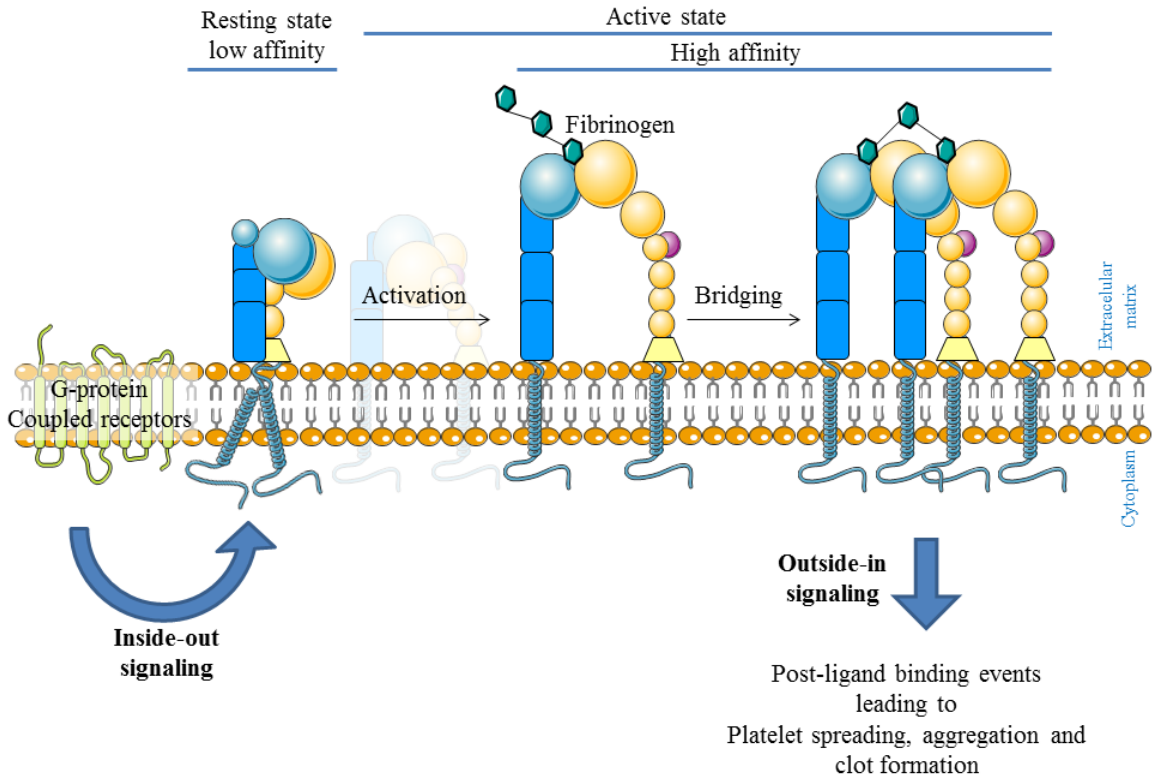

Figure 3 – Scheme of integrin αIIbβ3 activation on platelets membrane with inside-out, outside-in signaling mechanisms and consequent events (figure based on (Shattil et al., 1998)).

The conversion of the αIIbβ3 receptor from a low- to a high- affinity state can be reversibly triggered through an intracellular signalling cascade: inside-out signalling. This cascade starts with the binding of agonists to G-protein coupled receptors as TBXA2R, CXCR4, AGTR1, PAR1, and PAR4 (Topol et al., 1999) and involves talin, a cytoplasmic protein composed of an N-terminal head domain with ~ 50 kDa and a C-terminal rod domain with ~200 kDa (Winkler et al., 1997). Upon binding of agonists to G-protein coupled receptors (Figure 3), talin undergoes a conformational change that facilitates its binding via the phosphotyrosine-binding (PTB)-like domain to β3 subunit via its membrane proximal NPxY motif (Calderwood et al., 2002). Binding of talin causes a sterical disruption of the interactions between the cytoplasmic tails of αIIb and β3 integrin subunits (Wegener et al., 2007). The displacement of αIIb and β3 interactions leads to the opening of the C-terminal stalks, converts the receptor into an intermediate extended conformation with a close headpiece in which the receptor is activated but it is not yet able to bind a ligand, and finally to a fully extended or "open" conformation in which the head is situated more apart from the plasma membrane (Vinogradova et al., 2002) (Frelinger et al., 1991; Nishida et al., 2006;

Takagi et al., 2002; Xiong et al., 2001) (Figure 3). The interaction between talin and β3 subunit is sufficient to activate αIIbβ3 *in vitro* (Ye et al., 2010) but full integrin activation in platelets requires also protein kindlin-3 (Moser et al., 2009a). The mechanism is not completely understood but several studies point to cooperation between talin and kindlin in the regulation of integrin affinity for ligands (Calderwood et al., 1999; Calderwood et al., 2002; Ma et al., 2008; Montanez et al., 2008; Moser et al., 2008; Moser et al., 2009b).

Once in high-affinity state, αIIbβ3 binds extracellular peptides with xGD motif, where x can be a basic or a hydrophobic amino acid (Sanchez-Cortes and Mrksich, 2009). The predominant natural ligands of αIIbβ3 are fibrinogen and von Willebrand Factor (vWF), but it binds also fibronectin, thrombospondin-1 and vitronectin (De Marco et al., 1985; Jennings and Phillips, 1982; Plow et al., 2000; Savage et al., 1998). Binding to fibrinogen is dependent on two peptide sequences: the RGD sequence at position 572-4 on the fibrinogen Aα chain that binds to residues 109-171 of β3 integrin subunit (D'Souza et al., 1988; Santoro and Lawing, 1987); and a HHLGGAKQAGDV sequence at position 400-11 on the γ chain of fibrinogen that binds to residues 294-314 in αIIb integrin subunit (D'Souza et al., 1990; D'Souza et al., 1991). Notably, fibrinogen is the coagulation protein circulating at the highest concentration in blood (between 2.6 and 3.5 mg/ml) (Hantgan, 2001). Ultimately, binding of adhesive proteins like fibrinogen or vWF to the receptor creates bridges between receptors (Figure 3). In one hand, brigdes between receptors of different platelets allow platelets to aggregate and form thrombi (Bennett and Vilaire, 1979). In one other hand, bridges between receptors on one same cell form receptor clusters and a microenvironment in the plasma membrane (Isenberg et al., 1987) that facilitate subsequent outside-in signalling events (Abrams et al., 1994; Narumiya, 1996) contributing for actin polymerization and cytoskeletal reorganization (Reviewed by (Shattil et al., 1998)). In this way, the signalling through αIIbβ3 regulates the platelet spreading on a matrix containing vWF or fibrinogen (Savage et al., 1992; Savage et al., 1996). Moreover, as result of the outside-in signals occur granule secretion and secondary aggregation which regulates the size of a hemostatic plug or a pathological thrombus (Reviewed by (Shattil et al., 1998)).

1.2.2 – The Leu33Pro polymorphism of β3

The human platelet alloantigen 1 (HPA-1), also designed platelet antigen (Pl^A) is an antigen system existing in a diallelic form and is localized in the β3 subunit of the integrin

αIIbβ3. One of the forms is called HPA-1a and contains a Leucine at position 33 of β3 subunit, and the other form is called HPA-1b and contains a Proline at the same position (Leu33Pro). This Leu33Pro substitution results from a polymorphic 1565T>C substitution in exon 2 of the β3 subunit. The two variants were identified through sequencing and restriction enzyme-based analysis of PCR products obtained from platelet-derived mRNA from HPA-1a and HPA-1b individuals (Newman et al., 1989).

The allelic frequency distribution of the HPA-1b polymorphism varies according to the geographical region and ethnic background. Approximately 25% of the Europeans are heterozygotic for HPA-1 (Von dem Borne and Decary, 1990), 2% of the Caucasian population are homozygotic indivuals for HPA-1b (Newman et al., 1989), and the gene frequency of HPA-1b in Asians is lower than 1% (Kim et al., 1995).

The crystal structure of Leu33 β3 (Xiao et al., 2004) revealed that Leu33 residue is located on a long loop between strands A and B of the PSI domain (Xiong et al., 2004). The PSI and the contiguous hybrid domain constitute a rigid structure that functions as a lever, causing a widening of the angle between the legs of α and β and consequently leg extension and separation (Xiao et al., 2004). A structure for Pro33 β3 is still missing and therefore the exact structural consequences of the Leu33Pro substitution are not known, however the substitution, is likely to alter the conformation of β3 subunit due to two reasons: (i) the different nature of the residues. Leu is an alpha-helix-favoring amino acid while Pro is a helix-disrupting residue because it cannot form hydrogen bonds necessary to stabilize alpha-helix structures; (ii) the close proximity of another Pro residue (at position 36) that reinforces the destabilizing character of Pro33 on β3 conformation. Due to these reasons it has been discussed that Pro33 may confer more rigidity to the PSI domain which might cause a more prominent separation and/or greater stability of the open-head conformation after ligand binding (Reviewed by (Vijayan and Bray, 2006)).

1.2.2.1 – Clinical and epidemiological studies

A strong association between the HPA-1b polymorphism and acute coronary thrombosis was shown for the first time in 1996 (Weiss et al., 1996). This initial study showed that the prevalence of HPA-1b was 2.1 times higher among patients who suffered from myocardial infarction (MI) or unstable angina than among patients without known heart disease. In the subgroup of people under 60 years, this prevalence was 3.6 times higher. Identical association to the same polymorphism was described by other authors (Araujo et al., 1999; Ardissino et

al., 1999; Garcia-Ribes et al., 1998; Hooper et al., 1999; Pastinen et al., 1998; Zotz et al., 1998).Noteworthy, in subsequent studies no association between the HPA-1b genotype and an increased risk of myocardial infarction, stroke, venous thrombosis or acute coronary thrombosis was found (Anderson et al., 1999; Corral et al., 1997; Herrmann et al., 1997; Kekomaki et al., 1999; Ridker et al., 1997; Scaglione et al., 1998). The apparent contradiction between these two sets of studies could be attributed to significant differences in the patients cohorts in terms of geographical origin, ethnic background, age, gender, type of infarction, as well as to the choice of the control groups (Bray, 2000). In fact, considering the studies in which the choice of the patients was more homogenous (Anderson et al., 1999; Carter et al., 1997; Durante-Mangoni et al., 1998; Gardemann et al., 1998; Kastrati et al., 1999; Laule et al., 1999; Mamotte et al., 1998; Walter et al., 1997; Zotz et al., 2000), a consistent higher prevalence of HPA-1b in patients with MI could still be verified (Bray, 2000).

Notably the bleeding time in HPA-1b individuals is significantly shorter than the bleeding time in HPA-1a individuals (Szczeklik et al., 2000; Szczeklik et al., 2001), and HPA-1b is also associated with an increased platelet thrombogenicity, the tendency of platelets to produce thrombus/embolus (Zotz et al., 2000). In addition, HPA-1b allele carriers with coronary artery disease have an onset of MI 5.2 years earlier than non-carriers (Zotz et al., 2005). This shows that the HPA-1b genotype constitutes a risk factor for patients with an atherosclerotic lesion but it does not represent a risk factor for the development of an atherosclerotic lesion among healthy individuals. Despite that, the risk associated with HPA-1b genotype is considered much lower than the standard cardiovascular risk factors as hypercholesterolemia, smoking and others (Burr et al., 2003; Di Castelnuovo et al., 2005; Reiner et al., 2001).

1.2.2.2 – Functional in-vitro studies

Functional differences between the HPA-1a and HPA-1b variants have been investigated in-vitro and collectively the data from existing studies support the prothrombotic character suggested by the epidemiologic studies.

A study employing antibodies for flow cytometry, for radiometric and ELISA assays, showed that platelets from HPA-1b individuals have higher tendency for activation, for αIIbβ3 integrin receptor activation, and for binding to fibrinogen than platelets from HPA-1a individuals (Michelson et al., 2000). Another study focused on the evaluation of risk factors for cardiovascular disease used platelets from children and reported that the Pro33 allele was

associated with higher platelet aggregability in comparison with the Leu33 allele concluding that the observations provided an explanation for the association of Pro33 allele with the increased risk for cardiovascular disease (Feng et al., 1999).

Using Chinese hamster ovary (CHO) and Human embryonal kidney (HEK293) cell-lines as models expressing the Leu33 and Pro33 variants of the αIIbβ3 integrin receptor, it could also be shown that binding efficiency to immobilized fibrinogen, cell spreading, actin cytoskeleton rearrangement, and clot retraction were also increased in HPA-1b cells comparing to HPA-1a cells. These differences were suggested to be related with differences in post-receptor occupancy signalling events (outside-in signalling) that could eventually result from a structural difference in the αIIbβ3 integrin receptor caused by the polymorphism Leu33Pro (Vijayan et al., 2000). On another study using the same cell-line models it could be observed an increased adhesion activity, increased thrombus formation, and increased outside-in signalling under in-vitro simulated physiological and pathological flow conditions of cells expressing HPA-1b compared to cells expressing the HPA-1a (Scharf and Zotz, 2006). In this study the same results were also observed in HPA-1b platelets in comparison with HPA-1a platelets. Despite the suggestion of Vijayan et al. referred above there is no data linking the receptor structure with the fibrinogen binding or outside-in signalling.

1.3 –Technologies available to study the structure and function of αIIbβ3

Besides the functional studies involving the assays described above, technologies are available and could potentially be used to gain a new perspective on differences between the two HPA-1 receptor variants concerning their structure and forces implicated in receptor-ligand.

1.3.1 – Fluorescence Resonance Energy Transfer by the acceptor photobleaching method (FRET-APB)

The Förster or Fluorescence Resonance Energy Transfer (FRET), described by Theodor Förster in 1948 (Förster, 1948) consists on a physical process: the energy transfer between a fluorescent donor molecule and a fluorescent acceptor molecule. It is a distance-dependent method, the fluorophores must be less than 10 nm apart from each other and therefore it is applied to study proteins in close proximity. For the energy transfer process it is also required an overlap between the emision spectrum of the donor fluorophore and the excitation spectrum

of the acceptor fluorophore as well as the appropriated orientation of both fluorophores (Lakowicz, 2006). The distance range at which FRET occurs corresponds to the dimensions of many biological molecules potentiating the use of this technique. One can profit from the technology of FRET imaging microscopy getting deep information about the structure of proteins, structural changes and/or protein interactions more precisely the distance between sites/domains on multi-subunit proteins. Being non-invasive, this technique is applicable on cultured living-cells under physiological conditions (Ma et al., 2014) .

There are different methods to measure FRET. In the acceptor photobleaching method (FRET-APB), the acceptor fluorophore is specifically destroyed by a strong laser pulse (bleaching). In consequence of this, the transfer of energy between donor and acceptor can no longer occur and therefore will occur an increase in the donor's emmited fluorescence (Karpova et al., 2003b) (Figure 4A).

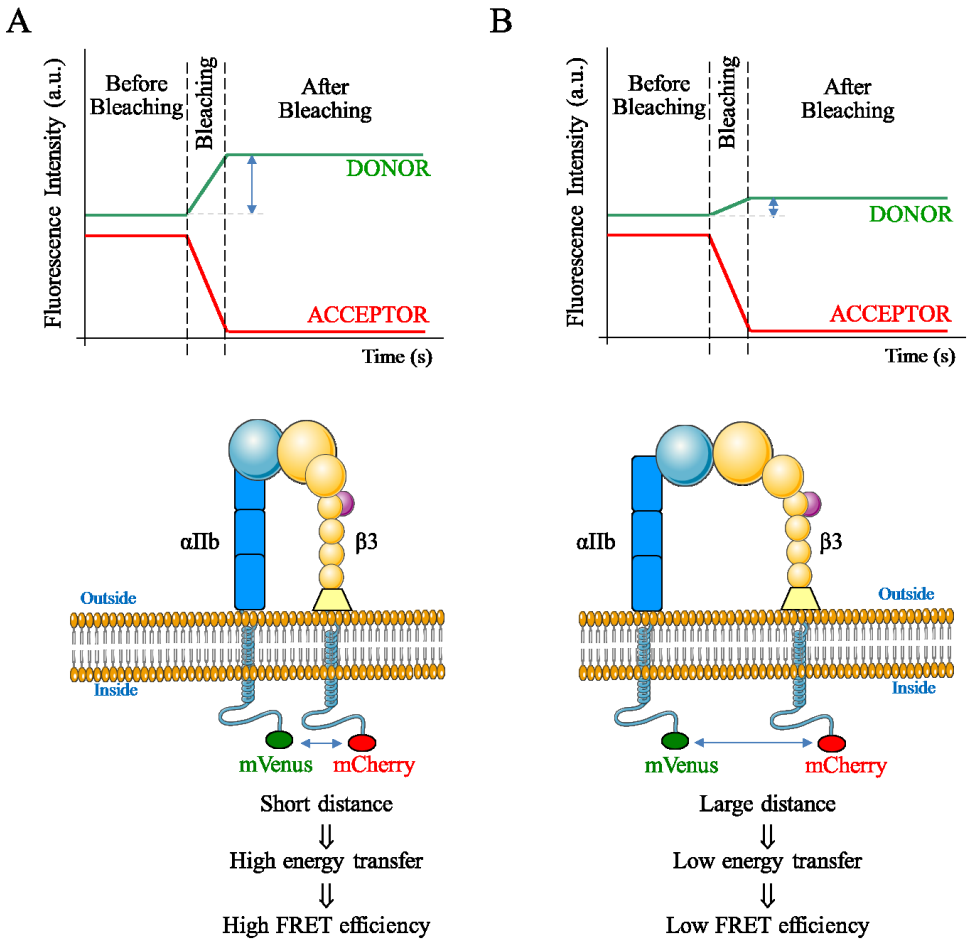

Figure 4 – FRET- acceptor photobleaching method for **(A)** a receptor in which the two subunits are spacially in close proximity **(B)** for a receptor in which the separation between the two subunits is larger. **(upper panels)** Variation of donor and acceptor fluorescence intensities with time. Figure based on (Stahl and Weidtkamp-Peters, 2015). In consequence of the bleaching that causes the destruction of the acceptor fluorophore, energy transfer

from the donor to the acceptor can no longer occur and the fluorescence intensity from the donor increases. This increase in donor fluorescent intensity is higher in the case of closer proximity of the two fluorophores. **(lower panels)** Schematic representation of αIIbβ3 receptor with the two fluorophores fused to the cytoplasmatic tails. In case of closer proximity of the tails, there is a higher energy transfer between the fused fluorophores and consequently a higher measured FRET-efficiency.

The differences in fluorescence intensity can be detected with a confocal microscope and can be quantified using appropriate software. If the two fluorophores are situated very close from each other, high levels of energy transfer occur between them and the increase on fluorescence intensity of the donor upon acceptor´s bleaching will be big. The more distant the two fluorophores are, the lower the levels of energy transfer are, and the lower will be the differences in donor´s emitted fluorescence detected upon acceptor bleaching (Figure 4B).

1.3.1 – Single-cell force spectroscopy (SCFS)

One other assay that can potentially be used to quantify interactions between biomolecules is the Atomic Force Microscopy (AFM), first reported in 1986 (Binnig et al., 1986). AFM is a high-resolution technique that monitors forces applied on a surface in the piconewton (ρN) range (Butt et al., 2005; Fuhrmann and Ros, 2010; Helenius et al., 2008; Hinterdorfer and Dufrene, 2006; Liang and Fernandez, 2009; Zlatanova et al., 2000). Single cell force spectroscopy (SCFS), is a special type of force experiment which can be performed with an AFM and it can be used to study the interaction between a cell and a substrate (Aliuos et al., 2013; Beckmann et al., 2013; Benoit et al., 2000; Benoit and Gaub, 2002; Boettiger and Wehrle-Haller, 2010; Dao et al., 2012; Elter et al., 2012; Friedrichs et al., 2010; Grandbois et al., 2000). In detail, in SCFS, a cantilever, working as a flexible spring, brings a single cell into contact with a substrate for a defined period of time and retracts afterwards. During retraction, the cantilever will deflect, thereby increasing the detachment force, until the cell detaches completely from the substrate. For measuring the force, the cantilever is aligned with a laser beam and reflects it onto a quadrant photodiode (Butt et al., 2005). The stronger the cell is adherent to the substrate, the higher will be the deflection of the cantilever while retraction, and the higher will be the signal of the photodiode. This signal is proportional to the forces involved in the adhesion of the cell to the substrate (Figure 5).

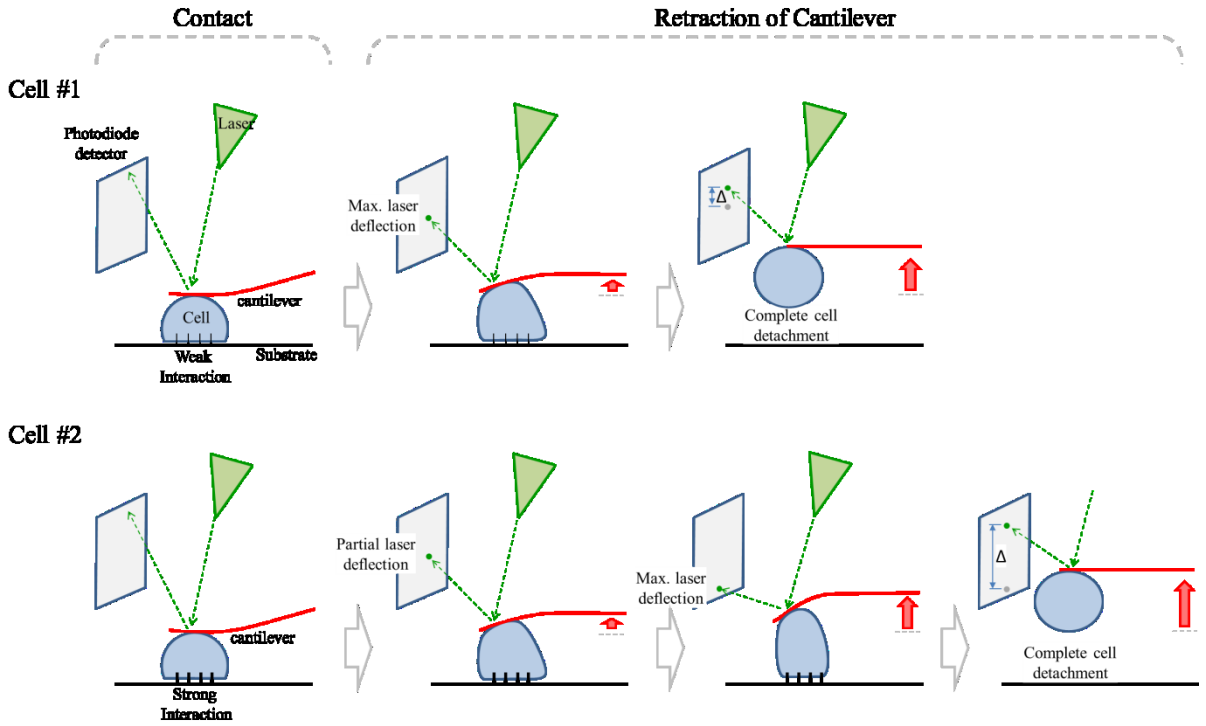

Figure 5 – Schematic representation of a single SCFS experiment for two cells. Due to the proportionality between the cantilever deflection and the laser signal detected, it is possible to infer about the force involved in the interaction between the cell and substrate. When the force involved is weak (Cell #1) the cantilever deflects slightly and the difference in the laser signal reflected on the photodiode is lower. If the force involved is stronger (Cell #2), the cantilever deflects more and the difference in the laser signal detected is higher.

2 – OBJECTIVES

The HPA-1 is polymorphic at position 33 where a Leu residue (HPA-1a) can be substituted by a Pro residue (HPA-1b). The HPA-1b variant is associated with an increased risk for myocardial infarction in patients with coronary artery disease. The epidemiologic evidences are supported by dispersed functional studies reporting the prothrombotic character of the HPA-1b receptor variant, however there is still a big gap in our knowledge about the impact of the Leu33Pro substitution in the receptor´s structure and how it can influence its function.

Implying techniques to analyse single cells at the molecular level, the work presented here aims at exploring structural and functional differences between the HPA-1a and HPA-1b variants, to narrow the gap in our knowledge on the relation existing between the structural features of the integrin αIIbβ3 and the phenotype associated to the HPA-1b. More concretely the main objectives for this work are:

1- Analyse the impact of the Leu33Pro polymorphism in the structure of the β3 subunit and consequently in the whole αIIbβ3 receptor. For this we will compare the physical separation between the cytoplasmic tails of αIIb and β3 subunits in both HPA-1a and HPA-1b variants of the receptor on a resting state, through FRET-APB. We will compare these FRET-APB results on the intracellular domain of HPA-1a and HPA-1b with results of computational structural studies by all-atom molecular dynamics (MD) simulations done for the extracellular fraction (ectodomain) of the same integrin isoforms.

2- Investigate if the Leu33Pro polymorphism has an impact in the function of the receptor. Recurring to SCFS, we will study and compare different parameters (maximal adhesion force, adhesion energy, single rupture force, tether force and tether length) involved on the interaction between the HPA-1a and HPA-1b isoforms of αIIbβ3 and its natural ligand fibrinogen.

3- Find a relation between the results obtained in this work through FRET-APB and SCFS and the clinical epidemiological and functional studies described before.

3 - MATERIALS AND METHODS

3.1 – MATERIALS

3.1.1 – cDNA

ITGA2B, αIIb - a kind gift from Dr. Sanford Shattil, University of California, San Diego, USA; ITGB3, β3 - a kind gift from Dr. Jonathan Jones, Northwestern University Medical School, USA.

3.1.2 – Plasmids

pcDNA3.1(-) - Invitrogen, USA*;* mVenus - a kind gift from Steven Vogel, Addgene, plasmid # 27794; mCherry - Clontech Laboratories, Inc., USA.

3.1.3 – Cell lines

HEK293 - Leibniz Institute DSMZ-German Collection of Microorganisms and Cell Cultures (DSMZ, no. ACC 305).

3.1.4 – Bacteria, enzymes, reagents, kits and antibodies

DH5α™ derivative competent *E. coli* (NEB, USA); S.O.C. medium (Invitrogen, USA); Ampicillin (Invitrogen, USA); Zeocin (Invitrogen, USA); Highspeed Plasmid Maxi Kit (QIAGEN, Germany); glycerol (Carl Roth, Germany); DMEM (Thermo Fischer Scientific, USA); Fetal Bovine Serum (FBS) (Thermo Fischer Scientific, USA); Penicillin-Streptomycin (Thermo Fischer Scientific, USA); EDTA (Sigma-Aldrich, USA), DPBS (Sigma-Aldrich, St. Louis, USA); Trypan Blue Solution 0.4% (Thermo Fisher Scientific, USA); Effectene Transfection Reagent (Qiagen, Germany); Fibrinogen from human plasma (Sigma-Aldrich, USA); Supersignal® West Dura Extended Duration Substrate (Thermo Scientific, USA); BSA (Sigma-Aldrich, Germany); 2-propanol (Sigma-Aldrich, USA); Plus Protein™ WesternC™ standards (Bio-Rad, Germany); StrepTactin-HRP conjugate (Bio-Rad, Germany); nitrocellulose membrane (Bio-rad, USA); Whatman® Gel Blot Paper (Whatman, USA); Tween 20 (Merck, Germany); rabbit anti-human integrin αIIb polyclonal antibody (clone H-160; Santa Cruz Biotechnology, Inc, USA); rabbit anti-human integrin β3 polyclonal antibody (Cell Signaling, Inc, USA) respectively; GAPDH (clone 6C5; Abcam, UK); Ecl anti-rabbit

IgG Horseradish secondary antibody (GE Healthcare, UK); Super Signal® West Dura Extended Duration Substrate (Thermo Scientific, USA); APC-conjugated mouse anti-human CD41 monoclonal antibody (clone MEM-06; Exbio, Czech Republic); phenol red free Fluorobrite™ DMEM (Life Technologies, USA); poly-L-lysine (Sigma-Aldrich, Germany); Abciximab (Lilly, Germany); In-Fusion HD PCR Cloning Kit (Clontech Laboratories, Inc., USA); Bacto-trypton (BD, USA); NaCl (Merck, Denmark); Yeast (BD, USA); Agar (Invitrogen, USA); 1.5 M NaCl (Merck, Denmark); 10% Triton X-100 (Sigma-Aldrich, Germany); 5% Sodium deoxycholate (Sigma-Aldrich, Germany); 0.2 M EDTA (Sigma-Aldrich, USA); cOmplete, Mini EDTA-free Easypack (Roche, Germany); Water for chromatography (Merck, Gemany); Trizma® base (Sigma- Aldrich, USA); HCl (Merck, Germany); 30% Acrylamide/0.8%Bisacrylamide (National Diagnostics, USA); 10% Ammoniumpersulfate (Sigma-Aldrich, USA); TEMED (Sigma-Aldrich, USA); SDS pure (Carl-Roth, Germany); Glycine (Carl-Roth, Germany); 20% SDS (Carl-Roth, Germany); Glycerol (Carl-Roth, Germany); DTT (Sigma-Aldrich, USA); Bromophenol blue (Merck, Germany); Methanol (Merck, Germany).

3.1.5 – Equipment and plasticware

Thermal block (Eppendorf, Germany); Biospectrophotometer (Eppendorf, Germany); Neubauer chamber (Assistant, Germany); 6-well plate (Greiner Bio-one, Germany); µ-Slide 4 Well ibiTreat chamber slide (Ibidi, Germany); Axiovert S100 inverted fluorescence microscope (Zeiss, Germany); 12.0 Monochrome w/o IR-18 monochromatic camera (Diagnostic Instruments, inc, USA); Genesys 10S UV-VIS spectrophotometer (Thermo Fischer Scientific, USA); disposable cuvettes (Sarstedt, Germany); PerfectBlue™ Double Gel System Twin S (Peqlab, Germany); PTC-200 Peltier Thermal Cycler (M J Research, USA); Mini Trans-blot® Electrophoretic Transfer Cell (Bio-Rad, USA); RM5-80V roll mixer (CAT, Germany); Molecular Imager (Chemidoc XRS, Biorad, USA); FACS Canto II flow cytometer (BD Biosciences, USA); µ-Slide 8 Well ibiTreat chamber slide (Ibidi, Germany); LSM 780 inverted microscope (Zeiss, Germany); heating frame (Pecon, Germany); cantilevers (Nano World, Switzerland); culture-insert 2 well dishes (Ibidi, Germany); CellHesion200 AFM (JPK Instruments, Germany); Petri dish heater (JPK Instruments, Germany); IX83 inverted microscope (Olympus, Germany); XM10 camera (Olympus, Germany); 10x UPLFLN2 / NA 0,3 objective (Olympus, Germany).

3.2 – METHODS

3.2.1 – Plasmid preparation for expression of αIIbβ3 integrin receptor

3.2.1.1 – Plasmid construction

Three plasmids (αIIbmVenus, β3Leu33mCherry, and β3Pro33mCherry) were used to express the two isoforms of the αIIbβ3 integrin receptor in HEK293 cells. The exact cloning strategy followed to obtain these plasmids is described in detail on Appendix 1 and the primers used are listed on Table A1.1 from the same Appendix. Briefly, initially two plasmids were created by cloning the cDNA of the alpha 2b human integrin gene (ITGA2B, αIIb) and the cDNA of the beta 3 human integrin gene (ITGB3, β3) downstream the Cytomegalovirus (CMV) promoter in the pcDNA3.1(-) plasmid. A third plasmid, containing the Leu33Pro substitution on β3 subunit was generated by site-directed mutagenesis (Kunkel, 1985). Subsequently, the coding sequence of mVenus was cloned downstream the αIIb coding sequence, and the coding sequence of mCherry was cloned downstream the β3Leu33 and β3Pro33 coding sequences in the respective plasmids. Importantly, mVenus and mCherry coding sequences were cloned in frame with the integrin subunits coding sequences with removal of the original stop codon of the integrin subunits for expression as fusion proteins. The sequences of the three resulting plasmids were confirmed by Sanger sequencing (Biological Medical Research Center (BMFZ, Heinrich Heine University Düsseldorf) using the primers listed on Table A1.2 from Appendix 1.

3.2.1.2 – Bacterial transformation, bacterial growth and isolation of plasmids

The bacterial transformation was performed to amplify the plasmids. Here DH5α^{TM} derivative competent *E. coli* was used and a heat shock was employed for the transformation process. The capacity of the bacterial cell to capture exogenous DNA (competency) can be conferred by several methods. The DH5α^{TM} was pre-treated with Calcium Chloride to make bacteria permeable allowing the DNA to pass through the membrane. Transformation was done according to manufacturer's protocol. Briefly, 50 μl of cells were transferred to an Eppendorf tube immersed on ice. 100 ηg of plasmid DNA were added, the tube was inverted 4-5 times to mix cells and let on ice for 30 minutes. A heat shock was achieved inserting the tube on a thermal block at 42°C for 30s followed by 5 minutes on ice. 950 μl of S.O.C.

medium was added to the mixture and the tube was placed on the thermal block at 37 °C for 60 minutes with 300 rpm agitation. The transformed bacteria were spread on LB agar plates (Table A2.1 from Appendix 2) previously warmed at 37°C and supplemented with 100 μg/ml of Ampicillin (in case of bacteria transformed with the plasmid αIIbmVenus), or 50 μg/ml of Zeocin (in case of plasmids β3Leu33mCherry and β3Pro33ZeomCherry). Due to the fact that plasmids contained a gene conferring resistance to antibiotic (Figure 7), only colonies effectively transformed and expressing the antibiotic-resistance gene are expected to survive. In the present work, after 12h of incubation at 37°C, resistant colonies were picked and grown O.N. at 37°C in 250 ml of LB medium (Table A2.2 from Appendix 1) containing the corresponding antibiotic. From the grown cultures, DNA was isolated using the Highspeed Plasmid Maxi Kit and, a glycerol stock (70μl bacterial suspension + 30μl of glycerol) was prepared and kept at -70°C for further applications. DNA concentration was determined by absorbance using a Biospectrophotometer. Isolated plasmids were subsequently used for transfecting human cell line cells.

3.2.2 – Expression of αIIbβ3 integrin receptor in HEK293 cells

3.2.2.1 – Cell culture

In the present work HEK293 cells were used, a commercially available cell line established from a human primary embryonal kidney transformed by adenovirus type 5 (Ad 5) (Graham et al., 1977). The HEK293 cells were purchased from the Leibniz Institute DSMZ-German Collection of Microorganisms and Cell Cultures (DSMZ, no. ACC 305) and cultured according to the recommended conditions in Dulbecco's Modified Eagle's Medium (DMEM) supplemented with 10% of Fetal Bovine Serum (FBS), and 1% Penicillin-Streptomycin. Cells passaging involved harvesting with 625 μM of etilenodiaminotetracetic acid (EDTA) in Dulbecco´s Phosphate-buffered saline (DPBS) followed by reaction stopping with DPBS. Prior to experiments, viable cells were counted using a Neubauer chamber and Trypan Blue Solution 0.4% according to standard protocols (Schmitz, 2011).

3.2.2.2 – Cell transfection

In order to bring HEK293 cells to express the complete αIIbβ3 integrin receptor in each of its two isoforms (αIIbβ3Leu33 or αIIbβ3Pro33), a double transient transfection was

performed with the plasmids αIIbmVenus and β3Leu33mCherry or β3Pro33mCherry. In order to prepare the proper donor controls for FRET-APB experiments, HEK293 cells were also double transfected with αIIbmVenusβ3Leu33 and β3Leu33 or β3Pro33 plasmids (Figure 6).

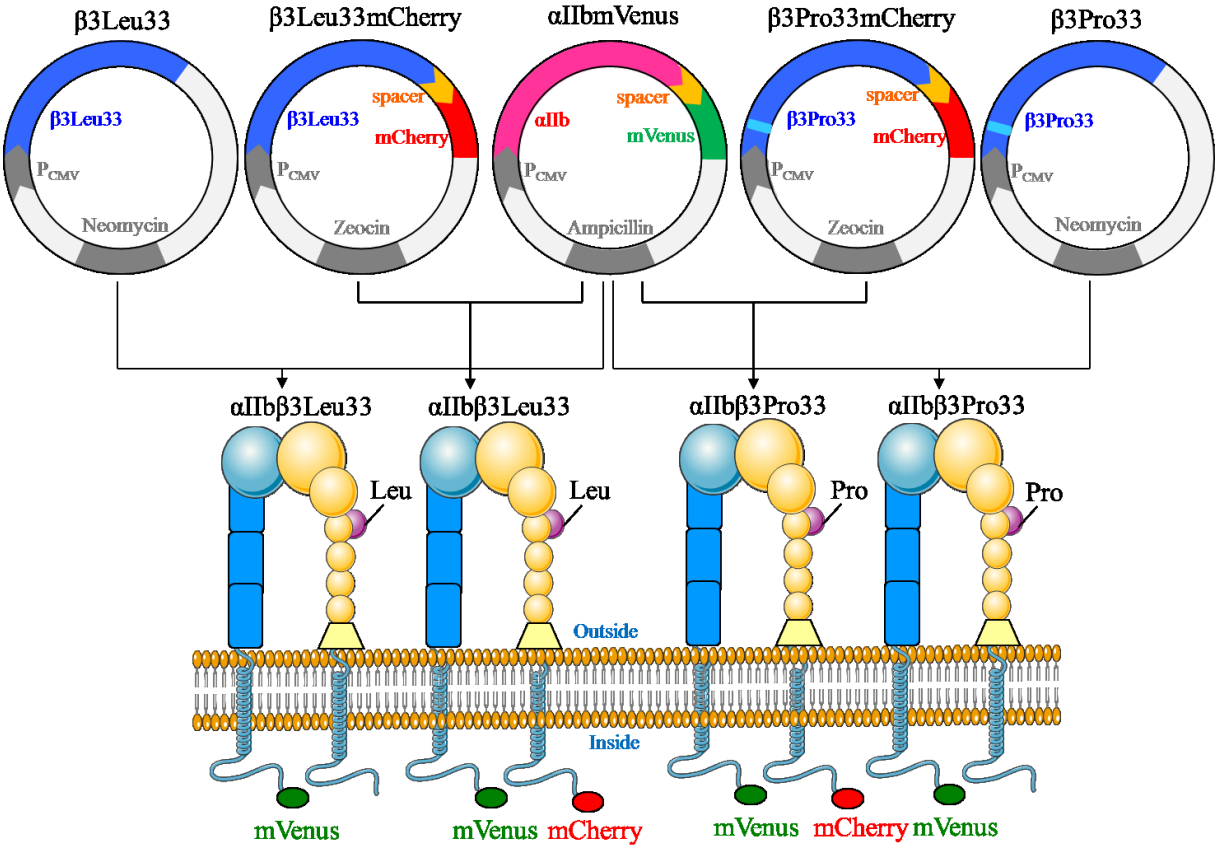

Figure 6 - Schematic representation of DNA constructs used in double transfections for expression of human αIIbmVenusβ3Leu33mCherry and αIIbmVenusβ3Pro33mCherry (plasmids designation) in HEK293 cells, including controls for FRET experiments αIIbmVenusβ3Leu33 and αIIbmVenusβ3Pro33 (plasmids designation).

A vector containing no integrin gene (vector-only control) was also transfected into the HEK293 cells, to be used later as negative control.

In this work a transient transfection was performed using the Effectene Transfection Reagent which is based on a non-lipossomal micelle component that coats the DNA forming a complex, facilitating the entrance of the DNA inside the cell. Briefly, 24h prior transfection, $1.6x10^5$ cells were seeded on a 6-well plate in culture medium. On the next day, 0.4 µg of integrin αIIb encoding plasmid and 0.4 µg of each β3 encoding plasmids were diluted in EB Buffer (total final volume of 100 µl), 3.2 µl of transfection enhancer was added, and the

mixture was incubated at room temperature for 5 min. Afterwards, 10 µl of Effectene was added and the mixture was incubated at room temperature for 10 min. Finally, 200 µl of cell culture medium was added and the mixture was carefully pipetted into the wells containing the cells. 24h after transfection the medium was replaced by standard cell culture medium. On such transient transfections, the expression of the protein coded in the plasmid is limited in time because the genetic material is not integrated into the genome and therefore can be lost by cell divison (Reviewed by (Kim and Eberwine, 2010)).

3.2.3 – Detection of the integrin αIIbβ3 expression in HEK293 cells

3.2.3.1 – Life-cell fluorescence microscopy

Live-cell imaging was performed to examine the cellular distribution of $\alpha_{IIb}\beta_3$-transfected HEK 293 cells expressing either isoform, Leu33 or Pro33. Twenty-four hours after transfection, $3.7x10^4$ cells in complete culture medium were allowed to settle for more 24 hrs in individual chambers in a µ-slide 4 well ibiTreat chamber slide (Ibidi, Germany) previously coated with 50 µg/ml of fibrinogen from human plasma (Sigma-Aldrich, USA) in PBS without Ca^{2+} and Mg^{2+} for 1 h at 37 °C. Live-cell imaging was performed with an Axiovert S100 inverted fluorescence microscope (Zeiss, Jena,, Germany), equipped with a 12.0 Monochrome w/o IR-18 monochromatic camera (Diagnostic Instruments, Inc, Sterling Heights, MI, USA) and a LEJ EBQ 100 isolated lamp (Leistungselektronik Jena GmbH, Jena, Germany). Images were obtained with a 63 x oil immersion objective lens using 5000 ms exposure time for mVenus, 100 ms for mCherry, and 300 ms for Brightfield. Image acquisition was performed with the Metamorph Software (v. 7.7.7.0, Zeiss, Germany). Background subtraction and image processing were obtained using Adobe Photoshop CS3 (Adobe, San Jose, CA, USA) software.

3.2.3.2 – Protein analysis

Western Blot is used to detect proteins on cell lysates. In the present work, Western Blot was performed in order to validate the expression of the two integrin subunits, αIIb and β3 (β3Leu33 or β3Pro33) in the transfected HEK 293 cells. Cell lysate is run via electrophoresis through a polyacrylamide gel to separate the protein according with its molecular weight. Via electroblotting the proteins are transferred from the gel onto a membrane that is afterwards

incubated with an antibody detecting a specific protein of interest. Detection of this first antibody used can be achieved by chemiluminescence. For that, the membrane is incubated with a secondary antibody raised against the species of the first antibody and coupled with Horseradish peroxidase (HRP). Subsequently, incubating the membrane with Supersignal® West Dura Extended Duration Substrate, a HRP substrate that becomes luminescence upon HRP cleavage, light is produced at the place where the antibodies and the specific protein of interest are located. This light can be detected by a camera and a digital image is produced. Using a molecular weight standard and with the information about the molecular weight of the protein to be detected we can conclude about the presence of the protein in the cell lysate.

3.2.3.2.1 – Crued cell extracts

For preparation of cell lysates, 48 h after transfection, cells were harvested, counted, and $3x10^6$ cells were pelleted by centrifugation at 400 g for 7 min and resuspended in 500 µl of 1 x Lysis Buffer (Table A2.3 from Appendix 2). This cell suspension was vortexed, incubated 1 h on ice for lysis, and centrifuged for 10 min at 16100 g at 4°C to separate the soluble protein content from insoluble membrane fragments. The supernatant containing the soluble cellular proteins was transferred into new eppendorf tubes and frozen at -20°C until further use. For protein quantification in cell lysates the Pierce Coomassie (Bradford) Protein Assay (Bradford, 1976) was used, a colorimetric method based in the modifications of the spectral characteristics of Pierce Coomassie reagent when it binds to proteins. When bound to a protein, the Pierce Coomassie dye exhibits an absorption maximum at 595 nm and the level of absorbance at this wavelength is directly proportional to the amount of protein in the sample (Bradford, 1976). Before absorbance measurement, cell lysate was first 1:8 diluted on a 1:1 mixture of lysis buffer and water. This mixture was also 1:50 diluted with filtered Bio-rad protein assay solution. The precise protein concentration of a sample was determined by comparing the absorbance at 595 nm of the samples with that detected in solutions of BSA (Sigma-Aldrich, Germany) at 100 µg/ml, 250 µg/ml, 500 µg/ml, 750 µg/ml, 1000 µg/ml and 1500 µg/ml similarly prepared on a 1:1 mixture of lysis buffer and water and diluted 1:50 in Bio-rad protein assay solution (a standard linear absorbance profile). The absorbance of the samples at 595nm was measured on a Genesys 10S UV-VIS spectrophotometer (Thermo Fischer Scientific, USA) using disposable cuvettes (Sarstedt, Germany). A 1:1 mixture of lysis buffer and water similarly diluted 1:50 in Bio-rad protein assay solution was used as blank measurement. Finally, it was determined an equation for the linear relation between the

concentration of the BSA solutions and the respective absorbance, and that equation was used to determine the protein concentration in the samples (Bradford, 1976).

3.2.3.2.2 – SDS-PAGE

SDS-PAGE gel was performed using the PerfectBlue™ Double Gel System Twin S. For each gel (10 cm x 10 cm), 9 ml of a separating gel (Table A2.5 from Appendix 2) was prepared quickly applied into the gel chamber, and let to polymerize for 15 min under a layer of 2-propanol. Following polymerization, 2-propanol layer was removed and 5 ml of freshly prepared stacking gel (Table A2.6 from Appendix 2) was quickly applied over the separating gel and let to polymerize for 15 min.. After polymerization, the gel was placed in the electrophoresis chamber. The chamber was filled with 500 ml of running buffer (Table A2.8 from Appendix 2). The electroforese was run at 20 mA/gel for 3h. Subsequently, the gel was incubated in 1 x transfer buffer (Table A2.10 and A2.11 from Appendix 2) for 10 min at RT with gentle shaking.

3.2.3.2.3 – Sample preparation

25µg of protein in 1x sample buffer (Table A2.9 from Appendix 2) were denatured at 95 °C for 5 min on a PTC-200 Peltier Thermal Cycler and used for each western blot.

To control the molecular weight of protein in the gel was used the Precision Plus Protein™ WesternC™ standards molecular weight marker. Before loading on the gel, 6 µl of the marker was mixed with 2 µl of StrepTactin-HRP conjugate.

3.2.3.2.4 – Western blot

The equipment used for blotting was the Mini Trans-blot® Electrophoretic Transfer Cell. Before blotting, a nitrocellulose membrane, two black foam pads and 2 Whatman® Gel Blot papers cut with the same size of the gel were incubated in cold 1x transfer buffer. A color-coded gel holder cassette was mounted using the components described before and inserted on the Mini Trans-blot® central core ensuring the proper orientation of the gel during transfer. Blotting was done at 100 V for 70 min. After that, cassette was disassembled and the blotting membrane was rinsed in Tris-buffered saline and 0.1% Tween 20 (TBS-T buffer) for 1 min at RT. The blocking was performed with 5% BSA solution prepared in TBS-T buffer for 1h at RT with gentle agitation on a RM5-80V roll mixer.

3.2.3.2.5 – Imunnodetection

For the subsequent detection of the αIIb integrin and β3 integrin proteins in the membrane, were used the rabbit anti-human integrin αIIb polyclonal antibody (clone H-160; 0.4 μg/ml) and the rabbit anti-human integrin β3 polyclonal antibody (0.01 μg/ml) respectively. As loading control the Glyceraldehyde 3-phopsphate dehydrogenase (GAPDH) detected by the respective mouse monoclonal antibody (clone 6C5; 0.33 μg/ml) was used. Each antibody was diluted in 5 % BSA/TBS-T and membranes were incubated ON at 4 °C plus 1-2 h at RT with gentle agitation. Afterwards, membrane was washed two times with 5 % BSA/TBS-T for 5 min with gently agitation. Before using the Ecl anti-rabbit IgG Horseradish secondary antibody (dilution 1:5000), this was mixed with the conjugate Precision Protein StrepTactin HRP (1:10000) in 5 % BSA/TBS-T. The mixed antibody and conjugate was incubated with the membrane for 1.5 h at RT, with gentle agitation. Subsequently, membrane was washed three times with 5 % BSA in TBS-T during 5 min with gentle agitation. The detection was done using the Super Signal® West Dura Extended Duration Substrate, mixing 1 ml of Super Signal West Dura Stable Peroxide Buffer with 1 ml of Super Signal West Dura Luminol and 2 ml of destilled water. The membrane was left over a glass and incubated for 5 min with the previous mixture. The detection was performed using a Molecular Imager with exposure times from 1 s to 60 s.

3.2.3.3 – Flow cytometry

As reviewed by Picot et al. the flow cytometry is a technique that uses a laser to detect physical and molecular properties of individual cells in droplets of a liquid stream (Picot et al., 2012). In the present work, flow cytometry was used to detect and quantify the expression of mVenus and mCherry (fused to the integrin subunits) and the expression of CD41, the complete integrin receptor, on transfected HEK293 cells. For analysis by flow cytometry, transfected cells at 70-80% confluence were harvested 24, 48 and 72 h after transfection. Subsequently, cells were pelleted by centrifugation at 400 g for 7 min and resuspended in 100 μl of DPBS (Dulbecco's phosphate-buffered saline). Staining with allophycocyanin (APC)-conjugated mouse anti-human CD41 monoclonal antibody (clone MEM-06; Exbio, Czech Republic; 0.15 μg/ml) was performed for 30 min at RT, protected from light. After staining, cells were washed once in DPBS and analyzed on a FACS Canto II flow cytometer (BD Biosciences, San Jose, CA, USA), equipped with 488 nm and 633 nm lasers for excitation,

and the FITC, PE and APC filters for detection of mVenus, mCherry, and APC, respectively. The compensation of the signals due to spectral overlay was performed. A gate strategy was set to identify mVenus, mCherry and APC triple-positive cells. The collected data were analyzed with the FACSDiva software V. 6.1.3 (BD Biosciences, USA).

3.2.4 – Structural and functional studies of αIIbβ3 expressed in HEK293 cells

3.2.4.1 – Förster/Fluorescence Energy Transfer using acceptor-photobleaching (FRET-APB)

FRET consists on the transfer of energy between two fluorescent molecules that are in close proximity of each other (Förster, 1948). This principle and associated technology were applied to compare the distance between the cytoplasmic tails of α and β subunits in both receptor isoforms, αIIbβ3Leu33 and IIbβ3Pro33. Basal FRET efficiency was measured by the FRET-APB method in which the fluorescence intensity of an energy donor (mVenus) was compared before and after specific photo-induced destruction of the acceptor (mCherry). For that, 24 h after transfection, cells were harvested and seeded in μ-Slide 8 well ibiTreat chamber slide (Ibidi, Germany). Subsequently, 24 h later (48 h after transfection) and before measuring FRET efficiency, the culture medium was substituted by identical medium but this time containing phenol red free Fluorobrite^{TM} DMEM (Thermo Fisher, formerly Life Technologies, USA).

The experiments were performed at the Center for Advanced Imaging, at the Heinrich Heine University Düsseldorf. Living cells were examined with a LSM 780 (Zeiss, Jena, Germany) inverted microscope, equipped with a C-Apochromat 40x/1.20 W Corr (from Correction ring) M27 water immersion objective lens, an AxioCam camera, and a HPX 120C lamp. FRET acceptor photobleaching experiments including image acquisition, definition of regions of interest for bleaching, and data readout were performed using the LSM Software package ZEN 2012 (Zeiss, Oberkochen, Germany). The chamber slide containing the living cells was mounted on a heating frame within a large incubation chamber (PeCon, Erbach, Germany) set to 37 ºC. mVenus was excited with the 488 nm line of an argon multi-line laser, and detected between 513-558 nm using a GaAsP detector, while mCherry was excited at 561 nm using a DPSS laser and detected between 599-696 nm. The beam splitter was MBS 488/561/633. In total, a time series of 20 frames (128x128 pixel, pixel size 0.33 μm) at a pixel time of 2 μs/pixel was acquired for each FRET experiment. After the 5th frame, an area

corresponding to half of a cell, with a constant dimension of 42x42 pixels (region of interest), was bleached by 30 iterations of the mCherry excitation wavelength (561 nm) using 100% laser power. After bleaching, 15 additional frames were recorded. The entire measurement including bleaching of mCherry was finished within 3.5 s. The mean intensity of mVenus fluorescence at the cell membrane within the bleached area was extracted and analyzed according to the following equation:

$$\text{FRET Efficiency} = \frac{\text{Intensity mVenus after bleaching} - \text{Intensity mVenus before bleaching}}{\text{Intensity mVenus after bleaching}} \times 100$$

whereby intensity mVenus after bleaching and intensity mVenus before bleaching correspond to the mean intensity values of mVenus fluorescence of five images before and after bleaching within the bleached area at the cell membrane (Bleckmann et al., 2010; Karpova et al., 2003a).

3.2.4.2 – Single-cell force spectroscopy (SCFS) using AFM technology

Single-Cell Force Spectroscopy (SCFS) was used to study the interaction between the two variants of αIIbβ3 receptor, expressed in HEK293 cells, and fibrinogen, its natural ligand. The SCFS assays were performed in the Institute of Physical Chemistry, University of Göttingen, in the group of Prof. Dr. Andreas Janshoff and directly with MSc. Susanne Karsch. 24 h prior the SCFS experiments the cantilevers (Arrow-TL2, Tipless Silicon SPM-Sensors) were washed with isopropanol, cleaned in argon plasma for 1 min, and subsequently coated with 0.1 mg/ml of poly-L-lysine in 1xPBS for 1 h. The positively charged poly-L-lysine facilitates the adhesion of cells, which contain a negatively charged cell membrane, to the cantilever through an electrostatic interaction. Finally cantilevers were dried and kept at RT until the experiments. On that same day, culture dishes were coated with fibrinogen. For that the outer part of culture-insert 2 well dishes (35 mm diameter) were coated with 100 µg/ml of Fibrinogen from human plasma and were kept at 4 °C overnight. In the day of the experiments, unbound fibrinogen was taken out from the culture dishes and these were washed two times with PBS. Then the inserts of the culture dishes were removed and the entire exposed surface was blocked with 1% BSA in PBS without Ca^{2+} and Mg^{2+} at 37 °C for 1 h. Before being used in the SCFS assay, the culture dishes were washed again two times with PBS. HEK293 cells were harvested in the same way as for prior experiments (section

3.2.2). 50000 cells were suspended in 0.5 ml of cell culture medium (section 3.2.2.1), and kept at 37 °C with 5% CO_2 during instrument setup.

SCFS measurements were performed using a CellHesion200 AFM equipped with a Petri dish heater set to 37°C, and mounted on top of an IX83 inverted microscope (Figure 7).

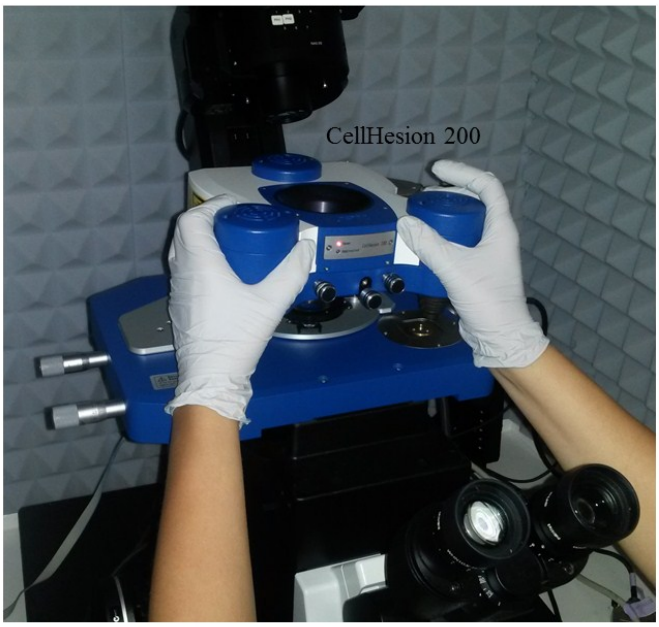

Figure 7 – CellHesion 200 mounted on Olympus IX81 microscope.

The microscope system was equipped with a XM10 camera-and a 10x UPLFLN2 / NA 0.3 objective. Before each experiment, laser detection system and cantilever were calibrated using a dish filled with 2 ml of phenol red free Fluorobrite^{TM} DMEM (measurement medium). The cantilever nominal spring constant (0.03 Nm^{-1}) was determined employing the thermal noise method (Hutter and Bechhoefer, 1993).

For the experiments, 20 µl of cell suspension was pipetted into the 2 ml measurement medium in the central area of the dish previously blocked with BSA. For the analysis, were selected single-cells with healthy appearance and expressing simultaneously mVenus and mCherry fluorescences (in order to guarantee the complete receptor). The analysis of fluorescence at the IX83 microscope was performed using 200 ms of exposure time and the CY3 Chroma 41002 fiter set (Ex. 535/50 nm; Em. 610/75 nm) for detection of mCherry fused to the β3Leu33 and β3Pro33 subunits, and the YFP Chroma 41028 filter set (Ex. 500/20 nm; Em. 535/30 nm) for detection of mVenus fused to the αIIb subunit. When identified, single-cells in the BSA area of the culture dish were picked with the cantilever using 30 s of contact

time, set point force of 1500 ρN in constant height mode, and approach/retraction velocity of 5 μms^{-1}. Before subsequent steps, a five minute- pause period was used to guarantee that the cell was firmly attached to the cantilever. Using the same approach/retraction velocity, the cell was carefully approached onto the fibrinogen-coated area of the culture dish with a set point force of 500 ρN for 5, 7.5, and 10 s in constant height mode. Each contact time was repeated a total of 10 times in 2 different areas. So a total of 30 measurements were done per individual cell. The two different areas of the culture dish were used to avoid errors caused by possible degradation of the fibrinogen substrate resulting from the repeated cell contact in the same area, and by possible differences of substrate concentration between areas of the dish. During each retraction of the cantilever, the force was recorded to identify differences in cell adhesion. The retraction curves were baseline corrected and the set point was automatically set at zero force in the retraction curve with the SPM software (Version 6.0.16) (JPK, Germany). Curves where no constant baseline was identified were rejected from further analysis. The adhesion events were quantified manually with a self-written Matlab Script. Parameters analysed were: maximal adhesion (minimum of retraction curve), single rupture (force jumps after a force increase), tether force (force jump after a constant force plateau, mostly at late retraction), tether length (length of a constant force plateau) and adhesion energy (area between baseline and retraction curve).

HEK293 cells that had been transfected 48h before with the αIIbmVenus and β3Leu33mCherry plasmids, and cells transfected with αIIbmVenus and β3Pro33mCherry plasmids expressing the complete receptor were used. As control, prior to the experiment, part of these harvested cells was incubated for 15 min at RT with 10 μg/ml of Abciximab (brand name: Reopro), a humanized form of a murine monoclonal antibody directed against αIIbβ3 and able to inhibit fibrinogen binding by steric hindrance and by an allosteric effect on the RGD-binding region (Artoni et al., 2004; Coller et al., 1983; Coller, 1985). One additional control consisted of HEK293 cells transfected with the vector-only control plasmid.

3.2.5 – Statistical Analysis

The statistical analysis was done based on the D'Agostino & Pearson omnibus normality test (D'Agostino and Pearson, 1973) and on the Mann-Whitney test, also called the Wilcoxon rank sum test (Wilcoxon, 1945). These tests were performed using GraphPad Prism version 6.00 for Windows, GraphPad Software, La Jolla California USA, www.graphpad.com.

4 – RESULTS

4.1 – Design and construction of plasmids

In order to drive the expression of the αIIbβ3 receptor in model cells and to evaluate the impact of the Leu33Pro substitution in its structure and function, we designed and constructed a total of six plasmids (Figure 8, Table 1).

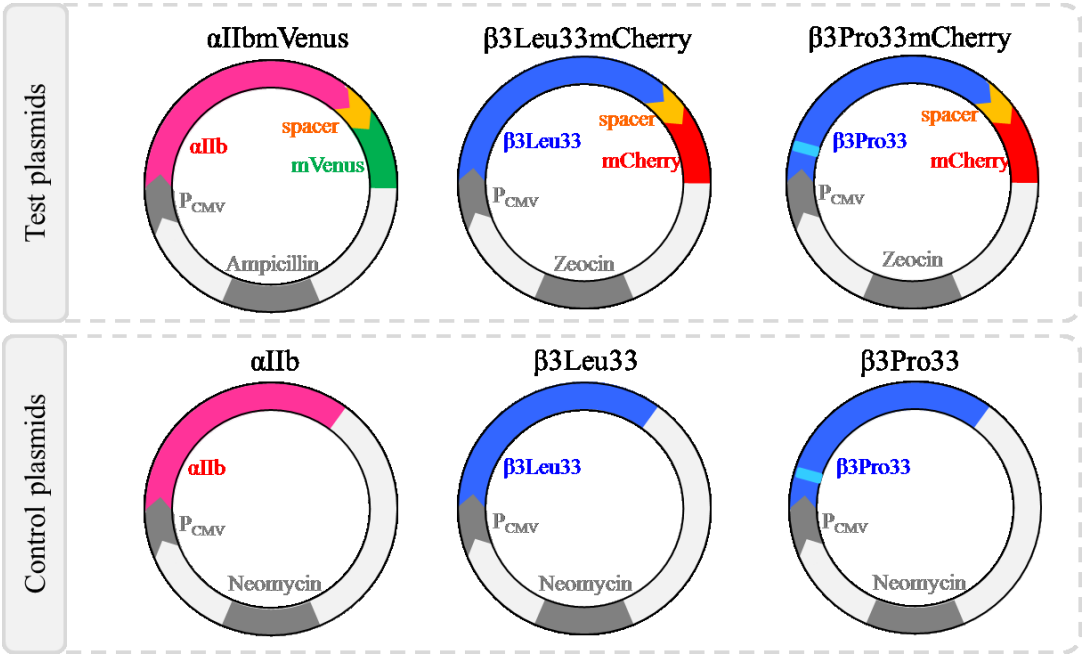

Figure 8 – Diagrams of the plasmids constructed for the present work (indicated genes are not proportional to their size).

Table 1 – Name, relevant attributes and size of the vectors constructed.

	Plasmid Name	Main characteristics	Size (bps)
Test plasmids	αIIbmVenus	Subunit αIIb fused to mVenus downstream of CMV promoter	9368
	β3Leu33mCherry	Subunit β3 fused to mCherry downstream of CMV promoter	6640
	β3Pro33mCherry	Subunit β3 containing Leu33Pro substitution and fused to mCherry downstream of CMV promoter	6640
Control plasmids	αIIb	Subunit αIIb downstream of CMV promoter	9957
	β3Leu33	Subunit β3 downstream of CMV promoter	8000
	β3Pro33	Subunit β3 containing Leu33Pro substitution downstream of CMV promoter	8000

Three plasmids (test plasmids) were designed to express each of the two subunits fused in their C-terminus to fluorescent proteins (αIIb fused to mVenus, and β3 fused to mCherry). Three other plasmids were constructed to express the subunits in their original form (not fused) and aimed to be used as controls in the different experiments (control plasmids).

After the cloning procedures (Appendix 1) and amplification in bacteria, we confirmed the integrity of the prepared plasmids. In one hand, the molecular weight of the constructs was estimated by agarose gel electrophoresis of the linearized plasmids. Linearization was performed by digesting the plasmids with single cutting restriction enzymes: ClaI for αIIbmVenus and AseI for β3Leu33mCherry and β3Pro33mCherry. The molecular weights that could be estimated from running the linearized plasmids in agarose gel (Figure 9) (~10000 bps for the αIIbmVenus and between 5000 and 7000 bps for β3Leu33mCherry and β3Pro33mCherry) fit with the expected ones (Table 1), indicating that no major sequences recombination events have occurred during the bacterial growth.

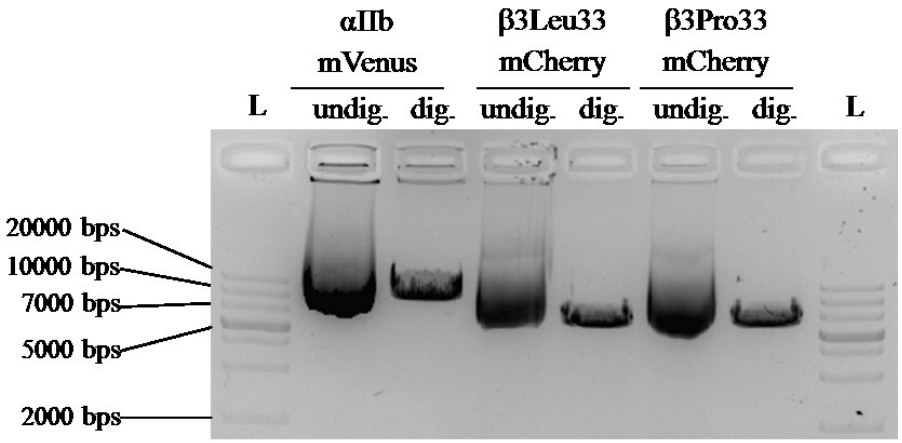

Figure 9 – Agarose gel electrophoresis obtained by digestion of the αIIbmVenus construct with ClaI restriction enzyme and of β3Leu33mCherry and β3Pro33mCherry constructs with AseI restriction enzyme. In both extremities of the gel are shown the ladder (L) used to evaluate the sizes of the originated fragments.

More in detail, by Sanger sequencing we could confirm the integrity of the plasmid elements more relevant for the present work, namely the CMV promoter, integrin subunit, spacer, and fluorescent protein. The αIIb protein coding sequence present in the plasmid was compared with the ITGA2B coding sequence (NCBI Reference Sequence NM_000419.4) while the β3 coding sequence was compared to the ITGB3 coding sequence (NCBI Reference Sequence: NM_000212.2) and no differences could be detected. Importantly, it could be verified the presence of the CTG codon coding for Leucine in position 33 of the β3 in the β3Leu33mCherry plasmid and the CCG codon coding for Proline at the same position in the

β3Pro33mCherry plasmid (Figure 10). The perfect match between plasmids´ sequences and the expected sequences indicates that the plasmids produced were correct and fit to the cloning strategy designed.

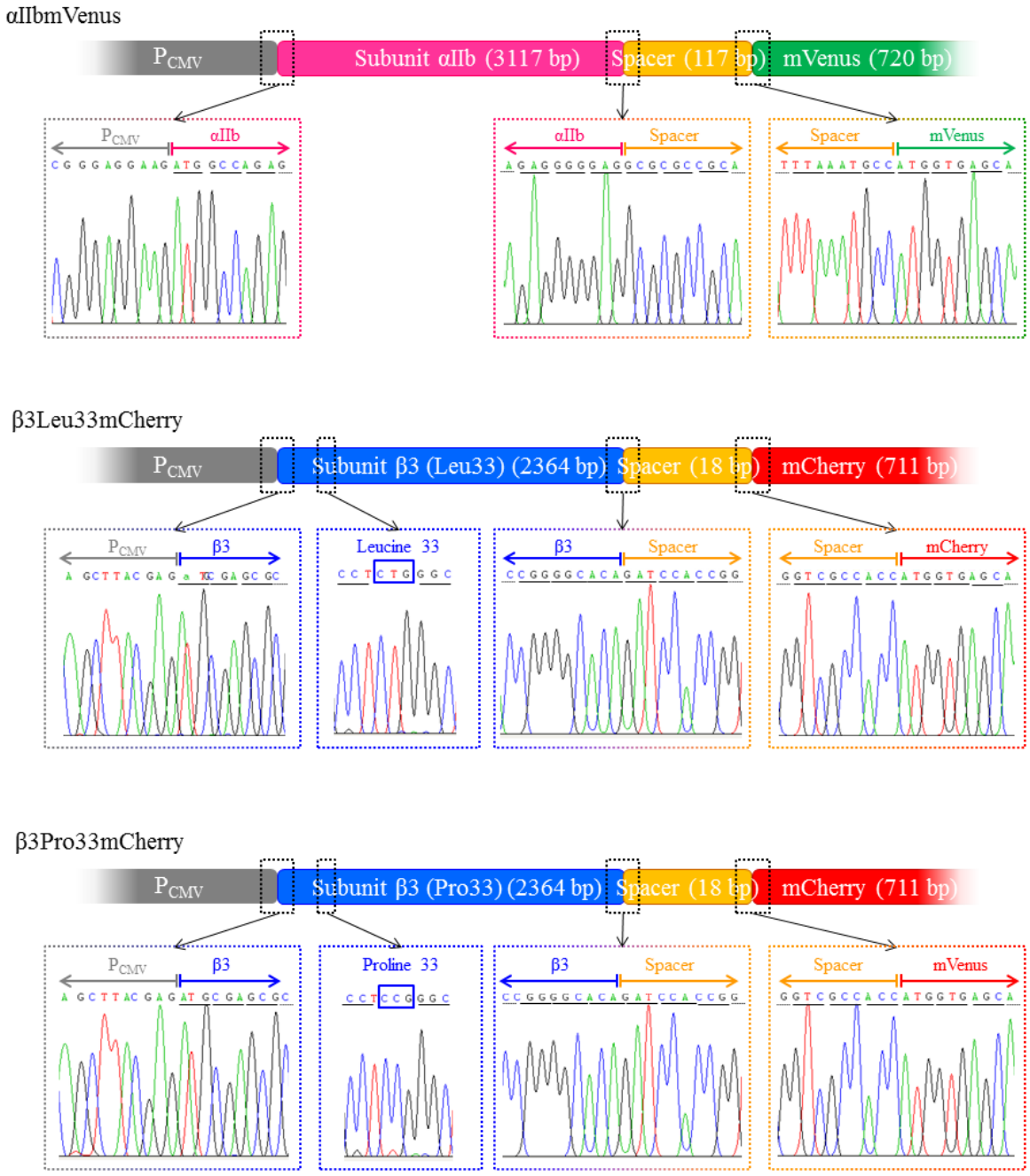

Figure 10 – The region of PCMV, integrin subunit, spacer and fluorescent protein are depicted for the αIIbmVenus (upper panel), β3Leu33mCherry (middle panel) and β3Pro33mCherry (lower panel) plasmids. For each plasmid, are shown short segments of the electropherograms encompassing the transition between the four main structural elements of the plasmid and the positions coding for Leucine or Proline in the β3 subunit. In each electropherogram, the underlining of the bases called indicates the codons in frame.

4.2 – Expression of integrin αIIbβ3 in HEK293 cells

The previously prepared plasmids were transfected into HEK293 cells according to the schemes depicted in Figure 6. Following transfection, we initially used western blotting to confirm the presence of both subunits in the respective protein cell lysates. The western blot showed that prominent bands at the expected molecular weight could be consistently detected in the different samples (Figure 11). In the αIIb western blot, when αIIbmVenus plasmid was used we could observe a prominent band at ~144 KDa that correspond to the complete fusion protein. When the αIIb plasmid was used the most prominent band appears at ~113 KDa which should correspond to the αIIb protein in its native form (ref. P08514.3 by SwissProt database). However, in samples transfected with the αIIbmVenus plasmid we could also detect the band at 113 KDa which suggest that in these samples αIIb protein can be expressed without its fluorescent tail. In addition, in all transfected samples we could detect two other less intense bands at approximately 109 and 103 KDa suggesting being two smaller isoforms of αIIb which may possibly be generated by alternative splicing (109 KDa ref. P08514-2; and 103 KDa ref. P08514-3). Interestingly, only the smaller isoform (103 KDa) could be detected in the lysate of platelets.

In the β3 western blot, a very prominent band at 121 KDa could be detected when the β3mCherry plasmids were used and which should correspond to the complete fusion protein. When the β3Pro33 plasmid was instead used that band was completely absent and replaced by a prominent band at 97 KDa corresponding to the β3 subunit alone. As expected, in platelets only the band at 97 KDa could be detected. Of note, when the β3mCherry plasmids were used, one other additional band between the 121 KDa and the 97 KDa bands could be seen but its origin is not clear. Of note, as for the αIIb, also three isoforms of the β3 subunit can be generated by alternative splicing of the sequence cloned (SwissProt identifiers: P05106-1; P05106-2 and P05106-3). However these isoforms differ very less in their molecular mass (87.1, 86.1 and 86.7 KDa) and therefore are an unlikely explanation for the additional band detected. Upon in-silico inspection of the β3mCherry plasmids, we could not detect the presence of any other putative protein coding sequence encompassing and in frame with the β3 coding region that could lead to a product of such molecular weight.

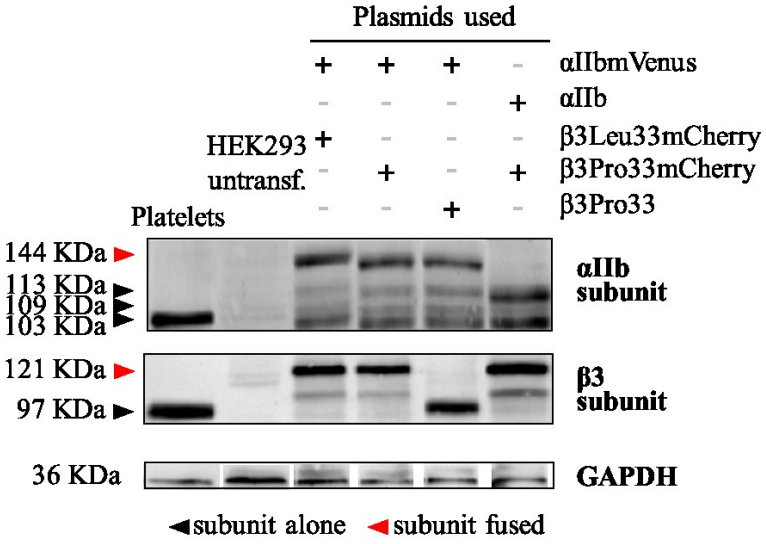

Figure 11 – Western Blots showing the expression of the different isoforms of αIIb and β3 subunits upon transfection of HEK293 cells with different combinations of plasmids. The molecular weight expected for the αIIb and β3 subunits in their natural form (alone) or fused to the mVenus or mCherry fluorescent proteins is indicated in the left side. Platelet protein lysate was used as positive control while untransfected HEK293 cells were used as negative control. GAPDH was used as loading control.

Subsequently, we used fluorescence microscopy to evaluate the cellular localization of the transfected subunits on HEK293 cells (Figure 12). The two subunits showed very similar distribution in the cells. They were localized predominantly at defined spots in the peri-nuclear region suggesting the Golgi complex, and at the cell membrane as expected for the functional αIIbβ3 receptor.

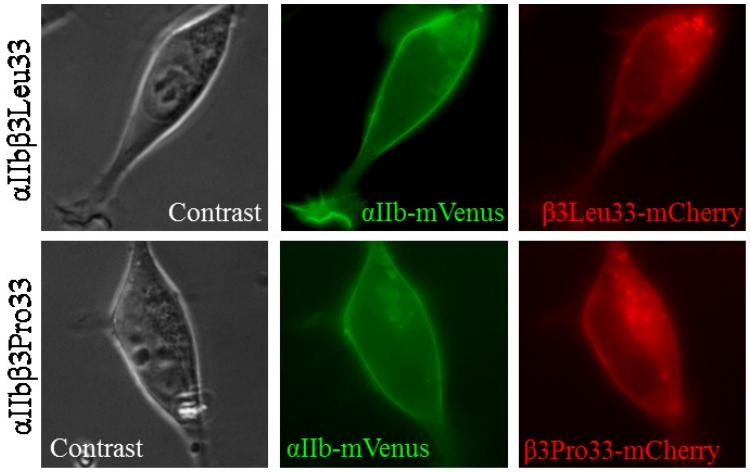

Figure 12 –Phase contrast and fluorescence microscopy images of one representative HEK293 cell transfected with α_{IIb}mVenus and β_3Leu33mCherry plasmids (upper panel), and one representative HEK293 cell transfected with α_{IIb}mVenus and β_3Pro33mCherry plasmids (lower panel) (63x objective).

Concordant with the presence of the receptor at the cellular membrane we could detect the complete αIIbβ3 receptor (recognized by an anti-CD41 antibody, clone MEM-06) by flow cytometry using a protocol for extracellular staining (Figure 13). In cells transfected with αIIbmVenus and β3Leu33 plasmids 45% of the intact defined upon forward and side scatter analysis, were positive for CD41-AP and mCherry ($CD41^{pos}$/$mCherry^{pos}$, Figure 13A1). 48.4% of the same cells were $CD41^{pos}$/$mVenus^{pos}$ (Figure 13A-3) and 47.5% were $mVenus^{pos}$/$mCherry^{pos}$ (Figure 13A-2). A very identical scenario was obtained for cells transfected with αIIbmVenus and β3Pro33 plasmids: 45.5% of the intact cells defined upon forward and side scatter analysis, were $CD41^{pos}$/$mCherry^{pos}$ (Figure 13B-1); 47.7% were $CD41^{pos}$/$mVenus^{pos}$ (Figure 13B-3); and 48.5% were $mVenus^{pos}$/$mCherry^{pos}$ (Figure 13B-2).

Of note, we could observe that among the cells transfected with αIIbmVenus and β3Leu33mCherry plasmids (13.4%, Figure 13A), some cells were positive for the complete CD41 receptor despite being negative for mCherry (13.4% of intact cells, Figure 13A-1) or negative for mVenus (6.6%, Figure 13A-3). Identical percentages were seen for cells transfected with the αIIbmVenus and β3Pro33 plasmids: 11.7% of intact cells were $CD41^{pos}$/$mCherry^{neg}$ (Figure 13B-1) and 6% were $CD41^{pos}$/$mVenus^{neg}$ (Figure 13B-3). As this could result from unspecific staining of the anti-CD41 antibody to incomplete receptors, we evaluated the specificity of the anti-CD41 antibody towards the complete receptor. For that we transfected HEK293 cells only with one integrin subunit using the αIIbmVenus plasmid, the β3Leu33mCherry plasmid, or the β3Pro33mCherry plasmid, and analysed the expression of CD41 with the same antibody. As untransfected HEK293 cells do not naturally express only one of the subunits (Western Blot, Figure 11) and here we transfected only one of the subunits, we expected only minimal or no detection by the CD41 antibody. In fact, only a minimal percentage of $CD41^{pos}$ could be detected upon single transfection with αIIbmVenus (2.5%, Figure 13C-1), with β3Leu33mCherry (1.72%, Figure 13C-2), and with β3Pro33mCherry (1.35%, Figure 13C-3). Interestingly, it was possible to observe that percentage of cells positive for mVenus (50.5%, Figure 13C-1) achieved in these single transfections controls was much higher than the number of cells positive for mCherry (3.7% and 3.0%, Figures 13C-2 and C3).

Another control used in order to confirm the specificity of the anti-CD41 antibody was performed using cells transfected with vector-only control. As expected no $CD41^{pos}$ cells were found (Figure 13D-3 and D4).

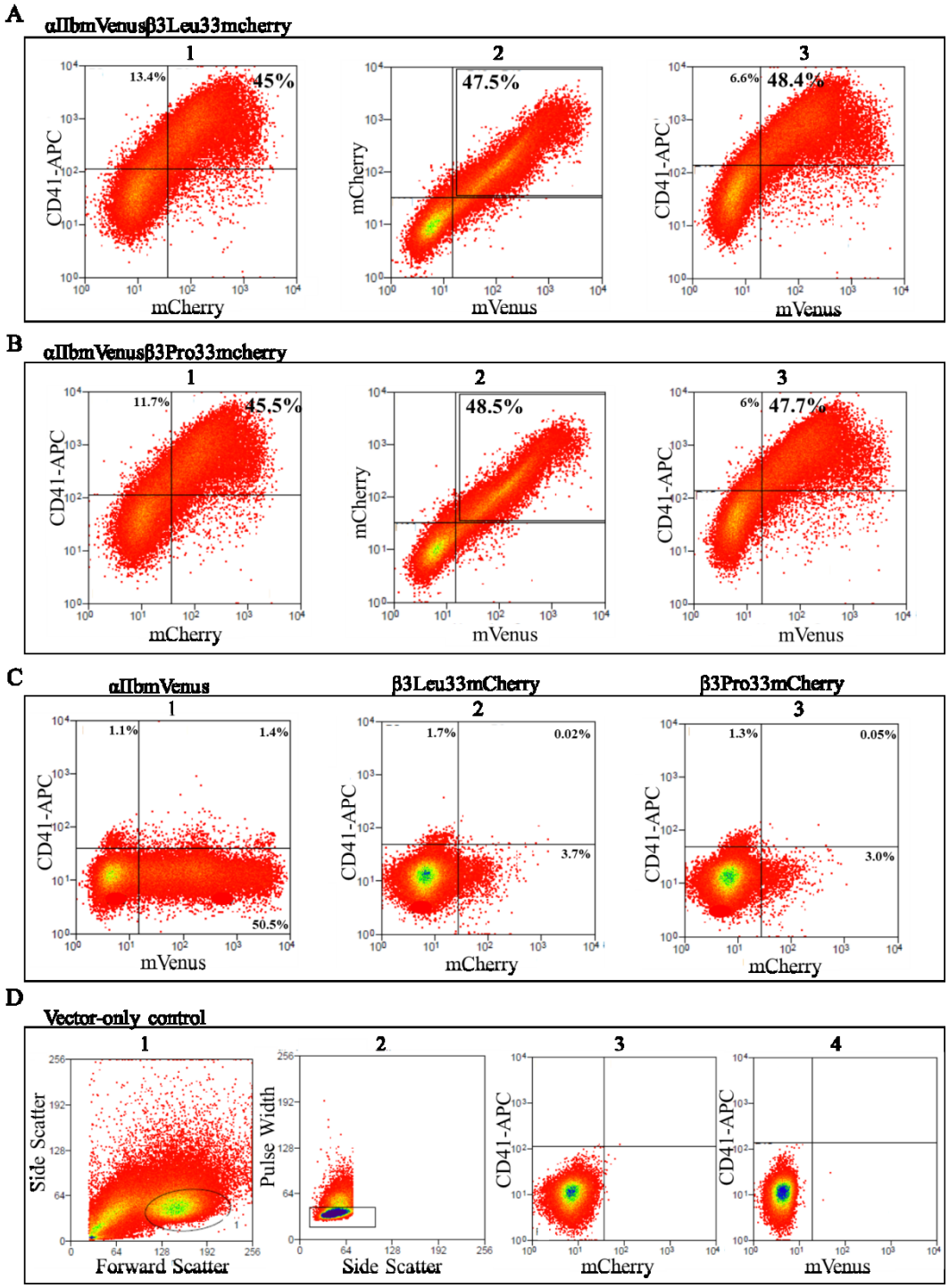

Figure 13 – Flow cytometry measurements of αIIbβ3 (CD41), mCherry and mVenus fluorescence intensity in HEK 293 cells transfected with: **(A)** αIIbmVenus and β3Leu33mcherry plasmids, **(B)** αIIbmVenus and β3Pro33 mcherry plasmids, **(C1)** αIIbmVenus, **(C2)** β3Leu33mCherry, **(C3)** β3Pro33mCherry, **(D)** vector-only control.

Notably, flow cytometry measurements of CD41 expression after five independent transfection experiments indicated that the levels of both αIIbβ3Leu33 and αIIbβ3Pro33 isoforms in the cells did not differ more than 10% in each experiment. Despite that we

verified that the expression level obtained for CD41 across the experiments was considerably different (Figure 14).

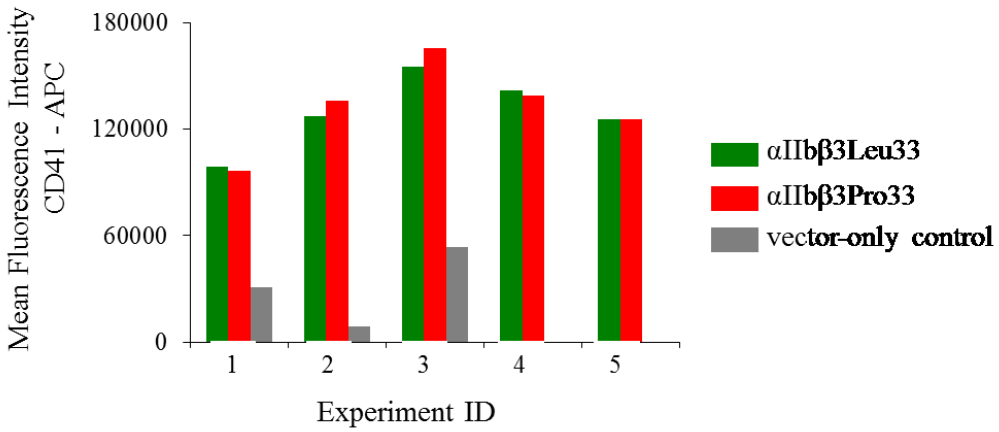

Figure 14 - Flow cytometric measurements of αIIbβ3 (CD41) in cells expressing the Leu33 isoform (αIIbβ3Leu33), the Pro33 isoform (αIIbβ3Pro33), or the vector-only control, performed 48 h after transfection in 5 independent experiments. Values represent mean fluorescence intensity measured for allophycocyanin (APC)-conjugated CD41 antibody, a complex-specific anti-αIIbβ3 antibody, in the population of APC, mVenus and mCherry positive cells.

4.3 – Structural and functional studies of αIIbβ3 expressed in HEK293 cells

4.3.1 – Spatial rearrangements of the cytoplasmic tails of αIIbβ3 upon Leu33Pro substitution

To investigate a possible influence of the Leu33Pro substitution on the spatial separation of α and β subunits, we performed FRET acceptor photobleaching (APB) analyses in individual cells transfected with αIIbmVenus and β3Leu33mCherry plasmids (Leu33 cells) and cells transfected with αIIbmVenus and β3Pro33mCherry plasmids (Pro33 cells). Using FRET, the spatial separation of the subunits is inferred from the amount of energy transferred between the fluorescent proteins mVenus and mCherry attached to the cytoplasmic tails of the subunits. As mVenus and mCherry are close, some of the energy emitted by the donor (mVenus) will be quenched by the acceptor (mCherry). With the specific photobleaching of the acceptor, the energy transfer is abolished resulting in an increase in the energy (fluorescence) emitted by the donor. The difference between the energy (fluorescence)

emitted by the donor before and after photobleaching of the acceptor is used to calculate the efficiency of energy transfer between donor and acceptor. As the quenching effect is increased with the proximity, the closer the donor and acceptor are, the higher will be the energy quenching before photobleaching and the higher will be the difference in fluorescence emitted by the donor upon ablation of the acceptor. For the experiment, we measured the difference in fluorescence emitted by mVenus before and after photobleaching of mCherry in single cells.

Upon photobleaching a defined cellular region (region of interest, ROI) encompassing part of the cell membrane at 561 nm, a complete ablation of mCherry fluorescence (energy acceptor) in that region was observed, a requisite for the experiment (Figure 15A and B). Consequently, in the same region, it could be detected an increase in the intensity of mVenus fluorescence compared to the values measured before photobleaching (Figure 15C and D). As expected, in cells transfected with the αIIbmVenus and β3Leu33 or β3Pro33 plasmids, mCherry fluorescence could not be detected (control condition, Figure 15E and F), and photobleaching at 561 nm caused no difference in the mVenus intensity (Figure 15G and H).

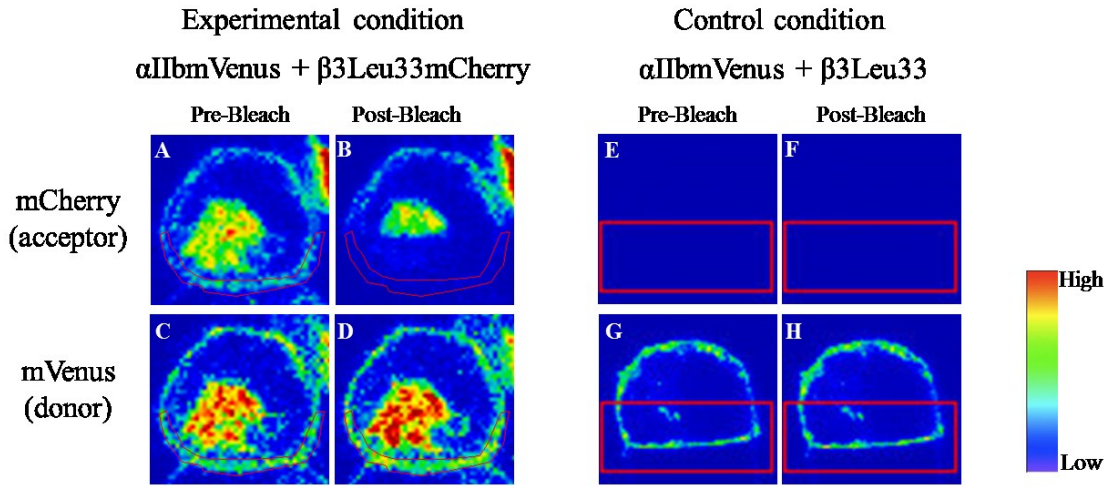

Figure 15 – Single-cell FRET-APB measurements in one representative HEK293 cell transfected with αIIbmVenus and β3Leu33mCherry plasmids and in one representative cell transfected with αIIbmVenus and β3Leu33 plasmids, a control lacking the fluorescence acceptor mCherry. The fluorescence of mVenus and mCherry was measured in a defined region of the membrane (red circled, ROI) before and after photobleaching of mCherry at 561 nm.

FRET-APB analyses could be performed in a total of 249 single cells chosen randomly: 88 cells transfected with αIIbmVenus and β3Pro33mCherry plasmids (Pro33 cells); 91 cells

transfected with αIIbmVenus and β3Leu33mCherry plasmids (Leu33 cells); 35 cells transfected with αIIbmVenus and β3Leu33 plasmids (Leu33 donor control); and 35 cells transfected with αIIbmVenus and β3Pro33 plasmids (Pro33 donor control).

According to the D'Agostino & Pearson omnibus normality test (D'Agostino and Pearson, 1973) performed, the data was not normally distributed. Therefore the statistical analysis was done based on the Mann-Whitney test (Wilcoxon, 1945) that assumes not normally distributed data.

FRET efficiency data obtained with the Leu33 donor control cells and Pro33 donor control cells were close to zero and did not differ significantly between the two groups of cells. Excitingly, FRET-APB efficiency between mVenus and mCherry in cells transfected with αIIbmVenus and β3Leu33mCherry (n= 91, median= 18.88, Interquartile range, IQR= 3.39) was significantly higher (P<0.0001, Mann-Whitney test) than in cells transfected with αIIbmVenus and β3Pro33mCherry (n= 88, median= 15.54, IQR= 3.88) (Figure 16).

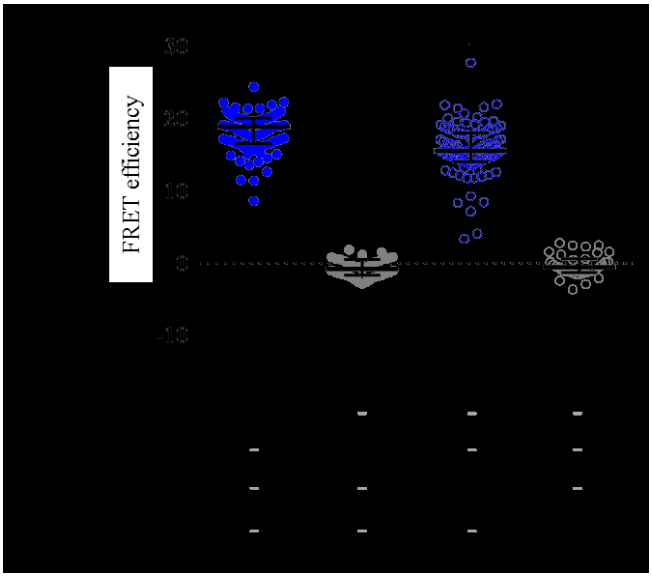

Figure 16 - FRET efficiency in cells transfected with different plasmids combinations: cells transfected with αIIbmVenus and β3Leu33mCherry plasmids (Leu33 cells), and respective control lacking the fluorescence acceptor mCherry; cells transfected with αIIbmVenus and β3Pro33mCherry plasmids (Pro33 cells), and respective control lacking the fluorescence acceptor mCherry. The P values presented result from statistical comparison done with non-parametric Mann-Whitney test. The lines correspond to the median with IQR.

Of note, the cells analysed were randomly chosen and we later observed that it resulted in the inclusion of cells considerably different in their mVenus and mCherry fluorescence intensities. To investigate a possible impact of this fact in the results, we compared in each individual cell the intensity of each of the two fluorescent proteins with the calculated efficiency of FRET-APB (Figure 17). The slope of the linear regression did not deviate

significantly from the zero value (linear regression was close to a horizontal line) indicating no general correlation/dependency from the FRET-APC efficiency on the intensity of mVenus nor mCherry.

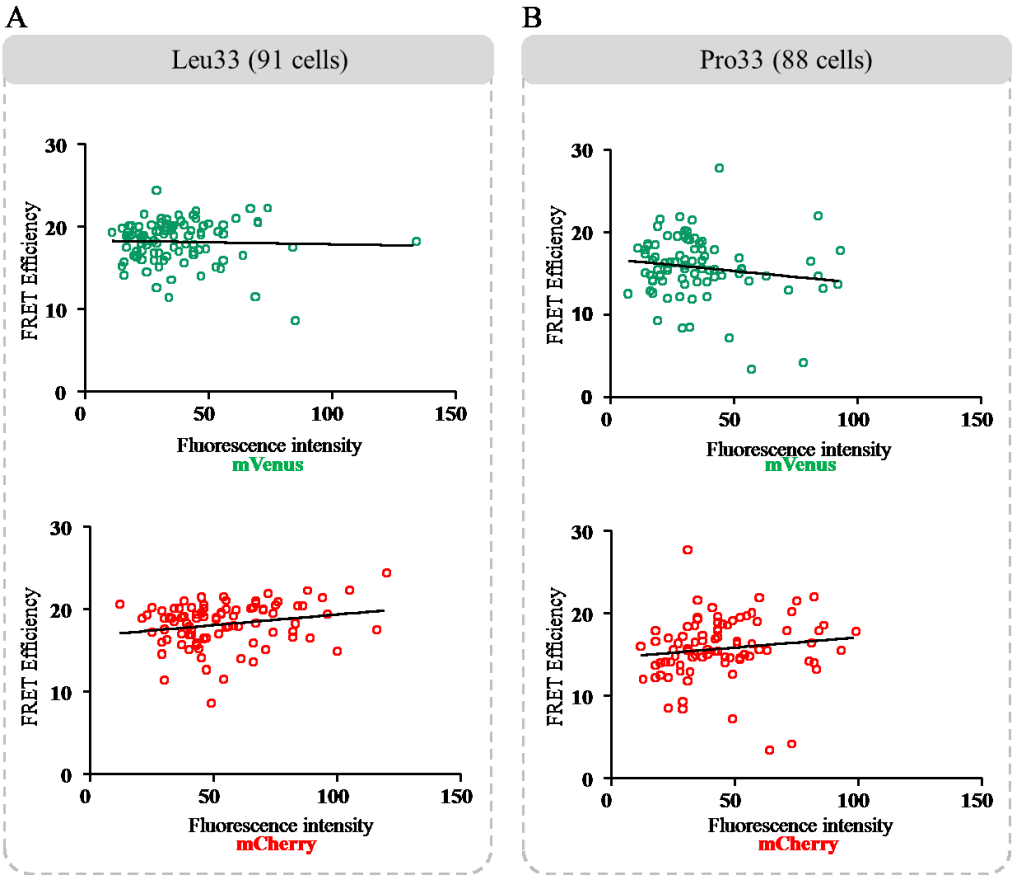

Figure 17 – Correlation between FRET efficiency and fluorescence intensity of mVenus and mCherry in individual cells. **(A)** Cells transfected with αIIbmVenus and β3Leu33mCherry plasmids (Leu33 cells) mVenus fluorescence intensity varied between 11 and 134 (median= 33), and mCherry varied between 12 and 120 (median= 49). **(B)** Cells transfected with αIIbmVenus and β3Pro33mCherry plasmids (Pro33 cells). mVenus fluorescence intensity varied between 7 and 93 (median= 31), and mCherry varied between 12 and 99 (median= 42.5).

In addition, comparing the intensities of both mVenus and mCherry in each cell, we observed that the relative intensities of the two fluorescent proteins differed considerably: (i) between the different cells as reflected by the very low R^2 values of the linear regressions; (ii) and within each cell as the slopes of the linear regressions were considerably distant from an optimal situation with slope equal to 1 where both energy donor (mVenus) and acceptor (mCherry) would be equally abundant (Figure 18).

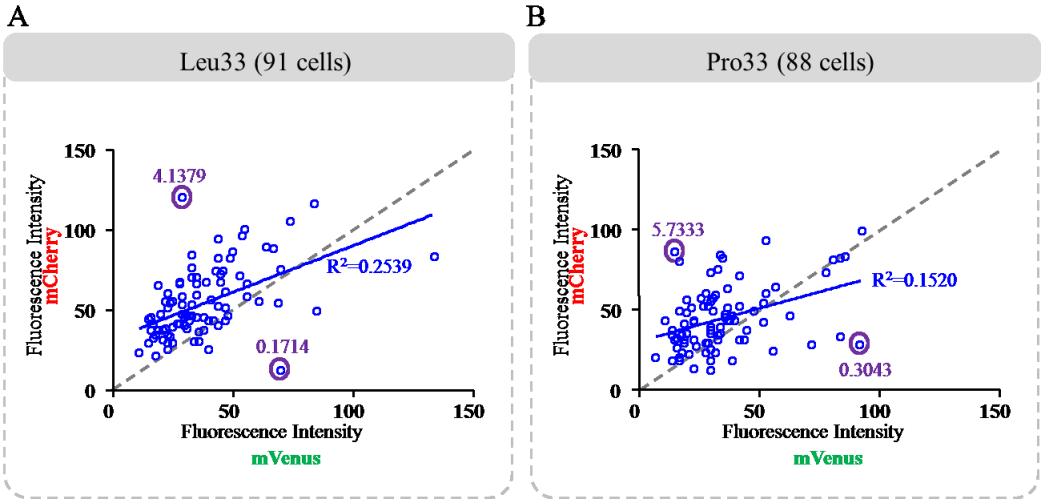

Figure 18 - Comparison between the intensities of mVenus and mCherry in each individual cell. **(A)** Cells transfected with αIIbmVenus and β3Leu33mCherry plasmids (Leu33 cells). The mCherry/mVenus ratio before bleaching varied between 0.1714 and 4.1379. **(B)** Cells transfected with αIIbmVenus and β3Pro33mCherry plasmids (Pro33 cells). The mCherry/mVenus ratio before bleaching varied between 0.3043 and 5.7333.

Moreover, we observed a significant difference between the intensities of mCherry between Leu33 and Pro33 cells (P=0.0022, Mann-Whitney test) (Figure 19).

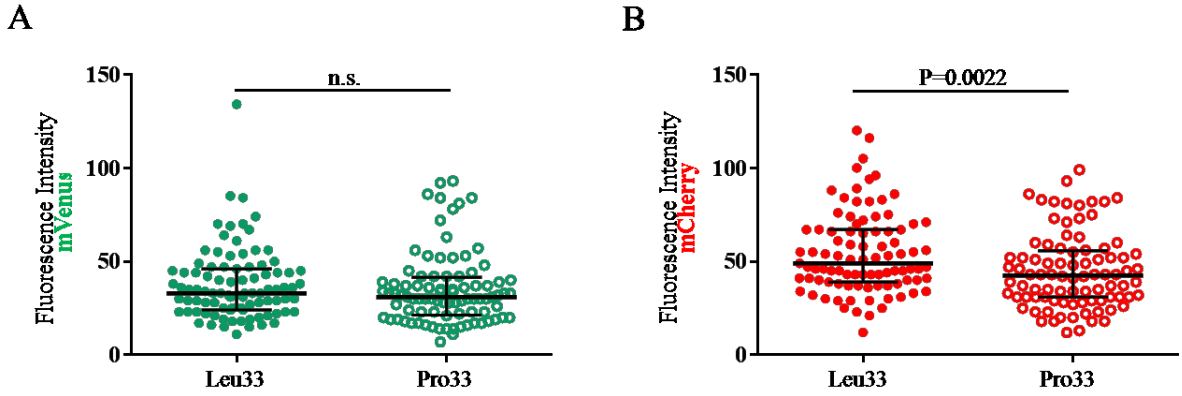

Figure 19 - Fluorescence intensities in the cells transfected with αIIbmVenus and β3Leu33mCherry plasmids (Leu33) and with αIIbmVenus and β3Pro33mCherry plasmids (Pro33). **(A)** Intensity of mVenus. **(B)** Intensity of mCherry. The P values presented result from statistical comparison done with non-parametric Mann-Whitney test. The lines correspond to the median with IQR.

Collectively, these results indicated some heterogeneity among the cells chosen randomly for analysis which could have an impact in the interpretation of results. This led us to apply some filters based on the relative intensities of mVenus and mCherry (in the pre-bleaching condition) in order to select a more homogeneous subset of cells for analysis. For

each cell, the relative intensity of mCherry to mVenus was determined and results were filtered with three filters allowing 30%, 20% and 10% of difference in the intensity of the two fluorophores. The idea was to gradually decrease the difference allowed between the intensities of the mVenus and mCherry within each cell. Increasing the stringency of the filter used resulted in a significant decrease in the number of cells available for analysis (Table 2).

Table 2 – Number of cells available for analysis after applying filters. These filters were based on the difference in the fluorescence intensities of mcherry and mVenus in the pre-bleaching condition.

	Filters			
	No Filter	30%	20%	10%
Number of Leu33 cells	91	26	21	12
Number of Pro33 cells	88	40	30	16

Comparing mVenus and mCherry fluorescences within the populations resulting after applying the filters we could observe that the R^2 values of the linear regression got gradually closer to 1, and the slope of the linear regression got gradually closer to the one of the optimal situation indicating a decrease in the the disparity of the populations (Figure 20).

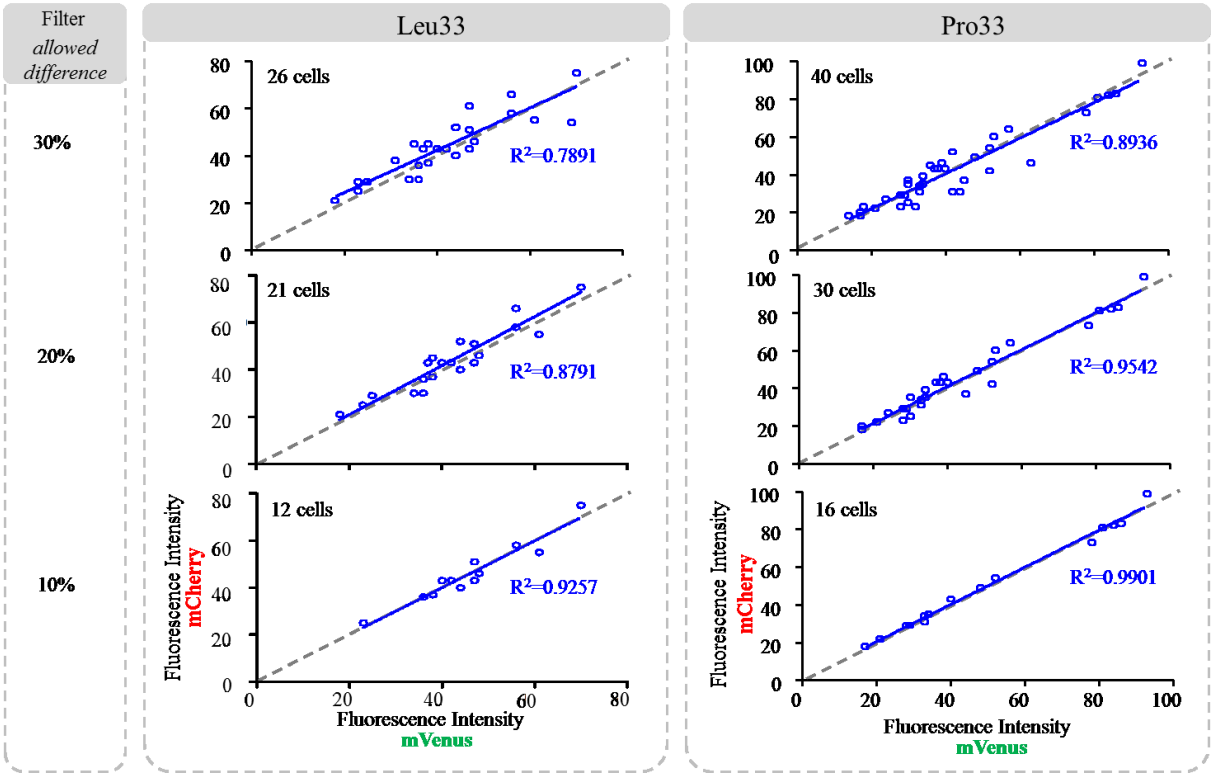

Figure 20 - Distribution of fluorescence intensities of mVenus in relation with mCherry in cells transfected with αIIbmVenus and β3Leu33mCherry plasmids (Leu33) and with αIIbmVenus and β3Pro33mCherry plasmids

(Pro33), applying filters of 30%, 20% and 10% of difference in the ratio fluorescence intensity of mCherry/fluorescence intensity of mVenus in the pre-bleaching condition, with R^2 values of linear regression.

Importantly, within each new subset of cells created upon filtering, there was no statistically significant difference in the intensity of mVenus nor mCherry between the two experimental conditions (αIIbmVenus + β3Leu33mCherry and αIIbmVenus + β3Pro33mCherry) (Figure 21).

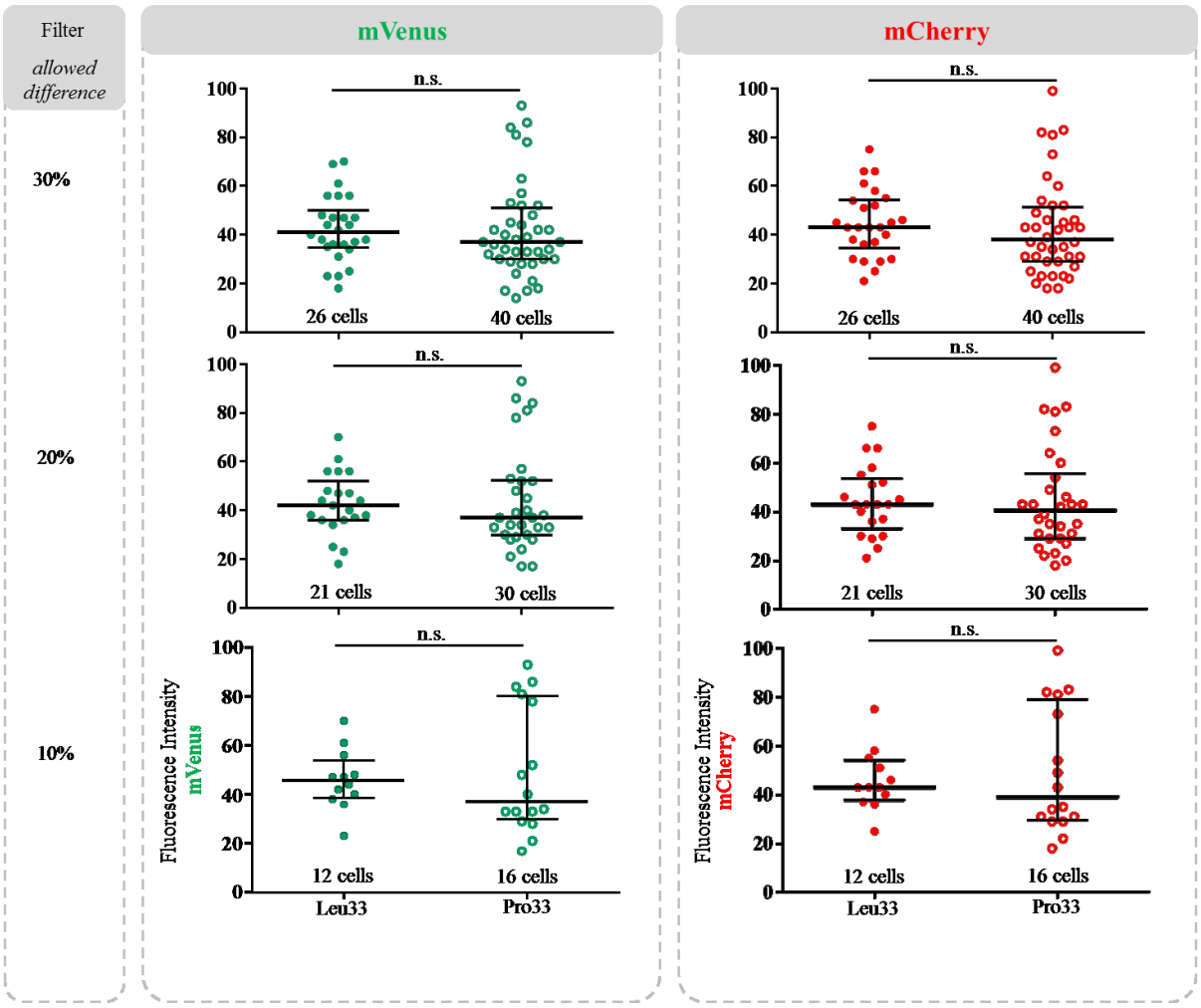

Figure 21 - Comparison of fluorescence intensities of mVenus and mCherry for categorized cells transfected with αIIbmVenus and β3Leu33mCherry plasmids (Leu33) and with αIIbmVenus and β3Pro33mCherry plasmids (Pro33). The P values presented result from statistical comparison done with non-parametric Mann-Whitney test. The lines correspond to the median with IQR.

Notably, despite the gradually lower number of cells available for analysis, the efficiency of FRET-APB between the two subunits of the αIIbβ3 receptor in its resting state

was always significantly lower (Mann-Whitney test) in the Pro33 cells compared to the Leu33 cells (Figure 22).

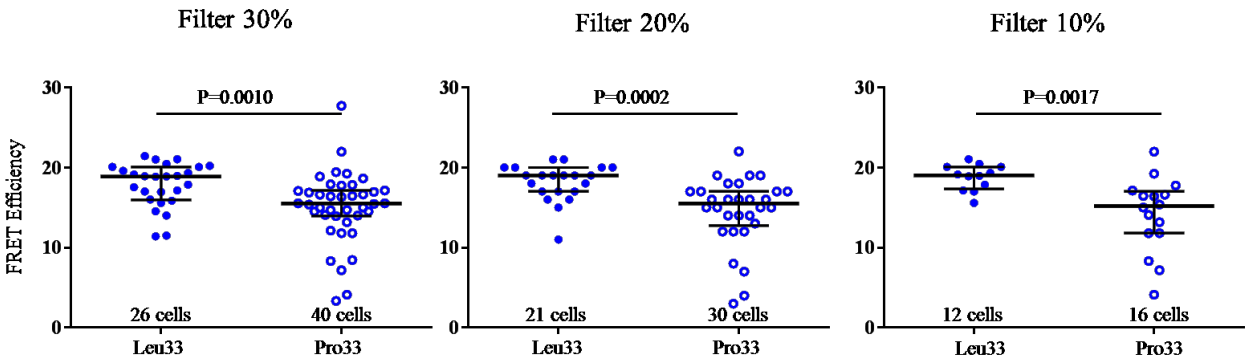

Figure 22 - Results of FRET efficiency calculated for individual cells transfected with αIIbmVenus and β3Leu33mCherry plasmids (Leu33) and transfected with αIIbmVenus and β3Pro33mCherry plasmids (Pro33), after classification in three different groups of filtered cells . The P values presented result from statistical comparison done with non-parametric Mann-Whitney test. The lines correspond to the median with IQR values.

Collectively, the results of FRET efficiency obtained in all filtered groups of cells (Figure 22), support and strength the initial observation done in the larger collective of randomly chosen cells (Figure 16). The significant differences in the efficiency of FRET-APB detected between the Leu33 and Pro33 isoforms, evidence a structural difference in the receptor induced by the Leu33Pro substitution and indicate that in the resting state there is a higher spatial separation between the cytoplasmic tails of the two subunits on the Pro33 variant than on the Leu33 variant.

4.3.2 – Force involved in the interaction of both variants of αIIbβ with fibrinogen

We used Single Cell Force Spectroscopy (SCFS) to investigate if the Leu33Pro polymorphism could also have an effect in the strength of integrin receptor binding to fibrinogen, one of its natural ligands. With this technique, individual cells adherent to a cantilever were multiple times brought in contact and retracted from a surface coated with fibrinogen (Figure 23).

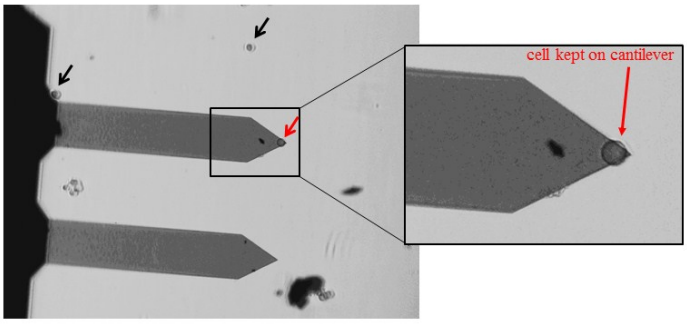

Figure 23 – Phase contrast image of a cell attached to the tip of a Poly-L-Lysin coated cantilever (red arrow) (20x Objective). In the image it is possible to see that other cells were in close proximity (black arrows).

During each retraction, a force-distance-curve is determined and from these curves, five different parameters were measured: maximal adhesion force, adhesion energy, single rupture force, tether force, and tether length (Figure 24A). In typical curves of experimental conditions (Figure 24A and B), at beginning of retraction, we observed that vertical deflection of cantilever dropped abruptly achieving an absolute minimum corresponding to the Maximal Adhesion Force between cell and substrate (Figure 24A-1). After this absolute minimum deflection, continuing of cantilever retraction has resulted in multiple local minimum values of deflection caused by disruption of individual bonds, and from which it can be determined the Single Rupture Force (Single Rupture Force, Figure 24A-3). Before the rupture events, the force decreases and consequently there was a decrease in the curve. Using the integral of the curve encompassing the maximum and all the relative minimums we could calculate the work necessary to detach the cell from the substrate (called Adhesion Energy) (Figure 24A-2). In the final part of the retraction, we could calculate the force of membrane tethers, thin membrane nanotubes involved in cell-cell adhesion and communication (Sun et al., 2005). Tethers are characteristics of membrane properties and membrane-cytoskeleton attachement and are represented in the force-distance curve by a plateau of constant force at larger retraction distances (Figure 24A-4) (Sun et al., 2005). In the negative control conditions involving cells transfected with the vector-only control (Figure 24C) and cells expressing the complete receptor but previously incubated with Abciximab, an antibody that blocks αIIbβ3 binding to fibrinogen (Figure 24D), the force-distance-curves obtained during retraction differed significantly. The absolute minimum deflection values (Maximal Adhesion Force) were in the range of -0.1 to -0.2 ρN and the curves usually lacked further discrete unbinding steps indicating no specific binding of cells to the fibrinogen coated surface.

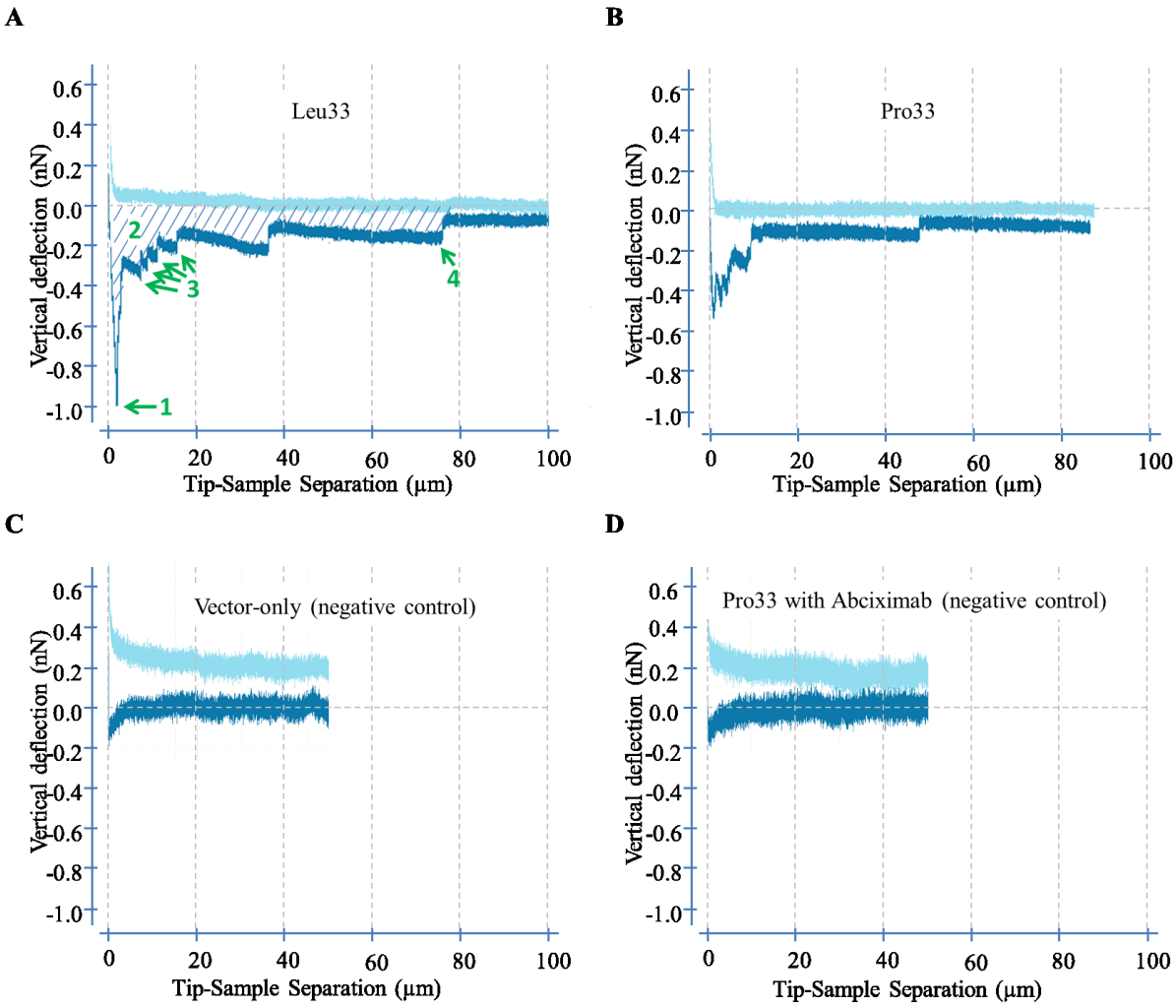

Figure 24 – Representative AFM force-distance-curves obtained for cells transfected with: **(A)** αIIbmVenus and β3Leu33mCherry plasmids (Leu33) (1-Maximal Adhesion Force, 2- Adhesion Energy, 3- Single Rupture Force, 4- Tether Force and Tether Length); **(B)** αIIbmVenus and β3Pro33mCherry plasmids (Pro33); **(C)** vector-only control plasmid; **(D)** Pro33 incubated previously with 10 µg/ml of Abciximab.

SCFS analyses could be performed and force-distance-curves could be determined for a total of 24 single-cells: 9 cells transfected with αIIbmVenus and β3Leu33mCherry plasmids (Leu33, 268 curves), 9 cells transfected with αIIbmVenus and β3Pro33mCherry plasmids (Pro33, 269 curves), 2 cells transfected with the empty vector (59 curves), 2 cells transfected with αIIbmVenus and β3Leu33mCherry plasmids incubated with Abciximab (Leu33, 58 curves), and 2 cells transfected with αIIbmVenus and β3Pro33mCherry plasmids incubated with Abciximab (Pro33, 61 curves). The curves were used to calculate five different parameters.

According to D'Agostino & Pearson omnibus normality test (D'Agostino and Pearson, 1973) performed, the data was not normally distributed. Therefore the statistical analysis was done based on the Mann-Whitney test (Wilcoxon, 1945).

Notably, the collective of values of maximal adhesion force in Pro33 cells (n cells= 9, n measurements= 269, median= 475 ρN, IQR= 787 ρN) was significantly higher (P<0.0001, Mann-Whitney test) than in Leu33 cells (n cells= 9, n measurements= 268, median= 359 ρN, IQR= 317.5 ρN) (Figure 25A). Importantly, considering separately the three different contact times (5, 7.5 and 10s), similarly significant differences could still be detected in the maximal adhesion force of Pro33 cells and Leu33 cells (Figure 25B).

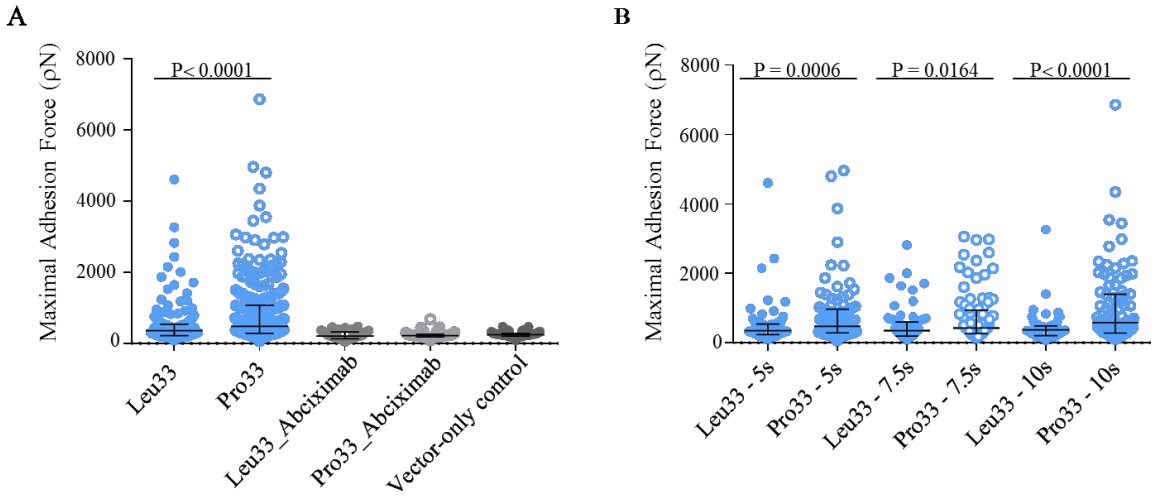

Figure 25 – **(A)** Maximal Adhesion Force calculated from all measurements for all contact times done for cells transfected with αIIbmVenus and β3Leu33mCherry plasmids (Leu33) (n= 268 from 9 cells), with αIIbmVenus and β3Pro33mCherry plasmids (Pro33) (n= 269 from 9 cells), with αIIbmVenus and β3Leu33mCherry plasmids and incubated with Abciximab (Leu33_Abciximab) (n= 58 from 2 cells), with αIIbmVenus and β3Pro33mCherry plasmids and incubated with Abciximab (Pro33_Abciximab) (n= 61 from 2 cells), and with the vector-only control (n= 59 from 2 cells). **(B)** Same data as in *(A)* but considering the different contact times. For Leu33 cells: n= 95 for 5s, n= 84 for 7.5s, n= 87 for 10s. For Pro33 cells: n= 87 for 5s, n= 87 for 7.5s, and n= 89 for 10s. The P values presented result from statistical comparison done with non-parametric Mann-Whitney test. The lines correspond to the median with IQR.

Similarly, Adhesion Energy of Pro33 cells (n=263, median= 4.54 fJ, IQR= 5.65 fJ) was significantly higher P<0.0001, Mann-Whitney test) than the Adhesion Energy of Leu33 cells (n=256, median= 2.49 fJ, IQR= 4.41 fJ) (Figure 26A).

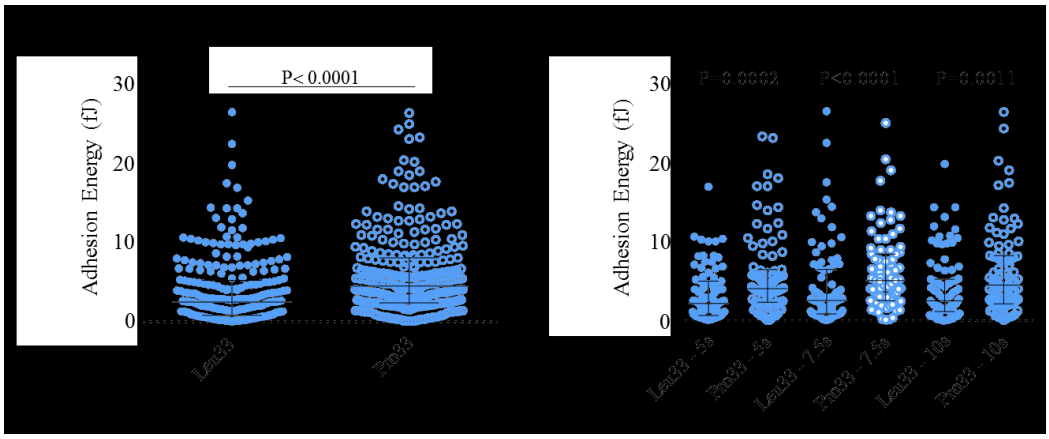

Figure 26 – **(A)** Adhesion Energy calculated from all measurements for all contact times done for cells transfected with αIIbmVenus and β3Leu33mCherry plasmids (Leu33) (n= 256 from 9 cells) or with αIIbmVenus and β3Pro33mCherry plasmids (Pro33) (n= 263 from 9 cells). **(B)** Same data as in *(A)* but considering the different contact times. For Leu33 cells: n= 95 for 5s, n= 84 for 7.5s, n= 87 for 10s. For Pro33 cells: n= 87 for 5s, n= 87 for 7.5s, and n= 89 for 10s. The P values presented result from statistical comparison done with non-parametric Mann-Whitney test. The lines correspond to the median with IQR.

The next parameter analyzed using the SCFS assay was the Single Rupture Force, which corresponded to the smallest detectable unbinding force units involved between a single integrin molecule and a single fibrinogen molecule (Figure 28). Also, the Single Rupture Force data obtained for Pro33 cells (n=1008, median= 58.3 ρN, IQR= 39.2 ρN) was significantly higher (P<0.0001, Mann-Whitney test) than single rupture force of Leu33 (n=766, median= 48.2 ρN, IQR= 24.3 ρN) (Figure 27A). This indicates that the energy involved in the disruption of single bonds is higher in the case of the β3Pro33 variant. As well as for the previous two parameters analyzed this difference was also significant considering each contact time separately (Figure 27B).

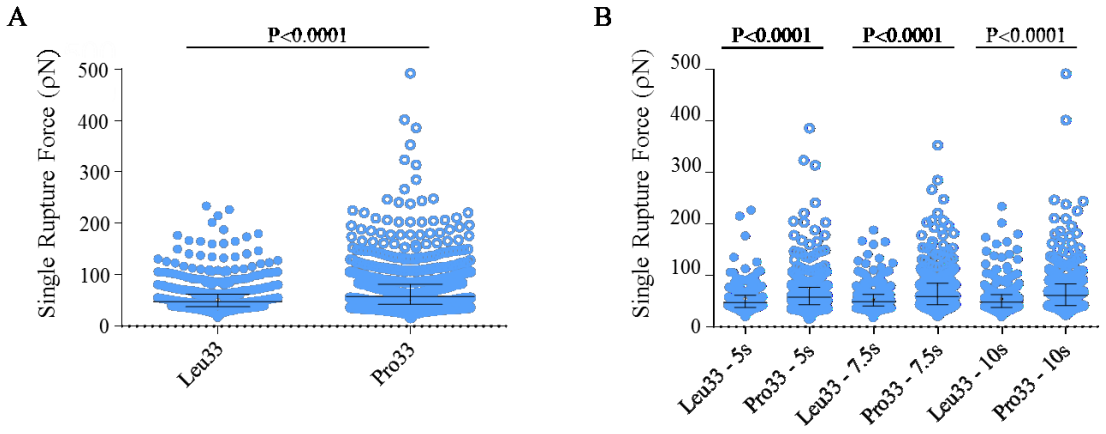

Figure 27 – **(A)** Single Rupture Force calculated from all measurements for all contact times done for cells transfected with αIIbmVenus and β3Leu33mCherry plasmids (Leu33) (n= 766 from 9 cells) or with αIIbmVenus and β3Pro33mCherry plasmids (Pro33) (n= 1008 from 9 cells). **(B)** Same data as in *(A)* but considering the different contact times. For Leu33 cells: n= 229 for 5s, n= 266 for 7.5s, and n= 271 for 10s. For Pro33 cells: n= 352 for 5s, n= 324 for 7.5s, n= 332 for 10s. The P values presented result from statistical comparison done with non-parametric Mann-Whitney test. The lines correspond to the median with IQR values.

In addition to the parameters directly correlated with the binding of integrin receptor to fibrinogen the Tether Force in cells transfected with αIIbmVenus and β3Pro33mCherry plasmids (n= 370, median= 59.75 ρN, IQR= 36.93 ρN) was significantly higher (tether force P<0.0001, Mann-Whitney test) than in cells transfected with αIIbmVenus and β3Leu33mCherry plasmids (n= 428, median= 47.05 ρN, IQR= 19.99 ρN). A statistically significant difference was also found between cells transfected with αIIbmVenus and β3Pro33 plasmids and cells transfected with αIIbmVenus and β3Leu33 plasmids when the different time contact points were considered separately (Figure 28B).

Plateau Lenght was also significantly higher (P= 0.0007, Mann-Whitney test) in cells transfected with αIIbmVenus and β3Pro33mCherry plasmids (n= 279, median= 10.72 μm, IQR= 19.79 μm) than in cells transfected with αIIbmVenus and β3Leu33mCherry plasmids (n= 360, median= 7.27 μm, IQR= 16.82 μm) (Figure 28A and C). With the exception of the Plateau Length in the measurements at 10s, a statistically significant difference was also found between cells transfected with αIIbmVenus and β3Pro33 plasmids and cells transfected with αIIbmVenus and β3Leu33 plasmids when the different time contact points were considered separately (Figure 28D).

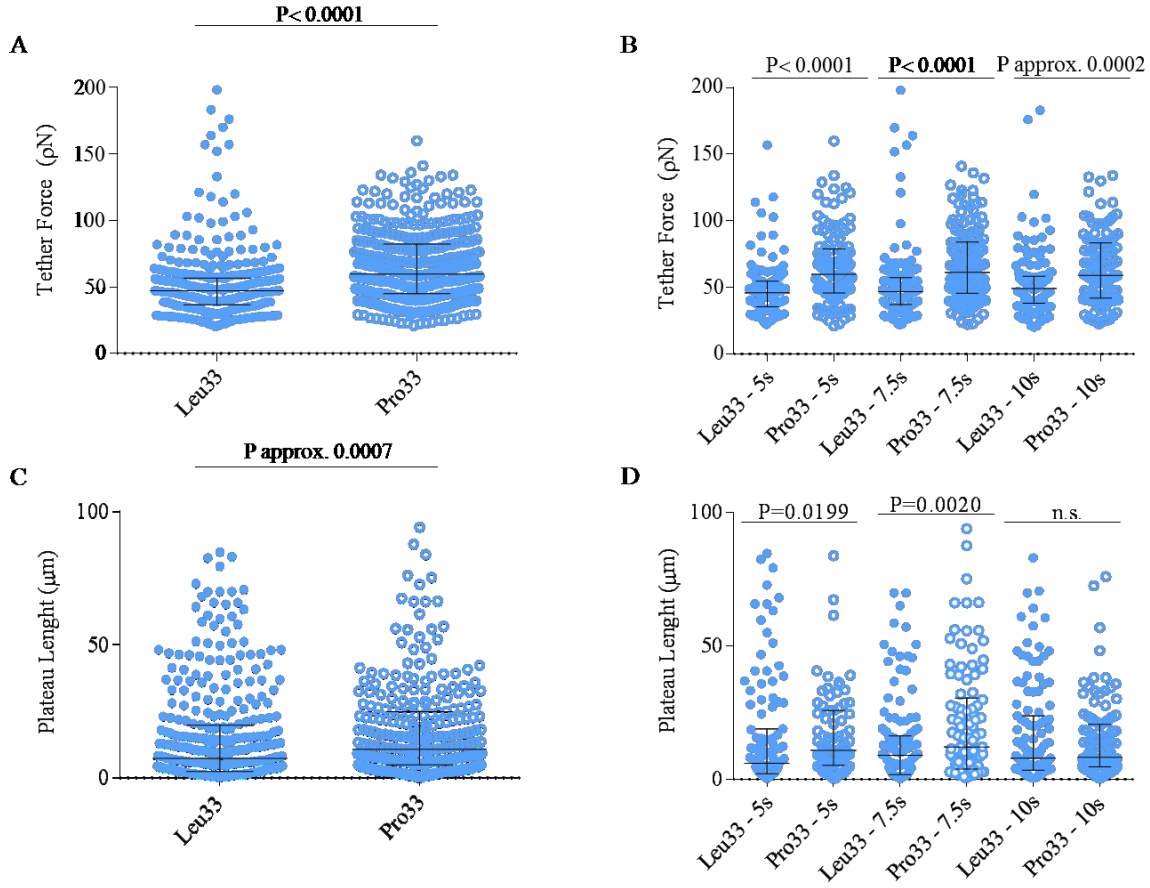

Figure 28 – **(A)** Tether force calculated from all measurements for all contact times done for cells transfected with αIIbmVenus and β3Leu33mCherry plasmids (Leu33) (n=428 from 9 cells) or with αIIbmVenus and β3Pro33mCherry plasmids (Pro33) (n=370, Cell from 9 cells). **(B)** Same data as in *(A)* but considering the different contact times. For Leu33 cells: n=138 for 5s, n=156, for 7.5s, and n=134 for 10s. For Pro33 cells: n=119 for 5s, n=139 n=9 for 7.5s, and n=112 for 10s. **(C)** Plateau Lenght calculated from all measurements for all contact times done for the same cells as in *(A)*. For Leu33 cells: n=360 from 9 cells. For Pro33 cells: n=279 from 9 cells. **(D)** Same data as in (C) but considering the different contact times. For Leu33 cells: n=111 for 5s, n=141 for 7.5s, and n=125 for 10s. For Pro33 cells: n=79 for 5s, n=98 for 7.5s, and n=102 for 10s. The P values presented result from statistical comparison done with non-parametric Mann-Whitney test. The lines correspond to the median with IQR.

Collectively, the results of all five parameters analyzed indicate that cells expressing the receptor with the β3Pro33 variant adhere more strongly to fibrinogen coated surface than cells expressing the β3Leu33 variant.

5 – DISCUSSION

The knowledge about platelets increased substancially in the last years and now platelets are acknowledged as cells involved on multidisciplinary functions. Despite all the newly uncovered roles of platelets, the most explored functions are still those related with Hemostasis and Thrombosis. In case of blood vessel damage, platelets are key elements keeping blood within the vessel through thrombus formation, as well as avoiding thrombosis by controlling the thrombus growth. For these physiological functions that rely on platelet aggregation, the integrin receptor αIIbβ3 has a pivotal role.

The integrin αIIbβ3 carries the human platelet antigen HPA-1 (Kunicki and Newman, 1992) which is polymorphic. Consequently individuals can be homozygotic for the wild type (HPA-1a), heterozygotic (HPA-1ab) or homozygotic for the polymorphic form (HPA-1b). The HPA-1b variant results from a single amino acid exchange in the β3 subunit of the integrin receptor αIIbβ3 – Leu33Pro – and leads to a conformation change in the extracellular domain (Valentin and Newman, 1994). Different clinical epidemiologic studies have shown that HPA-1b is associated with an increased risk of coronary disease (Burr et al., 2003), and HPA-1b men under forty years old were associated with three-fold and four-fold risk of ischaemic cardiovascular disease and myocardial infarction (Bojesen et al., 2003). Functional studies have grounded the idea that HPA-1b platelets have a prothrombotic character (Vijayan et al., 2000; Vijayan et al., 2003), and their authors have suggested that the conformation change in the β3 extracellular domain might affect receptor interaction with its ligand and have consequences for platelet function (Vijayan et al., 2000). Despite the suggestion, no concrete evidences for that have been presented so far.

5.1 – Experimental model for studies with the integrin αIIbβ3

Platelets are anucleated and therefore they are not amenable to genetic manipulation. This creates major obstacles for studies requiring plasmid-driven expression of proteins. Aiming the expression of the αIIb and β3 subunits for functional and structural studies we have chosen the HEK293 cell line, from human embryonic kidney origin, which do not express the αIIbβ3 receptor endogenously (Bodary and McLean, 1990). These cells have been already used by other authors to study adhesive properties of the HPA-1b receptor under static (Vijayan et al., 2000), and shear stress conditions (Vijayan et al., 2003), and in the

characterization of the different conformations of the αIIbβ3 receptor (Abraham et al., 1997), supporting the suitability of HEK293 cells for studies involving αIIbβ3.

Transient transfection with αIIbmVenus and β3Leu33mCherry plasmids and αIIbmVenus and β3Pro33mCherry plasmids resulted in the presence of detectable mVenus and mCherry in the membrane region, where the functional receptor is expected (Figure 12). mVenus and mCherry fluorescences could also be detected in intracellular perinuclear regions likely to be the endoplasmic reticulum and Golgi complex. After formation at the endoplasmic reticulum, the precursor form of the complex (Pro-IIb–IIIa) is transported to the Golgi complex for maturation and once mature, it is transported to the cell surface (Calvete et al., 1989; Duperray et al., 1987; Newman et al., 1985). In this way the fluorescence observed in intracellular regions is consistent with the formation of Pro-IIb-IIIa in the endoplasmic reticulum and the presence of Pro-IIb-IIIa on the Golgi complex before maturation and transport into the cell membrane.

Importantly, beyond the detection of both αIIb and β3 subunits through the fluorescence of mVenus and mCherry fused to their tails, it was also possible to detect the αIIbβ3 fuctional receptor at cell surface by flow cytometry (Figure 13) in approximately 50% of the cells using anti-CD41, a αIIbβ3 complex-specific antibody (O'Toole et al., 1989) which binds only the functional receptor. The CD41 positivity of 50% was not a limitant factor for this work once that the subsequent FRET and SCFS analyses were performed at a single-cell level, and double marker-positive cells could still be easely selected. Interestingly, we noticed a light unspecificity of this anti-CD41 antibody when both subunits (αIIbmVenus and β3Leu33mCherry or β3Pro33mCherry) were expressed (percentage of CD41pos cells that were negative for mVenus/mCherry) (Figures 13A1, A3, B1, B3, D1-3). It was also observed that the expression of mVenus was much higher (Figure 13D1) than the expression of mCherry when the cells were transfected with just one plasmid (Figures 13D2, D3) but very approximate when cells were transfected with two plasmids (Figures 13A1, A3 and B1, B3).

Notably, the expression levels achieved of the αIIbβ3Leu33 and αIIbβ3Pro33 receptors in the individual experiments were comparable. Differences in CD41-APC Mean Fluorescence Intensity values between αIIbβ3Leu33 and αIIbβ3Pro33 did not differ more than 10% (Figure 14), in conformity with recommendations of previous functional studies involving αIIbβ3 (Vijayan et al., 2000).

5.2 – Leu33Pro exchange imposes modifications in the global structure of the αIIbβ3 receptor

The impact of the Leu33Pro substitution in the structure of the β3 subunit and consequently in the αIIbβ3 receptor was initially investigated using FRET-APB technology. This technique allows inferring the distance between two fluorescent proteins by measuring the energy transfer occurring between them. In the present work, the two fluorescent proteins were mVenus (energy donor) and mCherry (energy acceptor) and were fused to the cytoplasmic tails of αIIb and β3 subunits, respectively. Consequently, energy transfer measured between mVenus and mCherry can be taken as an indirect measurement of the distance between the cytoplasmic tails of the two integrin subunits. Notably, in the presence of the αIIbβ3Pro33 variant, the efficiency of energy transfer was significantly reduced compared to the αIIbβ3Leu33variant. This observation indicates that in receptor's resting state exist a higher physical separation between the cytoplasmic tails of αIIb and β3 when αIIbβ3Pro33is present. Notably, this significant difference in energy transfer was valid in the whole collective of 91 αIIbβ3Leu33and 88 αIIbβ3Pro33cells analyzed (Figure 16) as well as in all different subsets presenting a more homogeneous relative expression of the two subunits (Figure 22).

Interestingly, our results on the cytoplasmic tail are in line with results of complementary structural studies by all-atom molecular dynamics (MD) simulations done at the Institute for Pharmaceutical and Medicinal Chemistry, University of Düsseldorf (group of Prof. Dr. Holger Gohlke, by MSc. Giulia Pagani) (Appendix 3). These MD simulations based on the X-ray structure of the αIIbβ3 extracellular fraction (Zhu et al., 2008), revealed that Leu33Pro substitution alters the structural dynamics of the integrin to a more unbent and splayed state. It could be calculated that Leu33Pro (i) reduces number of contacts between amino acids of the AB loop (which includes position 33) and residues from the adjacent EGF-1 and EGF-2 domains (Appendix 3 – Figure 5A) which leds to a less compact interface between the PSI domain and EGF-1 / EGF-2 domains; (ii) reduces the number of hydrogen bonds across the interface and within the EGF-1 / EGF-2 domains (Appendix 3 - Figure S6); (iii) and increases the radius of gyration of the entire ectodomain (Appendix 3 - Table S5). In addition the simulations could also show that upon the Leu33Pro exchange there is a bigger distance between the centre of mass (COM) of βA and βTD domains of β3 subunit, between the COM of Propeller and Calf-2 domains of the αIIb subunit, and also between the COM of β-tail domain of β subunit and the Calf-2 domain of the αIIb subunit (Appendix 3 - Figure 2).

Collectively, the MD simulations done for the extracellular domains and the spatial separation between the cytoplasmic tails inferred by the FRET experiments, suggest that the αIIbβ3Leu33variant shows a more compact, stable and bent geometry in which the interplay between the different domains is favoured, while the αIIbβ3Pro33variant shows a more flexible, stretched structure with higher spatial separation between α and β subunits (Figure 29).

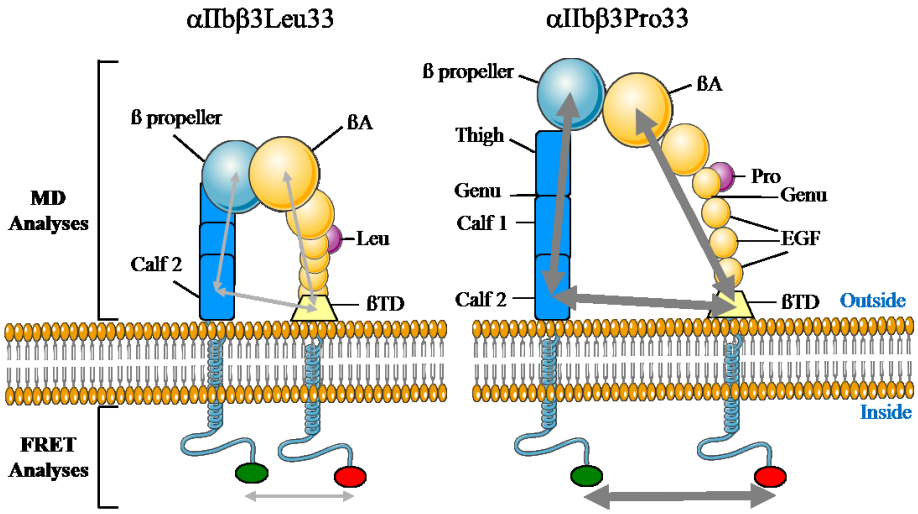

Figure 29 – Schematic representation of the spatial separation between domains measured by MD and by FRET in αIIbβ3Leu33 cells and in αIIbβ3Pro33 cells.

The Leu33Pro shifts the dynamic conformational equilibrium of αIIbβ3 integrin towards a more open, extended state, with a larger splaying of the legs. This state resembles more the active state, suggesting that the receptor can more easily reach its full activation, by that promoting the prothrombotic phenotype of Pro33 platelets (Appendix 3). As the consequences of the Leu33Pro substitution can be detected in regions (cytoplasmic tails) far away from the polymorphic site (in the ectodomain) the influence of the Leu33Pro exchange is allosteric.

Our results, obtained with the αIIbβ3 in its resting/unbound state, seem to contradict results from a previous study suggesting that only upon ligand binding would occur a widening of the angle between αIIb and β3Pro33 legs, favouring leg extension and separation (Xiao et al., 2004). In our present work, the αIIbβ3 Pro33 isoform appears to be closer from the active state even without the presence of a ligand.

A previous study by molecular dynamics simulations has already associated the Leu33Pro exchange with increased flexibility and mobility of the three domains constituting the β3Pro33 knee (PSI; I-EGF-1 and I-EGF-2) (Jallu et al., 2012). Interestingly, the study

suggested that, despite occurring in the PSI domain, the Leu33Pro exchange would not alter the local structure of that domain due to a very rigid structure formed by the residues 33 to 35. The physical constraints caused by the Pro33 residue would be counterbalanced by structural alterations within the rest of the PSI, the I-EGF-1, and the I-EGF-2 domains and in this way the Leu33Pro exchange was considered as responsible for modifying the structural equilibrium of the three domains collectively. However, this study has considered only the 3D model of β3Pro33 subunit and, ignoring the αIIb subunit, it could not report on the effect of Pro33 in the global structure of the receptor.

To our knowledge, the calculations done for the structure of the ectodomain of the receptor considering the two subunits, and the experimental evidences collected for the different relative position of the intracellular part of the αIIbβ3 receptor, constitute the most comprehensive structural analysis of this receptor.

As referred in the materials and methods section, the choice of the single cells to be analysed by FRET-APB was based on microscopic images, taking in consideration their apparent morphological integrity and their positivity for both fluorophores (mVenus and mCherry). Since the beginning of the experiments it was clear that the fluorescence intensities of both fluorophores varied considerably in each cell and between cells, a potential problem considering previous studies recommending the choice of the cells with comparable intensities for their fused fluorescence proteins (Vielreicher et al., 2007). When performing the experiments, choosing each single cell based on their fluorescence intensity would have been too time-consuming and it would have likely resulted on a very lower number of cells analysed. In the present work, we have selected the cells retrospectively. Attempting at a more homogeneous population of cells, it was possible to identify and select cells in which the intensities of both fluorophores did not differ more than 30%, 20%, and even 10% (Figure 21), and as expected that caused a strong reduction in the number of cells available for analysis. Notably, for all different subpopulations of cells, FRET efficiency proved to be significantly lower for the Pro33 isoform which strength our observations. The heterogeneity of the cells concerning the relative intensities of both fluorophores was likely associated with differences in success rate of transfection inherent to the transient transfection strategy. To minimize that problem, it was attempted the generation of HEK293-derived cells lines stably expressing the integrin receptor. As the plasmids contained genes coding for antibiotic resistance, integration of the plasmids in the cellular DNA was promoted by supplementing

the culture medium with antibiotic. However, it was not possible as cells systematically died upon introduction of antibiotic.

5.3 – Leu33Pro exchange increases the strength of the interaction with immobilized fibrinogen

In order to investigate if the structural alterations detected by FRET would have an impact in function of the receptor, it was used single cell force spectroscopy (SCFS). In this technique, a cell attached to a cantilever is allowed to contact with a surface for a short period of time and, subsequently, as the cantilever is pulled to retract, the cantilever deflections caused by adhesion of cells to the surface are measured. The profile of the cantilever deflections during retraction allows the measurement of the energy and strength of the interaction between cell and surface (Figure 24). In the present work, SCFS was used to investigate the impact of the Leu33Pro polymorphism on the forces involved on the adhesion of transfected cells to immobilized fibrinogen. The multiple parameters studied by SCFS indicate that the Pro33 isoform provides cells with increased capacity to bind immobilized fibrinogen.

Cells expressing the Pro33 variant showed a higher Maximal Adhesion Force (Figure 25) and higher Adhesion Energy (Figure 26) than cells expressing the Leu33 variant. The Maximal Adhesion Force is the maximal strength required to separate the cantilever-bound cell from the target surface (Helenius et al., 2008). In its turn Adhesion Energy is calculated by the integral of the curve resulting from the force exerted on the cell retraction over the whole trajectory of the cell until the detachment of the last αIIbβ3-fibrinogen bond. These two parameters allow inferring the overall stability of the binding between cell and fibrinogen and in that sense the results indicate that cells expressing the Pro33 variant bind more strongly and stably to immobilized fibrinogen than cells expressing the Leu33 variant. The Maximal Adhesion Force and Adhesion Energy result from the strength of each receptor-ligand bond (affinity) but it is also influenced by the total number of bonds (avidity) (Carman and Springer, 2003). Therefore there is a molecular and supramolecular dimension that might concur for the result observed. The Single Rupture Force, a parameter within the molecular dimension as it translates the force necessary to disrupt single non-covalent receptor-ligand bonds, was also significantly higher in Pro33 cells than in Leu33 cells. Of note, the values of Single Rupture Force calculated in the present work (25 to 120 ρN) (Figure 27) are in the

same magnitude of those for protein-ligand rupture forces in general calculated using similar experimental settings (20 and 200 ρN) (Weisel et al., 2003). Force values on this range were previously considered as corresponding indeed to single bimolecular ligand-integrin interactions (Litvinov et al., 2002). Notably, the calculated Single Rupture Force are very comparable with those previously calculated with SCFS for α5β1-fibronectin (50 to 100 ρN) (Kong et al., 2009; Li et al., 2003) and α2β1-collagen (50 ρN) (Franz et al., 2007; Taubenberger et al., 2007). A different study using aldehyde/sulfate latex spheres and a laser tweezers-based model system, has calculated Single Rupture Forces ranging 70 to 150 ρN for the interaction between αIIbβ3 and fibrinogen in platelets (Goldsmith et al., 2000; Litvinov et al., 2002).

The tether force and length were parameters also studied with the SCFS technology and the corresponding results indicate that they were also significantly higher when the Pro33 variant is present (Figure 27). In the force distance curves (Figure 23) the tether is represented by plateaus of constant force and these plateaus can be seen as a membrane reservoir that is getting empty upon pulling on the plasma membrane (Raucher and Sheetz, 1999). The tethers are thin membrane nanotubes constituted by a lipd bilayer, involved in cell-cell adhesion (Schmidtke and Diamond, 2000) and suspected to play a role in the intracellular and intercellular communication (Iglič et al., 2003; Koster et al., 2003; Roux et al., 2002; Rustom et al., 2004; Upadhyaya and Sheetz, 2004). Tether formation is a process that occurs ubiquitously, independent of cell type (Sun et al., 2005). Some of the factors that influence tether force are the major constitutents of the cytoskeleton actin and tubulin (Raucher and Sheetz, 1999), and the integrity of such cytoskeleton components is fundamental in the regulation of membrane´s biomechanics (Sun et al., 2005). In this sense, the higher tether force and length in the Pro33 cells observed in the present study (Figures 28A-D) seems to indicate an extraordinary organization of the cytoskeleton in those cells. In previous studies, the Leu33Pro polymorphism has already been suggested as a modulator of cytoskeleton reorganization. In concrete, it was revealed a greater spreading and extensive actin polymerization of Pro33 cells when compared to Leu33 cells on fibrinogen substrate. This highly structured cytoskeleton in Pro33 cells results from outside-in signalling events and leads to a signalling cascade involving multiple proteins (Vijayan et al., 2000; Vijayan et al., 2005). As for the previously mentioned parameters studied, also the values calculated for the tether forces (30 to 85 ρN) (Figure 28A and B) are in line with those of previous studies (10 to 60 ρN). These studies were not directly involving integrins but were focused on the

interactions between cytoskeleton and membrane structures on a variety of cell lines (Dai and Sheetz, 1995; Dai and Sheetz, 1999; Hwang and Waugh, 1997; Raucher and Sheetz, 1999; Sun et al., 2005).

Putative additional interactions between other molecules/proteins expressed in the cells and the fibrinogen could eventually concur to the results which are here being attributed only to the αIIbβ3 receptor. However the specificity of the measurements could be verified by the absence of any significant forces detected in SCFS controls experiments involving cells not expressing the αIIbβ3 integrin and cells expressing the receptor but pre-incubated with Abciximab, an antibody binding integrin αIIbβ3 and avoiding its interaction with fibrinogen. In such control experiments, the absence of force associated with a specific cell-substrate binding in SCFS experiments resulted in symmetric approach and retraction profiles in the force-distance-curves (Figure 24C and Figure 24D). The slight increase seen in in the approach curve before contact, and a tiny dip in the retraction, can be explained with hydrodynamics resulting from the movement of the cantilever in the medium solution.

As for the FRET analyses, the choice of the cells to be analysed by SCFS was made taking in consideration the apparent cell integrity and the presence of both mVenus and mCherry fluorophores. In the cells selected for SCFS, the fluorescence intensities could also be measured and they were very heterogeneous. However, it was not possible to detect any significant difference between the fluorescence intensities of both fluorophores in the cells transfected with Pro33 and Leu33 and neither was possible to establish any influence of that fact in the results.

Collectively, the results indicate that expression of Pro33 variant allows cells to bind more strongly and stably to immobilized fibrinogen. These results seem in line with those of previous studies showing that the number of cells adhering to immobilized fibrinogen in adhesion assays under static conditions is higher for cells expressing the Pro33 variant compared to Leu33 variant (Deckmyn et al., 2004; Vijayan et al., 2000). The αIIbβ3-fibrinogen binding has as consequence a series of outside-in signalling events that involve the activation of kinases and phosphatases and platelet cytoskeleton rearrangement that allow platelets to spread on an adhesive surface. In light of the results obtained here, it is consivable a difference in the nature or efficiency of outside-in signals between the Leu33 and Pro33 variants confering to the Pro33 variant a prothrombotic character. This prothrombotic character of the Pro33 variant may justify the shorter bleeding time verified on HPA-1b cells (Byzova and Plow, 2000; Reiner et al., 2001) and verified in healthy Pro33 variant individuals

(Szczeklik et al., 2000) and the increased risk of coronary heart disease associated with the Leu33Pro polymorphism (Burr et al., 2003).

Importantly, the results and observations done in the present work are grounded in SCFS experiments using a very controlled experimental setting and allowing measurements at the subcellular molecular level. This represents a clear distinct feature of the present work.

5.4 – General discussion

It is still missing a detailed mechanistic explanation linking the functional differences between the Leu33 and Pro33 variants seen in the SCFS experiments and the results from the conformational differences unveiled by the FRET and MD studies. However it seems undisputable that the more open conformation and the less stability of the PSI, I-EGF-1, and I-EGF-2 domains in the HPA-1b have indeed a significant impact in the functional properties of the receptor, namely in its capacity to bind fibrinogen. In one hand it is tempting to speculate on a direct link between the more opened structure with a larger space between the subunits and a better accommodation for the ligand which would result in a stronger binding. Supporting this idea, the PSI domain containing a Pro33 was also considered by other authors as a provider of greater stability to the open-head conformation after ligand binding than a PSI domain containing the Leu33 isoform (Vijayan and Bray, 2006). In one other hand, it is known that activation of integrin receptors involves major conformational changes resulting in the stretching of the legs of both α and β subunits (Zhu et al., 2008) in a process facilitated by the disruption of key molecular interactions (Matsumoto et al., 2008). Particularly, it has been suggested that the disulfide bonds located within the EGF domains should be intact to keep the αIIbβ3 in an inactive state and disruption of a single disulphide is enough to induce activation of αIIbβ3 (Kamata et al., 2004). In that sense, the less stability of the PSI, I-EGF-1, and I-EGF-2 domains, and the more open and flexible conformation of the HPA-1b could therefore favor a more rapid activation of the receptor. The structural state more close to the active state seen in HPA-1b facilitates reaching the fully active state in the presence of integrin ligands. Following blood vessel injury fibrinogen gets immobilized in the damaged surface and is one of the proteins to which platelets adhere (Hatton et al., 1989), following platelet spreading and activation by an agonist (Balasubramanian and Slack, 2002; Jirouskova et al., 2007). This adhesion of platelets can be more easily achieved if binding to immobilized fibrinogen does not require receptor activation (Savage and Ruggeri, 1991). HPA-1b might therefore reduce αIIbβ3 dependency of inside-out signalling for activation. However, binding

of integrins to immobilized ligands seems also to require an initial leg extension followed by separation of α and β subunits, which should be achieved by rearrangements in the β subunit knee area as suggested by observations done in the related integrin αLβ2 (Schurpf and Springer, 2011). If this is the case for the αIIbβ3 integrin, the increased flexibility verified on β3Pro33 subunit knee domains may promote these rearrangements and therefore favor immobilized ligand binding (Jallu et al., 2012).

Considering the role of platelets binding to fibrinogen in the formation of thrombi, the results of the present work seem to support the prothrombotic factor of HPA-1b and seem in line with results showing that thrombi formed with HPA-1b platelets persist more time than thrombi formed with HPA-1a platelets (Cadroy et al., 2001), and with the phenotypes previously described for HPA-1b patients as the increased risk of coronary heart disease (Bojesen et al., 2003; Burr et al., 2003).

6 – CONCLUSIONS AND PERSPECTIVES

This study aimed to provide mechanistic insights to narrow the gap between the Leu33Pro polymorphism and the prothrombotic character of the HPA-1b platelets, observed in previous functional studies.

Using two complementary approaches we could provide new evidences for consequences of the Leu33Pro exchange on the global structure of the αIIbβ3Pro33 receptor. Using the FRET technology we managed to demonstrate that in the resting state the cytoplasmic tails of αIIb and β3 subunits are more distant from each other in the αIIbβ3Pro33 receptor variant than in the αIIbβ3Leu33 receptor variant. In a complementary study using MD simulation it was determined a higher physical separation between the extracellular domains and a more stretched and flexible structure of the receptor in the presence of the Pro33 variant. With that here we could show that the Leu33Pro exchange shifts the dynamic conformational equilibrium of αIIbβ3 integrin towards a more open, extended state, with a larger splaying of the legs, a structural state more close to the active state.

Additionally, performing SCFS we extended our knowledge about the αIIbβ3 receptor binding to immobilized ligand and evaluated the functional consequences of the Leu33Pro exhange. We could observe that the forces implicated in both supramolecular and molecular dimensions of αIIbβ3-promoted cell binding to fibrinogen were significantly higher for the Pro33 variant. This higher propensity for ligand binding seems to facilitate the post-receptor occupancy events (outside-in signaling cascade) which results on the extraordinary organization of the cytoskeleton also suggested by the same SCFC experiments.

Collectively, our results point to a clear effect of the Leu33Pro exchange in the resting state structure and function of the αIIbβ3Pro33 receptor. All these effects seem to underline the results of other functional studies showing increased binding efficiency to immobilized fibrinogen, cell spreading, actin cytoskeleton rearrangement and clot retraction. Of utmost importance, all our observations seem to provide a molecular mechanistic basis for the association existing between the Leu33Pro polymorphism and the increased risk of coronary heart disease, as well as the association between the HPA-1b homozygosity and the increased risk of ischaemic cardiovascular disease and myocardial infarction, reported on the clinical epidemiological studies performed in the past twenty years.

Having uncovered some important structural features of the receptor in its resting state, it would be of great interest to obtain data also on the structure of the receptor upon activation

with different agonists followed by binding to immobilized and soluble fibrinogen. This study would give a full picture of the receptor structure in its different conformational states. In particular, to know if the adhesion to immobilized fibrinogen, or the activation followed by binding to soluble fibrinogen, would cause an alteration in the physical separation between subunits. Also, evaluate the strength of the interaction between receptor and ligand upon receptor activation, at supramolecular and molecular levels. Upon the work presented here, techniques as FRET and SCFC could be extremely valuable for that.

A deeper understanding of the αIIbβ3 structure in its different conformational states may foster the development of drugs focused on limiting the gain-of function action of the Pro33 variant, in order to prevent coronary heart disease in HPA-1b individuals.

7 – LIST OF ABBREVIATIONS

ADP – Adenosine Di- Phosphate

AFM – Atomic Force Microscopy

APC – Allophycocyanin

APS – Ammoniumpersulfate

ATP – Adenosine Tri-Phosphate

BMFZ – Biologisches Medizinisches Forschungszentrum

BSA – Bovine Serum Albumin

CFP – Cyan Fluorescent Protein

CHO – Chinese Hamster Ovarian

CMV - Cytomegalovirus

DMEM – Dulbecco's Modified Eagle's Medium

DNA - Desoxyribonucleic acid

DPBS – Dulbecco's Phosphate Buffered Saline

DPSS - Diode-Pumped Solid-State

DSMZ – Deutsche Sammlung von Mikroorganismen und Zellkulturen

DTT – Dithiothreitol

ECM – Extracellular Matrix

EDTA - Etilenodiaminotetracetic acid

EGF – Epidermal Growth Factor

FAK – Focal Adhesion Kinase

FACS – Fluorescence Activated Cell Sorter

FBS – Fetal Bovine Serum

FITC - Fluorescein Isothiocyanate

FRET-APB – Förster or Fluorescence Resonance Energy Transfer – Acceptor Photobleaching

GaAsp - Gallium arsenide phosphide

GAPDH - Glyceraldehyde 3-phosphate dehydrogenase

HEK – Human Embryonal Kidney

HPA – Human Platelet Polymorphism

HPX – High Pressure Xenon

HRP – Horseradish Peroxidase

IQR – Interquartile range

KDa - Kilodalton

LB – Luria-Bertani

LSM – Laser Scanning Microscope

MBS – Micro Beam-Splitter

MD – Molecular Dynamics

MI – Myocardial Infarction

MKs – Megakaryocytes

mRNA – messenger RNA

PBS - Phosphate Buffered Saline

PE – Phycoerythrin

PTB – Phosphotyrosine-binding

PSI – Plexin, Semaphorin and Integrin

RNA - Ribonucleic Acid

SCFS – Single-Cell Fluorescence Spectroscopy

SDS - sodium dodecyl sulphate

TBS-T - Tris-buffered saline-Tween

vWF – Von Willebrand Factor

YFP – Yellow Fluorescent Protein

βTD – β-Tail Domain

8 – LITERATURE

Abraham DG, Nutt EM, Bednar RA, Bednar B, Gould RJ, Duong LT. 1997. Arginine-Glycine-Aspartic acid mimics can identify a transitional activation state of recombinant aIIbb3 in human embryonic kidney 293 cells. Mol Pharmacol **52**:227–36.

Abrams C, Deng YJ, Steiner B, O'Toole T, Shattil SJ. 1994. Determinants of specificity of a baculovirus-expressed antibody Fab fragment that binds selectively to the activated form of integrin alpha IIb beta 3. J Biol Chem **269**(29):18781-8.

Aliuos P, Fadeeva E, Badar M, Winkel A, Mueller PP, Warnecke A, Chichkov B, Lenarz T, Reich U, Reuter G. 2013. Evaluation of single-cell force spectroscopy and fluorescence microscopy to determine cell interactions with femtosecond-laser microstructured titanium surfaces. J Biomed Mater Res A **101**(4):981-90.

Anderson JL, King GJ, Bair TL, Elmer SP, Muhlestein JB, Habashi J, Carlquist JF. 1999. Associations between a polymorphism in the gene encoding glycoprotein IIIa and myocardial infarction or coronary artery disease. J Am Coll Cardiol **33**(3):727-33.

Araujo F, Santos A, Araujo V, Henriques I, Monteiro F, Meireles E, Moreira I, David D, Maciel MJ, Cunha-Ribeiro LM. 1999. Genetic risk factors in acute coronary disease. Haemostasis **29**(4):212-8.

Ardissino D, Mannucci PM, Merlini PA, Duca F, Fetiveau R, Tagliabue L, Tubaro M, Galvani M, Ottani F, Ferrario M, Corral J, Margaglione M. 1999. Prothrombotic genetic risk factors in young survivors of myocardial infarction. Blood **94**(1):46-51.

Artoni A, Li J, Mitchell B, Ruan J, Takagi J, Springer TA, French DL, Coller BS. 2004. Integrin beta3 regions controlling binding of murine mAb 7E3: implications for the mechanism of integrin alphaIIbbeta3 activation. Proc Natl Acad Sci U S A **101**(36):13114-20.

Balasubramanian V, Slack SM. 2002. The effect of fluid shear and co-adsorbed proteins on the stability of immobilized fibrinogen and subsequent platelet interactions. J Biomater Sci Polym Ed **13**(5):543-61.

Beckmann J, Schubert R, Chiquet-Ehrismann R, Muller DJ. 2013. Deciphering teneurin domains that facilitate cellular recognition, cell-cell adhesion, and neurite outgrowth using atomic force microscopy-based single-cell force spectroscopy. Nano Lett **13**(6):2937-46.

Bennett JS, Vilaire G. 1979. Exposure of platelet fibrinogen receptors by ADP and epinephrine. J Clin Invest **64**(5):1393-401.

Benoit M, Gabriel D, Gerisch G, Gaub HE. 2000. Discrete interactions in cell adhesion measured by single-molecule force spectroscopy. Nat Cell Biol **2**(6):313-7.

Benoit M, Gaub HE. 2002. Measuring cell adhesion forces with the atomic force microscope at the molecular level. Cells Tissues Organs **172**(3):174-89.

Bevers EM, Comfurius P, Zwaal RF. 1983. Changes in membrane phospholipid distribution during platelet activation. Biochim Biophys Acta **736**(1):57-66.

Binnig G, Quate CF, Gerber C. 1986. Atomic Force Microscope. Phys Rev Lett **56**(9):930-3.

Bizzozzero G. 1882. Su di un nuovo elemento morfologico del sangue nei mammiferi e sulla sua importanza nella trombosi e nella coagulazione. L'Osservatore Gazz Clin **17**:785-7.

Bleckmann A, Weidtkamp-Peters S, Seidel CAM, Simon R. 2010. Stem Cell Signaling in Arabidopsis Requires CRN to Localize CLV2 to the Plasma Membrane. Plant Physiol. **152**(1):166-76.

Bodary SC, McLean JW. 1990. The integrin beta 1 subunit associates with the vitronectin receptor alpha v subunit to form a novel vitronectin receptor in a human embryonic kidney cell line. J Biol Chem **265**(11):5938-41.

Boettiger D, Wehrle-Haller B. 2010. Integrin and glycocalyx mediated contributions to cell adhesion identified by single cell force spectroscopy. J Phys Condens Matter **22**(19):194101.

Bojesen SE, Juul K, Schnohr P, Tybjaerg-Hansen A, Nordestgaard BG. 2003. Platelet glycoprotein IIb/IIIa Pl(A2)/Pl(A2) homozygosity associated with risk of ischemic cardiovascular disease and myocardial infarction in young men: the Copenhagen City Heart Study. J Am Coll Cardiol **42**(4):661-7.

Bradford MM. 1976. A rapid and sensitive method for the quantitation of microgram quantities of protein utilizing the principle of protein-dye binding. Anal Biochem **72**(1):248-54.

Bray PF. 2000. Platelet glycoprotein polymorphisms as risk factors for thrombosis. Curr Opin Hematol **7**(5):284-9.

Brecher G, Schneiderman M, Cronkite EP. 1953. The reproducibility and constancy of the platelet count. Am J Clin Pathol **23**(1):15-26.

Burr D, Doss H, Cooke GE, Goldschmidt-Clermont PJ. 2003. A meta-analysis of studies on the association of the platelet PlA polymorphism of glycoprotein IIIa and risk of coronary heart disease. Stat Med **22**(10):1741-60.

Butt H-J, Cappella B, Kappl M. 2005. Force measurements with the atomic force microscope: Technique, interpretation and applications. Surf Sci Rep **59**(1–6):1-152.

Byzova TV, Plow EF. 2000. The Pl(A2) allele and cardiovascular disease: the pro(33) and con. J Clin Invest **105**(6):697-8.

Cadroy Y, Sakariassen K, Grandjean H, Thalamas C, Boneu B, Sie P. 2001. The effect of platelet PlA polymorphism on experimental thrombus formation in man depends on blood flow and thrombogenic substrate. Thromb Haemost **85**(6):1097-103.

Calderwood DA, Yan B, de Pereda JM, Alvarez BG, Fujioka Y, Liddington RC, Ginsberg MH. 2002. The phosphotyrosine binding-like domain of talin activates integrins. J Biol Chem **277**(24):21749-58.

Calderwood DA, Zent R, Grant R, Rees DJ, Hynes RO, Ginsberg MH. 1999. The Talin head domain binds to integrin beta subunit cytoplasmic tails and regulates integrin activation. J Biol Chem **274**(40):28071-4.

Calvete JJ, Alvarez MV, Rivas G, Hew CL, Henschen A, Gonzalez-Rodriguez J. 1989. Interchain and intrachain disulphide bonds in human platelet glycoprotein IIb. Localization of the epitopes for several monoclonal antibodies. Biochem J **261**(2):551-60.

Carman CV, Springer TA. 2003. Integrin avidity regulation: are changes in affinity and conformation underemphasized? Curr Opin Cell Biol **15**(5):547-56.

Carter AM, Ossei-Gerning N, Wilson IJ, Grant PJ. 1997. Association of the platelet Pl(A) polymorphism of glycoprotein IIb/IIIa and the fibrinogen Bbeta 448 polymorphism with myocardial infarction and extent of coronary artery disease. Circulation **96**(5):1424-31.

Cohen JA, Leeksma CH. 1956. Determination of the life span of human blood platelets using labelled diisopropylfluorophosphonate. J Clin Invest **35**(9):964-9.

Coller BS. 1985. A new murine monoclonal antibody reports an activation-dependent change in the conformation and/or microenvironment of the platelet glycoprotein IIb/IIIa complex. J Clin Invest **76**(1):101-8.

Coller BS, Peerschke EI, Scudder LE, Sullivan CA. 1983. A murine monoclonal antibody that completely blocks the binding of fibrinogen to platelets produces a thrombasthenic-like state in normal platelets and binds to glycoproteins IIb and/or IIIa. J Clin Invest **72**(1):325-38.

Corral J, Gonzalez-Conejero R, Rivera J, Iniesta JA, Lozano ML, Vicente V. 1997. HPA-1 genotype in arterial thrombosis--role of HPA-1b polymorphism in platelet function. Blood Coagul Fibrinolysis **8**(5):284-90.

D'Agostino R, Pearson ES. 1973. Tests for Departure from Normality. Empirical Results for the Distributions of b₂ and √ b₁. Biometrika **60**(3):613-22.

D'Souza SE, Ginsberg MH, Burke TA, Lam SC, Plow EF. 1988. Localization of an Arg-Gly-Asp recognition site within an integrin adhesion receptor. Science **242**(4875):91-3.

D'Souza SE, Ginsberg MH, Burke TA, Plow EF. 1990. The ligand binding site of the platelet integrin receptor GPIIb-IIIa is proximal to the second calcium binding domain of its alpha subunit. J Biol Chem **265**(6):3440-6.

D'Souza SE, Ginsberg MH, Matsueda GR, Plow EF. 1991. A discrete sequence in a platelet integrin is involved in ligand recognition. Nature **350**(6313):66-8.

Dai J, Sheetz MP. 1995. Mechanical properties of neuronal growth cone membranes studied by tether formation with laser optical tweezers. Biophys J **68**(3):988-96.

Dai J, Sheetz MP. 1999. Membrane tether formation from blebbing cells. Biophys J **77**(6):3363-70.

Dao L, Weiland U, Hauser M, Nazarenko I, Kalt H, Bastmeyer M, Franz CM. 2012. Revealing non-genetic adhesive variations in clonal populations by comparative single-cell force spectroscopy. Exp. Cell Res **318**(17):2155-67.

De Marco L, Girolami A, Russell S, Ruggeri ZM. 1985. Interaction of asialo von Willebrand factor with glycoprotein Ib induces fibrinogen binding to the glycoprotein IIb/IIIa complex and mediates platelet aggregation. J Clin Invest **75**(4):1198-203.

Deckmyn H, Ulrichts H, Van de Walle G, Vanhoorelbeke K. 2004. Platelet antigens and their function. Vox Sang **87**:105-11.

Di Castelnuovo A, de Gaetano G, Benedetta Donati M, Iacoviello L. 2005. Platelet glycoprotein IIb/IIIa polymorphism and coronary artery disease: implications for clinical practice. Am J Pharmacogenomics **5**(2):93-9.

Donné A. 1842. De porigine des globules du sang, de leur mode de formation et du leur fin. C R Acad Sci **14**:366-8.

Duperray A, Berthier R, Chagnon E, Ryckewaert JJ, Ginsberg M, Plow E, Marguerie G. 1987. Biosynthesis and processing of platelet GPIIb-IIIa in human megakaryocytes. J Cell Biol **104**(6):1665-73.

Durante-Mangoni E, Davies GJ, Ahmed N, Ruggiero G, Tuddenham EG. 1998. Coronary thrombosis and the platelet glycoprotein IIIA gene PLA2 polymorphism. Thromb Haemost **80**(2):218-9.

Elter P, Weihe T, Buhler S, Gimsa J, Beck U. 2012. Low fibronectin concentration overcompensates for reduced initial fibroblasts adhesion to a nanoscale topography: single-cell force spectroscopy. Colloids Surf B Biointerfaces **95**:82-9.

Feng D, Lindpaintner K, Larson MG, Rao VS, O'Donnell CJ, Lipinska I, Schmitz C, Sutherland PA, Silbershatz H, D'Agostino RB, Muller JE, Myers RH, Levy D, Tofler GH. 1999. Increased platelet aggregability associated with platelet GPIIIa PlA2 polymorphism: the Framingham Offspring Study. Arterioscler Thromb Vasc Biol **19**(4):1142-7.

Fitzgerald LA, Steiner B, Rall SC, Jr., Lo SS, Phillips DR. 1987. Protein sequence of endothelial glycoprotein IIIa derived from a cDNA clone. Identity with platelet glycoprotein IIIa and similarity to "integrin". J Biol Chem **262**(9):3936-9.

Förster T. 1948. Zwischenmolekulare Energiewanderung und Fluoreszenz. Ann Phys **437**(1-2):55-75.

Franz CM, Taubenberger A, Puech PH, Muller DJ. 2007. Studying integrin-mediated cell adhesion at the single-molecule level using AFM force spectroscopy. Sci STKE **2007**(406):pl5.

Frelinger AL, 3rd, Du XP, Plow EF, Ginsberg MH. 1991. Monoclonal antibodies to ligand-occupied conformers of integrin alpha IIb beta 3 (glycoprotein IIb-IIIa) alter receptor affinity, specificity, and function. J Biol Chem **266**(26):17106-11.

Friedrichs J, Helenius J, Muller DJ. 2010. Quantifying cellular adhesion to extracellular matrix components by single-cell force spectroscopy. Nat Protoc **5**(7):1353-61.

Fuhrmann A, Ros R. 2010. Single-molecule force spectroscopy: a method for quantitative analysis of ligand-receptor interactions. Nanomedicine (Lond) **5**(4):657-66.

Fujimura K, Phillips DR. 1983. Calcium cation regulation of glycoprotein IIb-IIIa complex formation in platelet plasma membranes. J Biol Chem **258**(17):10247-52.

Fukami MH, Salganicoff L. 1977. Human platelet storage organelles. A review. Thromb Haemost **38**(4):963-70.

Garcia-Ribes M, Gonzalez-Lamuno D, Hernandez-Estefania R, Colman T, Pocovi M, Delgado-Rodriguez M, Garcia-Fuentes M, Revuelta JM. 1998. Polymorphism of the platelet glycoprotein IIIa gene in patients with coronary stenosis. Thromb Haemost **79**(6):1126-9.

Gardemann A, Humme J, Stricker J, Nguyen QD, Katz N, Philipp M, Tillmanns H, Hehrlein FW, Rau M, Haberbosch W. 1998. Association of the platelet glycoprotein IIIa PlA1/A2 gene polymorphism to coronary artery disease but not to nonfatal myocardial infarction in low risk patients. Thromb Haemost **80**(2):214-7.

Goldsmith HL, McIntosh FA, Shahin J, Frojmovic MM. 2000. Time and force dependence of the rupture of glycoprotein IIb-IIIa-fibrinogen bonds between latex spheres. Biophys J **78**(3):1195-206.

Graham FL, Smiley J, Russell WC, Nairn R. 1977. Characteristics of a human cell line transformed by DNA from human adenovirus type 5. J Gen Virol **36**(1):59-74.

Grandbois M, Dettmann W, Benoit M, Gaub HE. 2000. Affinity imaging of red blood cells using an atomic force microscope. J Histochem Cytochem **48**(5):719-24.

Hantgan RR, Simpson-Haidiris, P. J., Francis, C. W., Marder, V. J. 2001. Fibrinogen structure and physiology Philadelphia. 203-32 pp.

Hatton MW, Moar SL, Richardson M. 1989. Deendothelialization in vivo initiates a thrombogenic reaction at the rabbit aorta surface. Correlation of uptake of fibrinogen and antithrombin III with thrombin generation by the exposed subendothelium. Am J Pathol **135**(3):499-508.

Helenius J, Heisenberg CP, Gaub HE, Muller DJ. 2008. Single-cell force spectroscopy. J Cell Sci **121**(11):1785-91.

Herrmann SM, Poirier O, Marques-Vidal P, Evans A, Arveiler D, Luc G, Emmerich J, Cambien F. 1997. The Leu33/Pro polymorphism (PlA1/PlA2) of the glycoprotein IIIa (GPIIIa) receptor is not related to myocardial infarction in the ECTIM Study. Etude Cas-Temoins de l'Infarctus du Myocarde. Thromb Haemost **77**(6):1179-81.

Hewson W. 1771. An experimental inquiry into the properties of the blood. London.

Hewson W. 1780. Experimental inquiries: part the first, containing an inquiry into the properties of the blood. London **3**.

Hinterdorfer P, Dufrene YF. 2006. Detection and localization of single molecular recognition events using atomic force microscopy. Nat Methods **3**(5):347-55.

Hooper WC, Lally C, Austin H, Benson J, Dilley A, Wenger NK, Whitsett C, Rawlins P, Evatt BL. 1999. The relationship between polymorphisms in the endothelial cell nitric oxide synthase gene and the platelet GPIIIa gene with myocardial infarction and venous thromboembolism in African Americans. Chest **116**(4):880-6.

Hutter JL, Bechhoefer J. 1993. Calibration of atomic-force microscope tips. Rev Sci Instrum **64**(7):1868-73.

Hwang WC, Waugh RE. 1997. Energy of dissociation of lipid bilayer from the membrane skeleton of red blood cells. Biophys J **72**(6):2669-78.

Hynes RO. 1987. Integrins: a family of cell surface receptors. Cell **48**(4):549-54.

Hynes RO. 2002. Integrins: bidirectional, allosteric signaling machines. Cell **110**(6):673-87.

Iglič A, Hägerstrand H, Bobrowska-Hägerstrand M, Arrigler V, Kralj-Iglič V. 2003. Possible role of phospholipid nanotubes in directed transport of membrane vesicles. Phys Lett **310**(5–6):493-7.

Isenberg WM, McEver RP, Phillips DR, Shuman MA, Bainton DF. 1987. The platelet fibrinogen receptor: an immunogold-surface replica study of agonist-induced ligand binding and receptor clustering. J Cell Biol **104**(6):1655-63.

Italiano JE, Jr., Lecine P, Shivdasani RA, Hartwig JH. 1999. Blood platelets are assembled principally at the ends of proplatelet processes produced by differentiated megakaryocytes. J Cell Biol **147**(6):1299-312.

Jallu V, Poulain P, Fuchs PF, Kaplan C, de Brevern AG. 2012. Modeling and molecular dynamics of HPA-1a and -1b polymorphisms: effects on the structure of the beta3 subunit of the alphaIIbbeta3 integrin. PLoS One **7**(11):e47304.

Jennings LK, Phillips DR. 1982. Purification of glycoproteins IIb and III from human platelet plasma membranes and characterization of a calcium-dependent glycoprotein IIb-III complex. J Biol Chem **257**(17):10458-66.

Jirouskova M, Jaiswal JK, Coller BS. 2007. Ligand density dramatically affects integrin alpha IIb beta 3-mediated platelet signaling and spreading. Blood **109**(12):5260-9.

Kamata T, Ambo H, Puzon-McLaughlin W, Tieu KK, Handa M, Ikeda Y, Takada Y. 2004. Critical cysteine residues for regulation of integrin alphaIIbbeta3 are clustered in the epidermal growth factor domains of the beta3 subunit. Biochem J **378**(Pt 3):1079-82.

Karpova TS, Baumann CT, He L, Wu X, Grammer A, Lipsky P, Hager GL, McNally JG. 2003a. Fluorescence resonance energy transfer from cyan to yellow fluorescent protein detected by acceptor photobleaching using confocal microscopy and a single laser. J. Microsc. **209**:56-70.

Karpova TS, Baumann CT, He L, Wu X, Grammer A, Lipsky P, Hager GL, McNally JG. 2003b. Fluorescence resonance energy transfer from cyan to yellow fluorescent protein detected by acceptor photobleaching using confocal microscopy and a single laser. J Microsc **209**(Pt 1):56-70.

Kastrati A, Schomig A, Seyfarth M, Koch W, Elezi S, Bottiger C, Mehilli J, Schomig K, von Beckerath N. 1999. PlA polymorphism of platelet glycoprotein IIIa and risk of restenosis after coronary stent placement. Circulation **99**(8):1005-10.

Kekomaki S, Hamalainen L, Kauppinen-Makelin R, Palomaki H, Kaste M, Kontula K. 1999. Genetic polymorphism of platelet glycoprotein IIIa in patients with acute myocardial infarction and acute ischaemic stroke. J Cardiovasc Risk **6**(1):13-7.

Kim HO, Jin Y, Kickler TS, Blakemore K, Kwon OH, Bray PF. 1995. Gene frequencies of the five major human platelet antigens in African American, white, and Korean populations. Transfusion **35**(10):863-7.

Kim M, Carman CV, Springer TA. 2003. Bidirectional transmembrane signaling by cytoplasmic domain separation in integrins. Science **301**(5640):1720-5.

Kim TK, Eberwine JH. 2010. Mammalian cell transfection: the present and the future. Anal Bioanal Chem **397**(8):3173-8.

Kong F, García AJ, Mould AP, Humphries MJ, Zhu C. 2009. Demonstration of catch bonds between an integrin and its ligand. J Cell Biol **185**(7):1275-84.

Koster G, VanDuijn M, Hofs B, Dogterom M. 2003. Membrane tube formation from giant vesicles by dynamic association of motor proteins. Proc Natl Acad Sci U S A **100**(26):15583-8.

Kunicki TJ, Newman PJ. 1992. The molecular immunology of human platelet proteins. Blood **80**(6):1386-404.

Kunkel TA. 1985. Rapid and efficient site-specific mutagenesis without phenotypic selection. Proc Natl Acad Sci U S A **82**(2):488-92.

Lakowicz JR. 2006. Principles of fluorescence spectroscopy. Springer, Berlin, Heidelberg, New York.

Laule M, Cascorbi I, Stangl V, Bielecke C, Wernecke KD, Mrozikiewicz PM, Felix SB, Roots I, Baumann G, Stangl K. 1999. A1/A2 polymorphism of glycoprotein IIIa and association with excess procedural risk for coronary catheter interventions: a case-controlled study. Lancet **353**(9154):708-12.

Leewenhoeck AV. 1675. Microscopical observations concerning blood, milk, bones, the brain, spittle, and cuticula, etc. Phil Trans **9**(116):121-8.

Li F, Redick SD, Erickson HP, Moy VT. 2003. Force measurements of the alpha5beta1 integrin-fibronectin interaction. Biophys J **84**(2 Pt 1):1252-62.

Liang J, Fernandez JM. 2009. Mechanochemistry: one bond at a time. ACS Nano **3**(7):1628-45.

Litvinov RI, Shuman H, Bennett JS, Weisel JW. 2002. Binding strength and activation state of single fibrinogen-integrin pairs on living cells. Proc Natl Acad Sci U S A **99**(11):7426-31.

Ma L, Yang F, Zheng J. 2014. Application of fluorescence resonance energy transfer in protein studies. J Mol Struct **1077**:87-100.

Ma Y-Q, Qin J, Wu C, Plow EF. 2008. Kindlin-2 (Mig-2): a co-activator of β(3) integrins. J Cell Biol **181**(3):439-46.

Mamotte CD, van Bockxmeer FM, Taylor RR. 1998. PIa1/a2 polymorphism of glycoprotein IIIa and risk of coronary artery disease and restenosis following coronary angioplasty. Am J Cardiol **82**(1):13-6.

Mann KG, Bovill EG, Krishnaswamy S. 1991. Surface-dependent reactions in the propagation phase of blood coagulation. Ann N Y Acad Sci **614**:63-75.

Matsumoto A, Kamata T, Takagi J, Iwasaki K, Yura K. 2008. Key interactions in integrin ectodomain responsible for global conformational change detected by elastic network normal-mode analysis. Biophys J **95**(6):2895-908.

Michelson AD, Furman MI, Goldschmidt-Clermont P, Mascelli MA, Hendrix C, Coleman L, Hamlington J, Barnard MR, Kickler T, Christie DJ, Kundu S, Bray PF. 2000. Platelet GP IIIa Pl(A) polymorphisms display different sensitivities to agonists. Circulation **101**(9):1013-8.

Montanez E, Ussar S, Schifferer M, Bosl M, Zent R, Moser M, Fassler R. 2008. Kindlin-2 controls bidirectional signaling of integrins. Genes Dev **22**(10):1325-30.

Moser M, Bauer M, Schmid S, Ruppert R, Schmidt S, Sixt M, Wang HV, Sperandio M, Fassler R. 2009a. Kindlin-3 is required for beta2 integrin-mediated leukocyte adhesion to endothelial cells. Nat Med **15**(3):300-5.

Moser M, Legate KR, Zent R, Fassler R. 2009b. The tail of integrins, talin, and kindlins. Science **324**(5929):895-9.

Moser M, Nieswandt B, Ussar S, Pozgajova M, Fässler R. 2008. Kindlin-3 is essential for integrin activation and platelet aggregation. Nat Med **14**(3):325-30.

Mosher DF, Schad PE. 1979. Cross-linking of fibronectin to collagen by blood coagulation Factor XIIIa. J Clin Invest **64**(3):781-7.

Nachmias VT. 1983. Platelet and megakaryocyte shape change: triggered alterations in the cytoskeleton. Semin Hematol **20**(4):261-81.

Narumiya S. 1996. The small GTPase Rho: cellular functions and signal transduction. J Biochem **120**(2):215-28.

Newman PJ, Derbes RS, Aster RH. 1989. The human platelet alloantigens, PlA1 and PlA2, are associated with a leucine33/proline33 amino acid polymorphism in membrane glycoprotein IIIa, and are distinguishable by DNA typing. J Clin Invest **83**(5):1778-81.

Newman PJ, Martin LS, Knipp MA, Kahn RA. 1985. Studies on the nature of the human platelet alloantigen, PlA1: localization to a 17,000-dalton polypeptide. Mol Immunol **22**(6):719-29.

Nishida N, Xie C, Shimaoka M, Cheng Y, Walz T, Springer TA. 2006. Activation of leukocyte beta2 integrins by conversion from bent to extended conformations. Immunity **25**(4):583-94.

O'Toole TE, Loftus JC, Plow EF, Glass AA, Harper JR, Ginsberg MH. 1989. Efficient surface expression of platelet GPIIb-IIIa requires both subunits. Blood **74**(1):14-8.

Pabla R, Weyrich AS, Dixon DA, Bray PF, McIntyre TM, Prescott SM, Zimmerman GA. 1999. Integrin-dependent control of translation: engagement of integrin alphaIIbbeta3 regulates synthesis of proteins in activated human platelets. J Cell Biol **144**(1):175-84.

Pastinen T, Perola M, Niini P, Terwilliger J, Salomaa V, Vartiainen E, Peltonen L, Syvanen A. 1998. Array-based multiplex analysis of candidate genes reveals two independent and additive genetic risk factors for myocardial infarction in the Finnish population. Hum Mol Genet **7**(9):1453-62.

Picot J, Guerin CL, Le Van Kim C, Boulanger CM. 2012. Flow cytometry: retrospective, fundamentals and recent instrumentation. Cytotechnology **64**(2):109-30.

Piotrowicz RS, Orchekowski RP, Nugent DJ, Yamada KY, Kunicki TJ. 1988. Glycoprotein Ic-IIa functions as an activation-independent fibronectin receptor on human platelets. J Cell Biol **106**(4):1359-64.

Plow EF, Haas TA, Zhang L, Loftus J, Smith JW. 2000. Ligand binding to integrins. J Biol Chem **275**(29):21785-8.

Poncz M, Eisman R, Heidenreich R, Silver SM, Vilaire G, Surrey S, Schwartz E, Bennett JS. 1987. Structure of the platelet membrane glycoprotein IIb. Homology to the alpha subunits of the vitronectin and fibronectin membrane receptors. J Biol Chem **262**(18):8476-82.

Raucher D, Sheetz MP. 1999. Characteristics of a membrane reservoir buffering membrane tension. Biophys J **77**(4):1992-2002.

Reiner AP, Siscovick DS, Rosendaal FR. 2001. Platelet glycoprotein gene polymorphisms and risk of thrombosis: facts and fancies. Rev Clin Exp Hematol **5**(3):262-87; discussion 311-2.

Ridker PM, Hennekens CH, Schmitz C, Stampfer MJ, Lindpaintner K. 1997. PIA1/A2 polymorphism of platelet glycoprotein IIIa and risks of myocardial infarction, stroke, and venous thrombosis. Lancet **349**(9049):385-8.

Roux A, Cappello G, Cartaud J, Prost J, Goud B, Bassereau P. 2002. A minimal system allowing tubulation with molecular motors pulling on giant liposomes. Proc Natl Acad Sci U S A **99**(8):5394-9.

Rustom A, Saffrich R, Markovic I, Walther P, Gerdes H-H. 2004. Nanotubular Highways for Intercellular Organelle Transport. Science **303**(5660):1007-10.

Sanchez-Cortes J, Mrksich M. 2009. The platelet integrin alphaIIbbeta3 binds to the RGD and AGD motifs in fibrinogen. Chem Biol **16**(9):990-1000.

Santoro SA, Lawing WJ, Jr. 1987. Competition for related but nonidentical binding sites on the glycoprotein IIb-IIIa complex by peptides derived from platelet adhesive proteins. Cell **48**(5):867-73.

Savage B, Almus-Jacobs F, Ruggeri ZM. 1998. Specific synergy of multiple substrate-receptor interactions in platelet thrombus formation under flow. Cell **94**(5):657-66.

Savage B, Ruggeri ZM. 1991. Selective recognition of adhesive sites in surface-bound fibrinogen by glycoprotein IIb-IIIa on nonactivated platelets. J Biol Chem **266**(17):11227-33.

Savage B, Saldivar E, Ruggeri ZM. 1996. Initiation of platelet adhesion by arrest onto fibrinogen or translocation on von Willebrand factor. Cell **84**(2):289-97.

Savage B, Shattil SJ, Ruggeri ZM. 1992. Modulation of platelet function through adhesion receptors. A dual role for glycoprotein IIb-IIIa (integrin alpha IIb beta 3) mediated by fibrinogen and glycoprotein Ib-von Willebrand factor. J Biol Chem **267**(16):11300-6.

Scaglione L, Bergerone S, Gaschino G, Imazio M, Maccagnani A, Gambino R, Cassader M, Di Leo M, Macchia G, Brusca A, Pagano G, Cavallo-Perin P. 1998. Lack of relationship between the P1A1/P1A2 polymorphism of platelet glycoprotein IIIa and premature myocardial infarction. Eur J Clin Invest **28**(5):385-8.

Scharf RE, Zotz RB. 2006. Blood Platelets and Myocardial Infarction: Do Hyperactive Platelets Really Exist? Transfus Med Hemother **33**(2):189-99.

Schmidtke DW, Diamond SL. 2000. Direct observation of membrane tethers formed during neutrophil attachment to platelets or P-selectin under physiological flow. J Cell Biol **149**(3):719-30.

Schmitz S. 2011. Der Experimentator: Zellkultur. Spektrum Akademischer Verlag, Heidelberg.

Schultze M. 1865. Ein heizbarer Objecttisch und seine Verwendung bei Untersuchungen des Blutes. Arch Mikroskop Anat **1**:1-42.

Schurpf T, Springer TA. 2011. Regulation of integrin affinity on cell surfaces. EMBO J **30**(23):4712-27.

Shattil SJ, Kashiwagi H, Pampori N. 1998. Integrin signaling: the platelet paradigm. Blood **91**(8):2645-57.

Staatz WD, Rajpara SM, Wayner EA, Carter WG, Santoro SA. 1989. The membrane glycoprotein Ia-IIa (VLA-2) complex mediates the Mg++-dependent adhesion of platelets to collagen. J Cell Biol **108**(5):1917-24.

Stahl Y, Weidtkamp-Peters S. 2015. *In vivo* FRET measurements in plants: a practical guide. *In* EMBO Practical Course: *In vivo* Plant Imaging, Heidelberg, Germany.

Sun M, Graham JS, Hegedüs B, Marga F, Zhang Y, Forgacs G, Grandbois M. 2005. Multiple Membrane Tethers Probed by Atomic Force Microscopy. Biophys J **89**(6):4320-9.

Szczeklik A, Sanak M, Undas A. 2001. Platelet glycoprotein IIIa pl(a) polymorphism and effects of aspirin on thrombin generation. Circulation **103**(6):E33-4.

Szczeklik A, Undas A, Sanak M, Frolow M, Wegrzyn W. 2000. Relationship between bleeding time, aspirin and the PlA1/A2 polymorphism of platelet glycoprotein IIIa. Br J Haematol **110**(4):965-7.

Takagi J, Petre BM, Walz T, Springer TA. 2002. Global conformational rearrangements in integrin extracellular domains in outside-in and inside-out signaling. Cell **110**(5):599-11.

Taubenberger A, Cisneros DA, Friedrichs J, Puech PH, Muller DJ, Franz CM. 2007. Revealing early steps of alpha2beta1 integrin-mediated adhesion to collagen type I by using single-cell force spectroscopy. Mol Biol Cell **18**(5):1634-44.

Thornton MA, Poncz M, Korostishevsky M, Yakobson E, Usher S, Seligsohn U, Peretz H. 1999. The human platelet alphaIIb gene is not closely linked to its integrin partner beta3. Blood **94**(6):2039-47.

Topol EJ, Byzova TV, Plow EF. 1999. Platelet GPIIb-IIIa blockers. The Lancet **353**(9148):227-31.

Upadhyaya A, Sheetz MP. 2004. Tension in tubulovesicular networks of Golgi and endoplasmic reticulum membranes. Biophys J **86**(5):2923-8.

Valentin N, Newman PJ. 1994. Human platelet alloantigens. Curr Opin Hematol **1**(5):381-7.

Vielreicher M, Harms G, Butt E, Walter U, Obergfell A. 2007. Dynamic Interaction between Src and C-terminal Src Kinase in Integrin IIbbeta3-mediated Signaling to the Cytoskeleton. J B C **282**(46):33623-31.

Vijayan KV, Bray PF. 2006. Molecular mechanisms of prothrombotic risk due to genetic variations in platelet genes: Enhanced outside-in signaling through the Pro33 variant of integrin beta3. Exp Biol Med (Maywood) **231**(5):505-13.

Vijayan KV, Goldschmidt-Clermont PJ, Roos C, Bray PF. 2000. The Pl(A2) polymorphism of integrin beta(3) enhances outside-in signaling and adhesive functions. J Clin Invest **105**(6):793-802.

Vijayan KV, Huang TC, Liu Y, Bernardo A, Dong JF, Goldschmidt-Clermont PJ, Alevriadou BR, Bray PF. 2003. Shear stress augments the enhanced adhesive

phenotype of cells expressing the Pro33 isoform of integrin beta3. FEBS Lett **540**(1-3):41-6.

Vijayan KV, Liu Y, Sun W, Ito M, Bray PF. 2005. The Pro33 isoform of integrin beta3 enhances outside-in signaling in human platelets by regulating the activation of serine/threonine phosphatases. J Biol Chem **280**(23):21756-62.

Vinogradova O, Velyvis A, Velyviene A, Hu B, Haas T, Plow E, Qin J. 2002. A structural mechanism of integrin alpha(IIb)beta(3) "inside-out" activation as regulated by its cytoplasmic face. Cell **110**(5):587-97.

Von dem Borne AE, Decary F. 1990. Nomenclature of platelet-specific antigens. Hum Immunol **29**(1):1-2.

Wagner CL, Mascelli MA, Neblock DS, Weisman HF, Coller BS, Jordan RE. 1996. Analysis of GPIIb/IIIa receptor number by quantification of 7E3 binding to human platelets. Blood **88**(3):907-14.

Walter DH, Schachinger V, Elsner M, Dimmeler S, Zeiher AM. 1997. Platelet glycoprotein IIIa polymorphisms and risk of coronary stent thrombosis. Lancet **350**(9086):1217-9.

Wang Y, Reheman A, Spring CM, Kalantari J, Marshall AH, Wolberg AS, Gross PL, Weitz JI, Rand ML, Mosher DF, Freedman J, Ni H. 2014. Plasma fibronectin supports hemostasis and regulates thrombosis. J Clin Invest **124**(10):4281-93.

Wegener KL, Partridge AW, Han J, Pickford AR, Liddington RC, Ginsberg MH, Campbell ID. 2007. Structural basis of integrin activation by talin. Cell **128**(1):171-82.

Weisel JW, Shuman H, Litvinov RI. 2003. Protein–protein unbinding induced by force: single-molecule studies. Curr Opin Struct Biol **13**(2):227-35.

Weiss EJ, Bray PF, Tayback M, Schulman SP, Kickler TS, Becker LC, Weiss JL, Gerstenblith G, Goldschmidt-Clermont PJ. 1996. A polymorphism of a platelet glycoprotein receptor as an inherited risk factor for coronary thrombosis. N Engl J Med **334**(17):1090-4.

Wilcoxon F. 1945. Individual Comparisons by Ranking Methods. Biometrics **1**(6):80-3.

Winkler J, Lünsdorf H, Jockusch BM. 1997. Energy-Filtered Electron Microscopy Reveals that Talin is a Highly Flexible Protein Composed of a Series of Globular Domains. European Journal of Biochemistry **243**(1-2):430-6.

Wright JH. 1906. The origin and nature of the blood plates. Old Corner Book Store, Boston.

Xiao T, Takagi J, Coller BS, Wang JH, Springer TA. 2004. Structural basis for allostery in integrins and binding to fibrinogen-mimetic therapeutics. Nature **432**(7013):59-67.

Xiong JP, Stehle T, Diefenbach B, Zhang R, Dunker R, Scott DL, Joachimiak A, Goodman SL, Arnaout MA. 2001. Crystal structure of the extracellular segment of integrin alpha Vbeta3. Science **294**(5541):339-45.

Xiong JP, Stehle T, Goodman SL, Arnaout MA. 2004. A novel adaptation of the integrin PSI domain revealed from its crystal structure. J Biol Chem **279**(39):40252-4.

Ye F, Hu G, Taylor D, Ratnikov B, Bobkov AA, McLean MA, Sligar SG, Taylor KA, Ginsberg MH. 2010. Recreation of the terminal events in physiological integrin activation. J Cell Biol **188**(1):157-73.

Zhu J, Luo BH, Xiao T, Zhang C, Nishida N, Springer TA. 2008. Structure of a complete integrin ectodomain in a physiologic resting state and activation and deactivation by applied forces. Mol Cell **32**(6):849-61.

Zimrin AB, Gidwitz S, Lord S, Schwartz E, Bennett JS, White GC, 2nd, Poncz M. 1990. The genomic organization of platelet glycoprotein IIIa. J Biol Chem **265**(15):8590-5.

Zlatanova J, Lindsay SM, Leuba SH. 2000. Single molecule force spectroscopy in biology using the atomic force microscope. Prog Biophys Mol Biol **74**(1-2):37-61.

Zotz RB, Klein M, Dauben HP, Moser C, Gams E, Scharf RE. 2000. Prospective analysis after coronary-artery bypass grafting: platelet GP IIIa polymorphism (HPA-1b/PIA2) is a risk factor for bypass occlusion, myocardial infarction, and death. Thromb Haemost **83**(3):404-7.

Zotz RB, Winkelmann BR, Müller C, Boehm BO, März W, Scharf RE. 2005. Association of polymorphisms of platelet membrane integrins αIIbβ3 (HPA-1b/PlA2) and α2β1 (α2807TT) with premature myocardial infarction. J Thromb Haemost **3**(7):1522-9.

Zotz RB, Winkelmann BR, Nauck M, Giers G, Maruhn-Debowski B, Marz W, Scharf RE. 1998. Polymorphism of platelet membrane glycoprotein IIIa: human platelet antigen 1b (HPA-1b/PlA2) is an inherited risk factor for premature myocardial infarction in coronary artery disease. Thromb Haemost **79**(4):731-5.

Zucker MB, Nachmias VT. 1985. Platelet activation. Arteriosclerosis **5**(1):2-18.

Zwaal RF, Bevers EM. 1983. Platelet phospholipid asymmetry and its significance in hemostasis. Subcell Biochem **9**:299-334.

APPENDIX 1 – Cloning strategy for plasmid production

The following strategy was followed to obtain αIIbmVenus, β3Leu33mCherry and β3Pro33mCherry plasmids: a CFP and a YFP tags were cloned downstream the pcDNA3αIIb and pcDNA3β3 plasmids, respectively. This cloning work was done by Intelechon (Germany). Due to problems related with the lost of expression of CFP by the HEK293 cells after stable transfection, more reliable fusion proteins were chosen and a new cloning strategy was applied by the Protein Purification Facility from Heinrich Heine University in Düsseldorf (Germany). The plasmid αIIbmVenus was cloned with the In-Fusion HD PCR Cloning Kit according to the manufacturer's protocol. At first the Hygromycin resistance gene replaced the neomycin resistance gene of the plasmid αIIb. The plasmid αIIb was linearized by PCR with the primer pair p10X-DelNEO-for and p10X-DelNEO-rev (Table A1.1). The hygromycin resistance gene was amplified by PCR (amplifying the plasmid containing the hygromycin coding sequence cloned downstream the CMV promoter in the pcDNA3.1(-) plasmid) with the primers Inf-Hyg-for and Inf-Hyg-rev (Table A1.1), both primers with a homology to the vector for the In-Fusion reaction. Sequencing confirmed the resulting plasmid αIIbHyg.

In the second step the replacement of the CFP tag to the mVenus tag was performed again with the In-Fusion reaction. The plasmid αIIbHyg was linearized by PCR with the primers p101-Tag-for and p101-Tag-rev (Table A1.1). The mVenus tag was amplified by PCR using mVenus-C1 as template and the primer pair Inf-mVenus-for and Inf-mVenus-rev (Table A1.1). Sequencing confirmed the resulting plasmid αIIbmVenus.

The plasmid β3mCherry was also cloned with the In-Fusion HD PCR Cloning Kit according to the manufacturer's protocol. At first the Zeocin resistance gene replaced the KAN/NEO resistance gene of the plasmid β3. The plasmid β3Pro33 was linearized by PCR with the primer pair p10X-DelNEO-for and p10X-DelNEO-rev. The Zeocin resistance gene was amplified by PCR applying the plasmid Zeocin with the primers Inf-Zeo-for and Inf-Zeo-rev (Table A1.1), both primers with a homology to the vector for the In-Fusion reaction. Sequencing confirmed the resulting plasmid β3Pro33Zeo. In the second step the replacement of the YFP tag to the mCherry tag was performed again with the In-Fusion reaction, the plasmid β3Pro33Zeo was linearized by PCR with the primers p106-Tag-for and p106-Tag-rev (Table A1.1). The mCherry tag was amplified by PCR using pcDNA3mCherry as template (Clontech Laboratories, Inc., USA) and the primer pair Inf-mCherry-for and Inf-mCherry-rev (Table A1.1). The plasmid β3Leu33mCherry derived from β3Pro33mCherry. The amino acid

residue Pro33 was replaced by Leu33 using site-directed mutagenesis (Kunkel, 1985) and primer pair p105-for and p105-rev (Table A1.1). The plasmids β3Leu33 and β3Pro33 (without fusion proteins) combined with αIIbmVenus (αIIbmVenusβ3Leu33 and αIIbmVenusβ3Pro33) were used as controls in the Förster/Fluorescence Energy Transfer assay. In initial fusion constructs, the length of the linker between the C-terminus of each subunit and the N-terminus of the corresponding fluorescent protein (mVenus or mCherry) was varied (Kim et al., 2003) and combinations of these constructs were tested in transiently transfected HEK293 cell by acceptor-photobleaching to determine optimal basal FRET efficiency. Accordingly, the construct containing a linker of 39 amino acids between αIIb (C-terminus) and mVenus (N-terminus) and a linker of 6 amino acids between β3Leu33 or β3Pro33 (C-terminus) and mCherry (N-terminus) was chosen.

Table A1.1 – Primers sequences used in the cloning strategy in order to obtain αIIbmVenus, β3Leu33mCherry and β3Pro33mCherry plasmids.

Plasmid	Primer name	Primer sequence (5´-3´)
αIIbmVenus	p10X-DelNEO-for	GCGGGACTCTGGGGTTCGAAATG
	p10X-DeNEO-rev	CATGCGAAACGATCCTCATCCTGTCTC
	Inf-Hyg-for	GGATCGTTTCGCATGGATAGATCCGGAAAGCCTGAAC
	Inf-Hyg-rev	ACCCCAGAGTCCCGCCTATTCCTTTGCCCTCGGACGAG
	p101-Tag-for	TCGAATTCTGCAGTCGACGGTAC
	p101-Tag-rev	AGCTTGCCGTAGGTGGCATC
	Inf-mVenus-for	GCCACCTACGGCAAGCTGACC
	Inf-mVenus-rev	CGACTGCAGAATTCGATTACTTGTACAGCTCGTCCATG
β3Pro33 mCherry	p10X-DelNEO-for	GCGGGACTCTGGGGTTCGAAATG
	p10X-DeNEO-rev	CATGCGAAACGATCCTCATCCTGTCTC
	Inf-Zeo-for	GGATCGTTTCGCATGGCCAAGTTGACCAGTG
	Inf-Zeo-rev	ACCCCAGAGTCCCGCTCAGTCCTGCTCCTCGG
	p106-Tag-for	TAAAGCGGCCGCGACTCTAGATCATAATC
	p106-Tag-rev	CATGGTGGCGACCGGTGGATC
	Inf-mCherry-for	CCACCGGTCGCCACCATGGTGAGCAAGGGCGAGGAG
	Inf-mCherry-rev	GAGTCGCGGCCGCTTTACTTGTACAGCTCGTCCATGCC
β3Leu33 mCherry	p105-for	GAGGCCCTGCCTCTGGGCTCACCTC
	p105-rev	GAGGTGAGCCCAGAGGCAGGGCCTC

Table A1.2 – Primers sequences used for sequencing αIIbmVenus and β3mCherry.

Plasmid	Primer name	Primer sequence (5´-3´)
αIIbmVenus	T7minus1	AATACGACTCACTATAGGG
	Seq-p101-I	TGGGACAAGCGTTACTGTG
	Seq-p101-II	GACCGGGATGGCTACAATG
	Seq-p101-III	TCGAGATGAGGCAGACTTC
	Seq-p101-IV	CAGCAGAAGAAGGTGAGAG
	Seq-p101-mVenus	GGCAACTAGAAGGCACAGTC
	pEGFP-RP	AACAGCTCCTCGCCCTTG
β3mCherry	pEGFP-FP	TTTAGTGAACCGTCAGATC
	Seq-p106-I	CTTGCCCATGTTTGGCTAC
	Seq-p106-II	GGCCTCAAGTCTTGTATGG
	Seq-p106-III	TGGCAGCTGTGTCTGTATC
	pEGFP_C2-RP	TTTAAAGCAAGTAAAACCTC

APPENDIX 2 - Solutions

Table A2.1 – Preparation of LB (Luria-Bertani) agar for bacterial growth (1 L of solution).

Reagent	Amount (g)	Concentration (M)
Bacto-trypton	10	-
NaCl	5	0.086
Yeast	5	-
Agar	15	-
Distilled water	to 1L	

Table A2.2 – Preparation of LB (Luria-Bertani) medium for bacterial growth (1 L of solution).

Reagent	Amount (g)	Concentration (M)
Bacto-trypton	10	-
NaCl	5	0.086
Yeast	5	-
Distilled water	to 1L	

Table A2.3 – Preparation of 1 x Lysis buffer (amount necessary for 5 ml of solution).

Reagent	Amount	Concentration (M)
1M TrisHCl (pH7.4) *(please see Table A2.4)*	100µl	0.02
1.5 M NaCl	500µl	0.15
10% Triton X-100	500µl	0.016 (1%)
5% Sodium deoxycholate	500µl	0.012(0.5%)
0.2 M EDTA	125µl	0.005
cOmplete, Mini EDTA-free Easypack	0.5 tablet	-
Water for chromatography	to 5L	-

Table A2.4 – Preparation of 1 M TrisHCl (pH7.4) (500 ml of solution).

Reagent	Amount (g)	Concentration (M)
Trizma® base (Sigma- Aldrich, USA)	60.57	1
Distilled water	to 500ml	

Using 1N HCl, adjust the pH to 7.4 and filter the solution through a 0.22 µm sterile filter

Table A2.5 – Preparation of separating gel (amount necessary for one gel) (15.11 ml).

Reagent	Volume	Concentration (M)
30% Acrylamide/0.8%Bisacrylamide	3.5ml	-
4xTrisHCl/SDS (pH8.8) *(please see Tab. A2.7)*	3.75ml	-
Distilled water	7.75ml	-
10% Ammoniumpersulfate (APS)	100µl	0.438
TEMED	10µl	-

Table A2.6 – Preparation of stacking gel (amount necessary for one gel) (5 ml).

Reagent	Volume	Concentration (M)
30% Acrylamide/0.8%Bisacrylamide	650µl	-
4xTrisHCl/SDS (pH6.8) *(please see Tab. A2.7)*	1.25ml	-
Distilled water	3.05ml	-
10% APS	50µl	0.438
TEMED	5µl	-

Table A2.7 – Preparation of 4xTrisHCl/SDS (pH6.8/pH8.8) (100 ml of solution).

Reagent	Amount	Concentration (M)
Trizma® base	6.05g	0.499
SDS pure	0.4g	0.014
Distilled water	to 100 ml	

Using 1N HCl, adjust the pH to 6.8 or 8.8 and filter the solution through a 0.45µm seringe fitable filter

Table A2.8 – Preparation of 5 x Running buffer (1 L of solution).

Reagent	Amount	Concentration (M)
Trizma® base	15.1g	0.125
Glycine	72g	0.959
SDS 20%	25ml	0.347
Distilled water	to 1L	

Table A2.9 – Preparation of 6xSample buffer.

Reagent	Amount	Concentration (M)
4xTrisHCl/SDS (pH6.8) *(please see Tab. A2.7)*	7.0 ml	-
Glycerol	3.0 ml	-
SDS pure	1 g	0.347
Dithiothreitol (DTT)	0.93 g	0.603
Bromophenol blue	0.0011 g	0.0002

Table A2.10 – Preparation of 10xTransfer buffer (500 ml of solution).

Reagent	Amount	Concentration (M)
Trizma® base	15.14g	0.143
Glycine	72g	1.918
Distilled water	to 500 ml	

Table A2.11 – Preparation of 1xTransfer buffer (1L of solution).

Reagent	Amount	Concentration (M)
10 x Transfer Buffer	100ml	-
Methanol	200ml	-
20% SDS	2.5ml	-
Distilled water	to 1L	

APPENDIX 3 - Manuscript submitted (Ref. JBC/2017/000558 from 21/10/2017)

The Pro33 (HPA-1b) variant of $\alpha_{IIb}\beta_3$ allosterically shifts the dynamic conformational equilibrium of the integrin towards an active state

Giulia Pagani[1], Joana P. V. Pereira[2§], Volker R. Stoldt[2§], Andreas Beck[3], Rüdiger E. Scharf[2,4#], and Holger Gohlke[1,5#*]

[1]Institute for Pharmaceutical and Medicinal Chemistry, Heinrich Heine University Düsseldorf, Düsseldorf, Germany
[2]Division of Experimental and Clinical Hemostasis, Hemotherapy and Transfusion Medicine, Institute of Transplantation Diagnostics and Cell Therapeutics, Heinrich Heine University Medical Center, Düsseldorf, Germany
[3]Institute of Informatics, Heinrich Heine University Düsseldorf, Düsseldorf, Germany
[4]Biological Medical Research Center, Heinrich Heine University Düsseldorf, Düsseldorf, Germany
[5]John von Neumann Institute for Computing (NIC), Jülich Supercomputing Centre (JSC) & Institute for Complex Systems - Structural Biochemistry (ICS 6), Forschungszentrum Jülich GmbH, Jülich, Germany

Running title: Allosteric changes of $\alpha_{IIb}\beta_3$ induced by the Pro33 variant

To whom correspondence should be addressed: Prof. Dr. Holger Gohlke, Institute for Pharmaceutical and Medicinal Chemistry, Heinrich Heine University Düsseldorf, Universitätsstr. 1, D-40225 Düsseldorf, Germany. Telephone: (+49) 211 81 13662; Fax: (+49) 211 81 13847; E-mail: gohlke@uni-duesseldorf.de or h.gohlke@fz-juelich.de

Keywords: Molecular dynamics, conformational changes, fluorescence resonance energy transfer (FRET), integrin, polymorphism, platelet, thrombus, structural dynamics, activation

[§]Current affiliation: Dept. of General, Visceral and Pediatric Surgery, Heinrich Heine University Medical Center & Faculty of Medicine, Heinrich Heine University Düsseldorf, Düsseldorf, Germany
[#]Share senior authorship

Abstract

The HPA-1 polymorphism of $\alpha_{IIb}\beta_3$ arises from a Leu→Pro exchange at residue 33 of the β_3 subunit, resulting in Leu33 (HPA-1a) or Pro33 (HPA-1b) isoforms. Clinical observations provided conflicting results, but some studies suggested an increased thrombogenicity of Pro33 platelets. Under flow-dynamic conditions, the Pro33 variant displays prothrombotic properties, characterized by increased platelet adhesion, aggregate/thrombus formation, and outside-in signaling. However, the molecular nature underlying this prothrombotic phenotype has remained elusive. As residue 33 in the genu is located > 80 Å away from extracellular binding sites or transmembrane domains, we hypothesized that the Leu→Pro exchange allosterically shifts the dynamic conformational equilibrium of $\alpha_{IIb}\beta_3$ towards an active state. We therefore performed multiple microsecond-long all-atom molecular dynamics simulations of the ectodomain of Leu33 and Pro33 isoforms. Our analyses provide evidence that the Leu→Pro exchange weakens inter-domain interactions at the genu and alters the structural dynamics of the integrin to a more unbent and splayed state. Upon FRET analysis of fluorescent proteins fused with $\alpha_{IIb}\beta_3$ in transfected HEK293 cells, the Pro33 variant in its resting state displays a lower energy transfer than the Leu33 isoform. This finding is indicative of a larger spatial separation of the cytoplasmic tails in the Pro33 variant. Together, our results demonstrate that the Leu→Pro exchange allosterically shifts the dynamic conformational equilibrium of $\alpha_{IIb}\beta_3$ to a structural state closer to the active one. This may promote reaching the fully active state and foster the prothrombotic phenotype of Pro33 platelets.

Introduction

Integrins are heterodimeric cell adhesion receptors formed of α and β subunits. Each subunit is divided into three parts: a large extracellular domain (ectodomain), a single-pass transmembrane domain (TMD), and a short cytoplasmic tail connecting the extracellular to the intracellular environment (1). In addition to their biomechanical role (2), integrins transmit signals allosterically (3) in both directions across the membrane (termed "outside-in" and "inside-out" signaling) by binding to intra- and extracellular components (4). In the present study, we focused on $\alpha_{IIb}\beta_3$ (5-8), which is expressed on the platelet surface and essential for platelet aggregation (8).

The ectodomain can be divided into two parts (9,10). The "head" of the receptor is formed by the propeller and βA domains, and the "legs" are formed by the thigh and CALF domains (α_{IIb} subunit) as well as EGF domains together with the β-tail domain (β_3 subunit) (4). The genu located between the thigh and CALF-1 domain as well as the EGF-1 and EGF-2 domains in the α_{IIb} and β_3 subunits, respectively, forms a region of interdomain flexibility (11). Integrin structural dynamics is characterized by at least three states: a closed, bent, low-affinity one; a closed, extended, low-affinity one; and an open, extended, high affinity one (12). Although the magnitude of conformational changes has remained a matter of discussion (6,10,13), the majority of crystal structures of $\alpha_v\beta_3$ (14), $\alpha_{IIb}\beta_3$ (9), and $\alpha_x\beta_2$ (15) integrins show their ectodomain in a bent conformation (14,16,17). Here, the head is flexed towards the membrane at an angle of 135° (7) related to the legs, with the genu being the angle's vertex.

According to current models, the genu plays a critical role in conformational transitions between the three structural states, as a straightening in the genu region leads to a separation of the head from the legs and thus an unbending of the conformation. This motion is associated with reduced interactions between the two subunits, resulting in a spatial separation ("splaying") of the α and β subunit legs (18). With respect to our study, the role of the plexin-semaphorin-integrin domain (PSI), being part of the β_3 genu (5), is of particular interest in integrin activation. Located > 80 Å away from the extracellular binding site and > 90 Å away from the membrane (estimated from PDB ID 3FCS), the domain's involvement in integrin activation has been proven (19,20). Specifically, the domain is believed to have a biomechanical role in the allosteric signal transmission across the structure (21).

The human platelet antigen-1 (HPA-1) polymorphism of the β_3 gene of $\alpha_{IIb}\beta_3$ arises from a Leu→Pro exchange at residue 33 of the mature β_3 subunit (22,24), resulting in Leu33 (HPA-1a) or Pro33 (HPA-1b) platelets. This amino acid exchange, located within the PSI domain, leads to an inherited dimorphism that can be of clinical relevance (22). For example,

the HPA-1b allele was significantly more frequent among young patients with acute coronary syndrome than among age-matched healthy subjects (23). In the LURIC trial, an association study including more than 4,000 individuals, we documented that patients with coronary artery disease (CAD)[1], who are carriers of the HPA-1b allele, experience their myocardial infarction five years earlier in life than CAD patients who are HPA-1b negative (22,24). In a prospective study on CAD patients undergoing saphenous-vein coronary-artery bypass grafting, we demonstrated that HPA-1b is a hereditary risk factor for bypass occlusion, myocardial infarction, or death after coronary-artery bypass surgery (25). These results suggest that the Leu→Pro exchange may modulate functional properties of $\alpha_{IIb}\beta_3$, resulting in a prothrombotic integrin variant. Prothrombotic properties are also displayed by Pro33 platelets under flow-dynamic conditions (26). However, the molecular mechanism underlying the suggested prothrombotic phenotype of the Pro33 (HPA-1b) variant has remained elusive.

We hypothesized that the Leu→Pro exchange allosterically shifts the dynamic conformational equilibrium of $\alpha_{IIb}\beta_3$ towards an active state. This, in turn, would facilitate reaching the fully active state in the presence of integrin ligands. To examine this hypothesis, we performed multiple microsecond-long all-atom molecular dynamics (MD) simulations of the ectodomain and Förster resonance energy transfer (FRET) measurements of $\alpha_{IIb}\beta_3$-transfected HEK293 cells expressing either isoform, Leu33 (HPA-1a) or Pro33 (HPA-1b). Our MD simulations provide evidence that the Leu→Pro exchange weakens inter-domain interactions at the genu and alters the structural dynamics of the integrin to a more unbent and splayed state, resulting in overall conformational changes that have been linked to integrin activation (18,27). In accord with these results, FRET analyses of $\alpha_{IIb}\beta_3$ transfectants reveal that the Pro33 (HPA-1b) variant in the resting state displays a significantly lower energy transfer than the Leu33 (HPA-1a) variant.

Results

Platelet thrombus size in relation to $\alpha_{IIb}\beta_3$ HPA-1 isoforms under flow conditions in vitro

Given the prothrombotic phenotype of Pro33 platelets, we initially focused on platelet thrombus formation under arterial flow conditions comparing Leu33 (HPA-1a) with Pro33 (HPA-1b) platelets. To study the dynamics of platelet thrombus formation, mepacrine-labeled citrated whole blood from healthy volunteers genotyped for HPA-1 of $\alpha_{IIb}\beta_3$ and α_2C807T of $\alpha_2\beta_1$ was perfused at shear rates $> 500\ s^{-1}$ through a flow chamber coated with collagen type I. Image acquisition was achieved by a series of stacks corresponding to confocal sections from the bottom to the apex of forming platelet thrombi. For quantitation of thrombus formation *in vitro*, we applied a voxel-based method for 3D visualization of real time-resolved volume data, using the ECCET software (www.ECCET.de) (28). As depicted in **Fig. 1A**, ECCET allows determination of the number, bottom area, height, and volume of single platelet thrombi formed *in vitro*.

Using these tools, we detected that, upon perfusion over 10 min, platelets homozygous for Pro33 (HPA-1b) formed single thrombi that were significantly higher than those of platelets homozygous for Leu33 (HPA-1a) (**Fig. 1B**). This difference in mean single thrombus volume was due to an increased thrombus height, whereas the number and bottom area of thrombi (**Fig. 1C**) did not differ between the HPA-1 isoforms. Platelet adhesion and subsequent aggregate/thrombus formation under flow were abrogated by the monoclonal antibody LJ-Ib1 (a gift from Dr. Z.M. Ruggeri, La Jolla, CA, USA) that completely inhibits binding of von Willebrand factor (VWF) to the platelet glycoprotein (GP) Ib-IX-V complex or by the monoclonal antibody 5C4 (a gift from Dr. M. Gawaz, Tübingen, Germany) that blocks the platelet collagen receptor GPVI (data not shown). As depicted in the schematic illustration (**Fig. 1D**), with increasing time, the flow path of the perfusion chamber becomes narrowed, as the thrombi are growing. Consequently, shear rates gradually increase, and formed platelet thrombi, especially at their apex, are exposed to higher shear than initially applied. Thus, the difference in mean single thrombus volumes between the HPA-1 isoforms can be indicative of a higher thrombus stability of Pro33 (HPA-1b) than Leu33 (HPA-1a) platelets, as reported before (29).

Structural variability of $\alpha_{IIb}\beta_3$ HPA-1 isoforms in MD simulations of the integrin ectodomain

To provide an atomistic view on the effect of the Leu→Pro exchange, the Leu33 (HPA-1a) and Pro33 (HPA-1b) isoforms were investigated by all-atom MD simulations, using the respective integrin ectodomains in the bent conformation as starting structures. Three independent MD simulations of 1 μs length each were carried out. The convergence of the MD simulations was tested by computing the root-mean-square deviation (RMSD) average correlation (RAC), as described in ref. (30) (**Fig. S1**). The RAC is a measure of the time scales, on which structural changes occur in MD simulations. From the bumps in the curves, we can estimate that observed structural changes occur within ~50 - 200 ns. For time intervals > 200 ns, the curves are smooth, suggesting that no large structural changes happen during the investigation period. The analyses are indicative of the extent, by which the conformational ensembles of examined ectodomain structures are converged. Unless stated otherwise, all results of the MD simulations are expressed as means over the respective simulations from the last 800 ns of simulation time.

The structural similarity of the conformations obtained by MD simulations with respect to the starting structure was explored in terms of the RMSD of C_α atoms after a mass-weighted superimpositioning. Similarly to our previous MD studies performed on integrin $\alpha_5\beta_1$ (18,27), the simulations revealed minor structural changes of the single domains, as mirrored by RMSD values that were largely below 3 Å, with the exception of the highly flexible β-tail (14) (RMSD up to ~ 5 Å) (**Table S3**, **Fig. S2**). In contrast, when aligning only the head region, the mean RMSD increased up to ~ 21 Å (**Table S4**, **Fig. S3**), with the highest values found for the CALF-2 and β-tail domains of the legs. Hence, these larger structural changes must arise from relative movements of the domains (or subunits) with respect to each other, considering that the single domains were structurally rather invariant. Comparing both isoforms of $\alpha_{IIb}\beta_3$, a larger mean RMSD (~ 9.5 Å) was found for Pro33 than Leu33 (~ 7.3 Å) (in both cases, SEM < 0.1 Å) (**Fig. 2A**). In accord with that, the mean radius of gyration (R_{og}) of the overall structure was larger for the Pro33 (~ 40.3 Å) than the Leu33 isoform (~ 39.7 Å) (in both cases, SEM < 0.01 Å) (**Fig. 2A**, **Table S5**). Taken together, the sampled conformational space of both $\alpha_{IIb}\beta_3$ isoforms varied significantly ($p < 0.001$) with respect to the difference of the mean values of these structural parameters. To conclude, the Pro33 variant displayed significantly larger structural deviations from the starting bent structure and became less compact than the Leu33 isoform during MD simulations.

Conformational changes of the ectodomains of $\alpha_{IIb}\beta_3$ HPA-1 isoforms towards a more open, extended conformation

To further characterize the structural differences between the $\alpha_{IIb}\beta_3$ isoforms, we monitored geometric parameters along the MD trajectories that have been linked with conformational changes of the ectodomain from an inactive to an active state (18,27) (**Table S6**).

First, we investigated possible variations in the region of the center of helix α1 and the N-terminus of helix α7 (27,31). This region was shown to form a "T-junction" upon activation (21,27). We computed the kink angle of helix α1 (**Fig. 2B**), which revealed a mean value over three MD trajectories that is larger by 15° in the Pro33 (~ 154°) than the Leu33 isoform (~ 137°) (SEM ~ 0.1°) (**Fig. 2C**). Hence, helix α1 straightens more in Pro33 and thus shows a stronger tendency to form the "T-junction" than in Leu33. The bimodal distribution found for Pro33 (**Fig. 2B**) resulted from a rapid and pronounced increase of the kink angle, which was initially ~ 143° (calculated from PDB ID 3FCS) within the first 200 ns in two of the three MD simulations (**Fig. S4A**).

Second, we evaluated the unbending of the structure in terms of the separation of the head region and the terminal part of the legs (CALF-2 domain and β-tail) (**Fig. 2D**). Furthermore, we monitored the spatial separation ("splaying") of the integrin's legs (**Fig. 2F**). Similar parameters were successfully used previously (18). The bending angle was ~ 6° larger in the Pro33 (50°) than in the Leu33 isoform (~ 44°) (in both cases, SEM < 0.01°; $p < 0.001$) (**Fig. 2E**, **Fig. S4B**). The difference remained significant ($p < 0.05$) when one MD trajectory of the Pro33 variant was excluded from the analysis that showed the largest values of the bending angle **(Table S6)**. The splaying angle was ~ 3° larger in Pro33 (~ 28°) than in Leu33 (~ 25°) (in both cases, SEM < 0.01°; $p < 0.001$) (**Fig. 2G**). In the latter

case, in two MD simulations, the time evolution of the splaying angle revealed a decrease of ~22° within the last 200 ns of the simulation (**Fig. S4C**), yielding a bimodal distribution (**Fig. 2G**). As additional indicators of structural changes, we evaluated the opening of the structure in terms of changes in internal distances between the N- and C-terminus of each subunit and between the C-terminus of the two subunits (**Fig. S4E**). The differences between distances in the Leu33 and Pro33 isoforms were significant in all cases ($p < 0.001$) (**Fig. S4D**). To conclude, our results revealed significant differences in the conformational states of both $\alpha_{IIb}\beta_3$ isoforms, with the ectodomain of Pro33 displaying a stronger tendency to move towards the extended conformation with more splayed legs.

Experimental evidence for spatial rearrangements of the cytoplasmic tails of $\alpha_{IIb}\beta_3$ upon Leu→Pro exchange

To investigate a possible influence of the Leu→Pro exchange on the spatial separation of α and β subunits, we performed FRET acceptor photobleaching (APB) analyses in individual cells transfected with α_{IIb}mVenus and β_3Leu33mCherry (HPA-1a) or β_3Pro33mCherry plasmids (HPA-1b), respectively. Using FRET, the spatial separation of the subunits is inferred from the amount of energy transferred between the fluorescent proteins mVenus and mCherry attached to the cytoplasmic tails of the subunits.

By fluorescence microscopy performed 48 h after transfection, we verified that both subunits were co-localized at the cell membrane (**Fig. 3A**). Concordant with the presence of the integrin at the plasma membrane, we detected the complete $\alpha_{IIb}\beta_3$ receptor (recognized by a complex-specific anti-$\alpha_{IIb}\beta_3$ antibody, anti-CD41, clone MEM-06) by flow cytometry. Functional integrity of both integrin isoforms and correct membrane insertion were documented by intact activation of $\alpha_{IIb}\beta_3$ in transfected cells upon phorbol 12-myristate 13-acetate (PMA)-induced stimulation of protein kinase C and specific binding of Alexa647 fibrinogen (Fg) to $\alpha_{IIb}\beta_3$ upon inside-out activation (32). Notably, flow cytometry measurements of CD41 expression upon five independent transfection experiments indicated that the $\alpha_{IIb}\beta_3$ levels expressing either the Leu33 (HPA-1a) or Pro33 (HPA-1b) isoform differed by ≤ 10% between each other (**Fig. 3B**).

Using these transfectants, photobleaching of mCherry at 561 nm on a defined cellular region (region of interest, ROI) encompassing part of the cell membrane led to a complete loss of energy transfer and, consequently, to an increase in mVenus fluorescence intensity (**Fig. 3C**). For control, cells transfected with α_{IIb}mVenus and β_3Leu33 or β_3Pro33 plasmids (without mCherry) were used, a condition that abrogated any energy transfer (data not shown). To focus on non-activated $\alpha_{IIb}\beta_3$-tranfectants, as evidenced by absent binding of Alexa647 Fg or PAC1, an activation-dependent anti-$\alpha_{IIb}\beta_3$ monoclonal antibody (data not shown), cells were left resting on chamber slides with culture medium for 24 h prior to FRET analyses, all of which were subsequently carried out with minimal manipulation of the cells to prevent any possible cellular activation.

FRET-APB analyses were performed in a total of 249 single cells: 91 Leu33 cells, 88 Pro33 cells, 35 Leu33 donor control cells, and 35 Pro33 donor control cells. FRET-APB efficiency was computed according to equation 2 (see **Experimental Procedures**; (33,34)). Notably, FRET-APB efficiency between mVenus and mCherry in Leu33 cells (mean ± SEM, 18.20 ± 0.276) was significantly higher ($p < 0.0001$) than in HPA-1b cells (15.74 ± 0.395) (**Fig. 3D**). This difference in energy transfer upon photobleaching of both $\alpha_{IIb}\beta_3$ isoforms suggested a larger spatial separation in the Pro33 than the Leu33 isoform, when both isoforms are examined in their bent conformation. This observation is indicative of a state more prone to activation as a consequence of the Leu→Pro exchange at residue 33 in the ectodomain of the β subunit of $\alpha_{IIb}\beta_3$.

Short- and mid-range structural, dynamics, and stability changes induced by the Leu→Pro exchange

The two-dimensional (2D) RMSD of C_α atoms of the EGF-1/EGF-2/EGF-3 domains along the MD trajectories was computed after mass-weighted superimposition onto the respective starting structures of the domains. The 2D RMSD values indicated that the domains showed larger differences from the initial starting structure in the Pro33 than the Leu33 isoform (see also **Table S3**) but also that the two isoforms adopted conformational states that largely deviated from each other (RMSD up to 8

Å) **(Fig. 4A)**. Next, we computed the residue-wise root-mean-square fluctuations (RMSF) of the PSI domain, a measure of atomic mobility, to identify differences in the conformational variations associated with the Leu→Pro exchange. The results revealed a marked increase in atomic mobility for residues Glu29 to Pro37 of the loop between strands A and B in the PSI domain (**Fig. 4B**), with a significant difference ($p < 0.05$) found at residue 33 (Leu or Pro). Beyond this region, the amino acid exchange did not affect the atomic mobility (**Fig. 4B)**. Likewise, we did not detect significant differences in the secondary structure propensity of the AB loop residues between the Leu33 and Pro33 isoform, except for a small decrease of the α-helix propensity in the helix C-terminal to the loop (**Fig. S5**). To conclude, in both isoforms, the PSI domain did not undergo marked changes in structure (see also **Table S3**) as a consequence of the polymorphism at residue 33 of the β_3 subunit. This was in contrast to the EGF domains, which revealed marked structural changes in Pro33. However, the structural dynamics of the AB loop of the PSI domain increased in the Pro33 variant.

As this loop faces the EGF-1 and EGF-2 domains (35), the Leu→Pro exchange may also impact the structure, interactions, and stability of this interface. Therefore, we monitored the time evolution of the distance between the C_α atoms of residues Leu33 or Pro33 with Ser469 and Gln481 to investigate how compact the interface between the PSI domain and the EGF-1 / EGF-2 domains is **(Fig. 4C)**. In the bent conformation of $\alpha_{IIb}\beta_3$, the C_α atom at residue 33 is separated by 9.4 Å and 15.8 Å from the C_α atoms of Ser469 and Gln481 (estimated from the PDB ID 3FCS), respectively.

Comparing both isoforms of $\alpha_{IIb}\beta_3$, we found a mean value for the Leu33Pro···Ser469 distance that is smaller by ~ 3.6 Å in Leu33 (~ 8.0 Å) than in Pro33 (~ 11.6 Å) (SEM < 0.1 Å). A mean value smaller by ~ 5.6 Å in Leu33 (~ 6.4 Å) than in Pro33 (~ 12.0 Å) (SEM < 0.1 Å) was found for the Leu33Pro···Gln481 distance (**Fig. 4D**). The pronounced decrease from the initial structure observed in the L33 isoform (~ 9 Å) for the Leu33···Gln481 distance is in line with the description of a contact area between these two domains in the closed, low-affinity, bent state (35). This contact is lost in the extended conformation (35). These results indicated that the interface between the PSI domain and the EGF-1 / EGF-2 domains is more tightly packed in the Leu33 than the Pro33 isoform.

In addition, we computed the number of contacts present in the starting structure ("native contacts") and those formed over the course of the MD simulations ("non-native contacts"). Contacts were evaluated between the nine residues of the AB loop and residues of the adjacent EGF-1 and EGF-2 domains, applying a distance cut-off of 7 Å between the side chain atoms. In all three MD simulations of the Pro33 variant, the total number of contacts was ~ 20% lower than in the Leu33 isoform (**Fig. 5A**). This difference became even more pronounced when only non-native contacts were considered (2-fold decrease). The same holds true for specific interactions (hydrogen bonds and salt bridges) that were conserved in the Leu33 isoform only (**Fig. S6**). In the segment connecting the EGF-1 domain with the EGF-2 domain, Gln481 is hydrogen-bonded to Ser469 with a high occupancy (~ 70% along the MD trajectories) and/or with Gln470 (~ 27%). Additional stable intra-domain hydrogen bond interactions (> 60%) were found within the EGF-2 domain, which involve Cys492 that also forms a disulfide bridge with Cys473 of the EGF-1 domain (**Fig. S6**). To conclude, the Leu→Pro exchange leads to a less compact interface between the PSI domain and EGF-1 / EGF-2 domains. Moreover, fewer interactions across the interface and within the EGF-1 / EGF-2 domains were found in the Pro33 variant compared with the Leu33 isoform.

Changes in structural stability of the EGF domains occur at long range from residue 33

To analyze changes in the structural stability of the interface between the PSI domain and EGF-1 / EGF-2 domains resulting from the Leu→Pro exchange, we performed Constraint Network Analysis (CNA) on the β_3 leg (hybrid domain/PSI and EGF domains) of both $\alpha_{IIb}\beta_3$ isoforms, Leu33 or Pro33. In CNA, (36), a molecular system is represented as a network of nodes (atoms) connected by constraints (non-covalent bonds). This network is analyzed applying rigidity theory (37), revealing rigid (i.e., structurally stable) clusters and flexible links in between (38). By rigidity analysis, long-range effects on the stability of distant structural parts due to a local structural change can be detected (39). Performing a constraint dilution

simulation (40), a stability map (41) rc_{ij} (with i, j being residue numbers) is obtained that reports on the hierarchy of structural stability of the molecular system. The difference stability map calculated as rc_{ij}(Leu33) – rc_{ij}(Pro33) then reports on the influence on structural stability due to the Leu→Pro exchange (blue (red) colors in **Fig. 5B, C** indicated residues that were less stable in the Leu33 (Pro33) isoform, respectively). The AB loop (**Fig. 5B, C**) showed a local increase in structural stability, which results from the overconstrained five-membered ring of Pro33 compared to the flexible side-chain of Leu33 (42). By contrast, the loop connecting the EGF-1 to the EGF-2 domain and pointing towards the AB loop (21), which is > 15 Å apart from residue 33, became less stable in the Pro33 variant **(Fig. 5B, C**; the segment formed by residues Ser469 – Gln481 is highlighted). The EGF-3 domain, although not directly interacting with the PSI domain, has been suggested to be important for keeping the integrin in its bent conformation (20). Residues Gly519-Cys536 of the EGF-3 domain > 30 Å apart from residue 33 became less structurally stable in the Pro33 variant. To conclude, the Leu→Pro exchange leads to long-range decreases in the structural stability of the EGF domains.

Discussion

In this study, we verified the hypothesis that the Pro33 variant of $\alpha_{IIb}\beta_3$ allosterically shifts the dynamic conformational equilibrium of the integrin towards a more active state. This finding can provide an explanation for the prothrombotic phenotype of Pro33 platelets that has been suggested in several clinical association studies (22-25) but also in experimental settings (26,32,43).

Both clinical and laboratory data regarding a possible impact of the HPA-1 polymorphism of $\alpha_{IIb}\beta_3$ on modulating platelet function have been discussed controversially. Specifically, it has been debated whether or not the Leu→Pro exchange at residue 33 of the β_3 subunit induces an increased thrombogenicity of Pro33 platelets. We therefore studied initially the dynamics of platelet thrombus formation, using a collagen type I matrix in an established perfusion system, simulating arterial flow conditions. Quantitation of thrombus growth *in vitro* demonstrated that the mean volume of single thrombi formed by Pro33 platelets is significantly higher than that of the Leu33 platelets **(Fig. 1)**. The initial adhesion of circulating platelets with a collagen matrix is complex, involving platelet capture ("tethering") by immobilized VWF via GPIbα of the platelet GPIb-IX-V complex, subsequent GPIb-IX-V-dependent signaling, and direct interaction with collagen via $\alpha_2\beta_1$ and GPVI, the platelet collagen receptors, inducing platelet activation (44,45). To block some of these interactions, we therefore used specific monoclonal antibodies such as LJ-Ib1 that completely inhibits VWF binding to the platelet GPIb-IX-V complex or 5C4 that blocks the platelet GPVI receptor (data not shown). The expression of $\alpha_2\beta_1$ on the platelet surface is genetically controlled and modulated by nucleotide polymorphisms in the α_2 gene (46). Moreover, since the $\alpha_2$807TT genotype of $\alpha_2\beta_1$ has also been suggested to be a prothrombotic integrin variant (22), volunteers of this series of experiments were carefully selected by recruiting only carriers of the $\alpha_2$807CC genotype.

A specific feature of the experiments summarized in **Fig. 1** is that the difference in single thrombus volumes between Pro33 and Leu33 platelets is due to differences in apical thrombus growth **(Fig. 1B)**. This is remarkable, especially since apical thrombus segments become exposed to increasing shear over time, exceeding an initial wall-near shear rate of 500 s^{-1} **(Fig. 1D).** Our finding is indicative of a higher thrombus stability of Pro33 than Leu33 platelets, as reported before (29). By contrast, considering the fact that neither the number nor the bottom area of formed thrombi differ between both isoforms of $\alpha_{IIb}\beta_3$, it appears rather unlikely that the initial adhesive interactions between the collagen matrix and platelets under flow had a significant effect on the results.

Assuming that the difference in thrombus volumes between both $\alpha_{IIb}\beta_3$ isoforms is indeed due to increased thrombus stability in the Pro33 variant, it would be an attractive assumption that the Leu→Pro exchange has an impact on the mechanotransduction mediated by the integrin. Such a contention is in line with previous observations, documenting a significantly more stable adhesion of Pro33 than of Leu33 platelets onto immobilized fibrinogen at shear rates ranging from 500 to 1,500 s^{-1} (26). Moreover, it has been shown that the Pro33 variant displays increased outside-in signaling (47). These

findings suggest that the HPA-1 polymorphism of $\alpha_{IIb}\beta_3$ modulates the function and activity of the integrin.

However, the molecular nature underlying this modulation has remained elusive so far. In this context, a marked concern has been in the past that the point mutation at residue 33 of the β_3 subunit is located > 80 Å away from relevant functional domains of $\alpha_{IIb}\beta_3$ such as extracellular binding sites or transmembrane domains. Conversely, due to its distant location, it appears quite appropriate to exclude that the Leu→Pro exchange would directly influence interactions with ligands at the extracellular or even intracellular binding sites. It is more likely that an increased activity of $\alpha_{IIb}\beta_3$ results from a change in the structural dynamics of the integrin. To probe this assumption, we have performed microsecond-long MD simulations on the ectodomains of both $\alpha_{IIb}\beta_3$ isoforms, Leu33 and Pro33. The ectodomains of either isoform initially only differed in the side-chains of residue 33.

Ectodomains of integrins have been successfully used in previous studies by us (18,27) and others (48,49) as model systems to explore possible influences of structure and solvent on integrin activation. The present simulations were started from the bent conformation with closed legs as present in the crystal structure (50), representing a low-affinity, inactive state of the integrin (51). As depicted, our simulation findings reveal that the Pro33 variant displays significantly larger structural deviations from the bent starting structure and becomes less compact than the Leu33 isoform **(Fig. 2)**. Furthermore, we evaluated geometric parameters within the βA domain ("T-junction formation" between helices α1 and α7, **Fig. 2B, C**) and variables characterizing the bending and splaying of the structure **(Fig. 2D, E, F, G)**, which had been used successfully in related studies to characterize inactive-to-active transitions (27,31,52). The results display significant differences in the conformational states of both isoforms of $\alpha_{IIb}\beta_3$, with the ectodomain of the Pro33 variant showing a stronger tendency to move towards an open, extended conformation with more splayed legs than the Leu 33 isoform. The results are consistent across three independent MD simulations for each isoform. This demonstrates the robustness of our approach. We are aware that the magnitudes of the changes of the bending or splaying angles do not correspond to those described for a fully open, extended ectodomain conformation (8). However, in consideration of the simulation times used here, this finding is in complete accord with the timescale of integrin activation in the absence of biomechanical forces, ranging from microseconds to seconds (49,53).

As an independent approach to explore the impact of the Leu→Pro exchange on the structural dynamics of full-length $\alpha_{IIb}\beta_3$ integrin, FRET measurements on α_{IIb}mVenus and β_3Leu33mCherry or β_3Pro33-mCherry transiently co-transfected in HEK293 cells were performed **(Fig. 3A-C)**. HEK293 cells have previously been shown to be a suitable cellular model for functional studies involving $\alpha_{IIb}\beta_3$ (54,55). The transfectants display a significantly higher efficiency of energy transfer between the α and β subunit in the Leu33 than the Pro33 isoform. This difference is indicative of a smaller spatial separation between the cytoplasmic tails of the Leu33 isoform in its resting state. Conversely, the lower energy transfer obtained in the Pro33 variant is reflecting a larger spatial separation of its cytoplasmic domains that is already present in the resting state **(Fig. 3D)**. This observation is in good agreement with the findings of the MD simulations.

Taken together, both the MD simulations and FRET experiments reveal structural changes in the ectodomain of $\alpha_{IIb}\beta_3$ or the full-length integrin for the Pro33 variant that relate to a conformational change from a closed, bent structural state with closed legs to a more open, extended state with splayed legs. According to current models (14,16,56) such a conformational change is required for integrin activation. Considering that in both the MD simulations and FRET measurements the integrin—has been examined in the resting state, our results provide evidence that the Leu→Pro exchange can shift the dynamic conformational equilibrium of $\alpha_{IIb}\beta_3$ in such a way that a structural state more similar to the active conformation is present.

The effect of the Leu→Pro exchange appears to have some similarity to stimulatory monoclonal antibodies, which have been suggested to shift the dynamic conformational equilibrium in favor of those forms that lead to an increase in the proportion of a high-affinity integrin (50). As the effect induced by the amino acid substitution

manifests in regions far away from the mutation site, the influence of the Leu→Pro exchange must be allosteric. Our results clearly go beyond a previous study (57) that used MD simulations of the β_3 subunit only to investigate possible effects of the HPA-1 polymorphism on the structure of the β_3 subunit.

To explore a possible mechanism of how the Leu→Pro exchange exerts an allosteric effect, applying MD simulations and rigidity analyses, we examined short- and mid-range structural, dynamics, and stability changes in the PSI domain and neighboring domains. Although the overall architecture of the PSI domain remains largely unchanged by the amino acid substitution, particularly the EGF domains show marked structural alterations in the Pro33 variant **(Fig. 4)**. The EGF-1 and EGF-2 domains, although sequentially distant from the mutation located at residue 33, are spatially close to the AB loop of the PSI domain in the bent state, which carries the HPA-1 polymorphism (5,19,21). Parts of the AB loop are significantly more mobile in the Pro33 variant **(Fig. 4B)**. Related to these changes, our analyses reveal that the Leu→Pro exchange leads to a less compact interface between the PSI domain and EGF-1 / EGF-2 domains **(Fig. 4C, D)**. Specifically, fewer native and non-native contacts are formed across the interface and within the EGF-1 / EGF-2 domains in the Pro33 variant than the Leu33 isoform **(Fig. 5A)**. These conformational and dynamic alterations are related to a change in the structural stability of the EGF-1 and EGF-2 domains, which percolates from the interface region through these domains **(Fig. 5B,C)**.

Notably, similar changes in these regions have been related to integrin activation before. For example, the displacement of the PSI domain of about 70 Å, described to act as a mechanical lever upon outside-in signaling (21), alters the interface formed with the EGF-1 and EGF-2 domains (58). Furthermore, activating mutations have been identified in the N-terminal part of the PSI domain, the EGF-2 domain, and parts of the EGF-3 domain of $\alpha_x\beta_2$ integrin (20). These regions are thought to form the area of contact between α and β subunits in the bent conformation. Finally, when generating integrin chimera by combining α and β subunits from different species, direct interactions between the subunits could not be formed, and the integrin did no longer appear locked in the closed conformation (20).

The results of this study provide an explanation for the prothrombotic phenotype of the Pro33 variant of $\alpha_{IIb}\beta_3$. Specifically, the shift of the dynamic conformational equilibrium of the Pro33 variant─towards an active state may promote a fully active state in the presence of immobilized adhesive ligands such as fibrinogen or VWF and, consequently, favour outside-in signaling. This, in turn, may facilitate and accelerate platelet aggregation and subsequent formation of stable platelet thrombi. Our results, thus, lend support to previous clinical (22-25,29,43) and experimental findings (26,29,32,43) suggesting that the Leu→Pro exchange confers prothrombotic properties to $\alpha_{IIb}\beta_3$.

Experimental procedures

Parallel plate flow chamber. A custom-made rectangle flow chamber was used (flow-channel width 5 mm, height 80 µm, length 40 mm). Glass cover slips forming the lower surface of the chamber were glutted by flame, cooled down, and coated with 0.04 µml/mm^2 collagen type S (concentration 3 mg/ml) containing 95 % type I and 5 % type III collagen (Roche, Mannheim, Germany). The perfusion system was flushed and filled with PBS buffer (pH = 7.3) containing 2% BSA to block unspecific adhesion onto the glass-slide. A syringe pump (Harvard Apparatus Inc. Holliston, MA, USA) was used to aspirate mepacrine-labeled citrated whole blood through the flow chamber for 10 min at a constant flow rate of 9.6 ml h^{-1}, producing an initial wall-near shear rate of 500 s^{-1}.

Labeling of platelets. Platelets were stained in whole blood by direct incubation with the fluorescent dye mepacrine (quinacrine dihydrochloride; 10 µM final concentration). Although this dye also labels leukocytes, these cells could be readily distinguished from platelets by their relatively large size and sparsity; moreover, leukocyte attachment to the surface tested was negligible under the conditions used. Mepacrine accumulates in the dense granules of platelets and had no effect on normal platelet function at the concentration used. Platelet secretion after adhesion did not prevent their visualization. Furthermore,

mepacrine did not affect platelet adhesion or platelet aggregate/thrombus formation.

Picture acquisition and digital image processing. The fluorescence signal of mepacrine-stained platelets was detected by a Zeiss Axiovert 100M / LSM 510 confocal laser scanning microscope. During the flow period of 10 min, 25 stacks of images were acquired. One stack consisted of 30 slices with a height of 30 µm. Digitized images had a standard size 512 x 512 pixels and an optical resolution of 1 µm.

Volumetry of single platelet thrombi. The stacks were reconstructed 3-dimensionally and analyzed with the custom-made software package ECCET (www.eccet.de). The software integrated the slices of every stack and divided the 3-dimensional space into multiple "voxel" (3-dimensional equivalent to a pixel). All fluorescence signals were smoothened by a separate linear Gaussian filter in all 3 planes (Filter sigma 2). Voxels with a grey value > 10 were marked as thrombus; voxels with lower grey values were disregarded. Thus, background noise of fluorescence signals from adjacent focus planes and single platelets was suppressed. Thrombi were then categorized by volume, and only platelet aggregates exceeding the cut-off volume of 100 µm³ were assessed to avoid interference by non-stationary objects, e.g., moving platelets.

Starting structures for molecular dynamics simulations. The starting structure for MD simulations of $\alpha_{IIb}\beta_3$ in the bent, closed form representing the inactive state of the Leu33 isoform was obtained from the coordinates of the X-ray structure of the ectodomain of $\alpha_{IIb}\beta_3$ integrin (PDB ID 3FCS) (9). In the PDB entry, the α_{IIb} subunit contains two unresolved regions within the CALF-2 domain (residues 764 to 774 (AB loop) and 840 to 873 (XY loop)), and the β_3 subunit has two unresolved regions within the EGF domain (residues 75 to 78 and 477 to 482). Residues unresolved in the α_{IIb} subunit were not included in the starting structures as the high flexibility of the residues implies that they will not contribute significantly to stabilizing the bent conformation of the $\alpha_{IIb}\beta_3$ integrin. The short regions of unresolved residues of the β_3 subunit were modeled and refined using the automatic loop refinement ModLoop (59). The structure was finally refined by reverting the engineered residues Cys598 and Cys688 to the natural residues, Leu 598 and Pro 688, respectively. Modeller v9.9 (60) was applied allowing the modeling of the two Cys residues only. The Pro33 variant was obtained by mutating residue Leu33 to Pro33, using SwissPDBviewer (61), without changing the coordinates of any of the other amino acids. As a final step, we capped the charges at the N-terminal residues, Glu764 and Gly840, and the C-terminal residues, Asp774 and Gln873, using the leap module of Amber 12 (62). All structural ions present in the protein were modeled as Mg^{2+} ions. Integrin sequence numbers used throughout this study are according to Uniprot.

Molecular dynamics simulations. Each starting structure of the two HPA-1 isoforms, Leu33 or Pro33, was subjected to three replicates of all-atom MD simulations of 1 µs length each in explicit solvent summing up to 6 µs of aggregate simulation time for production. MD simulations were performed with the AMBER 12 suite of programs (62), using the force field ff99SB, initially described by Cornell *et al.* (63) and modified according to Simmerling *et al.* (64). Parameters for the Mg^{2+} ions were taken from Aquist (65). The total charge of the system was neutralized by adding eight Na^+ counter ions with the leap module of AMBER 12 (62) and placed into an octahedral period box of TIP3P water molecules (66). The distance between the edges of the water box and the closest atom of the protein was at least 11 Å, resulting in systems of ~200,000 atoms. The particle mesh Ewald method (67) was used to treat long-range electrostatic interactions, and bond lengths involving bonds to hydrogen atoms were constrained using the SHAKE algorithm (68). The time step for integrating Newton's equations of motion was 2 fs with a direct space, non-bonded cut-off of 8 Å. Applying harmonic restraints with force constants of 5 kcal mol^{-1} $Å^{-2}$ to all solute atoms, MD simulations in the NVT (constant number of particles, volume, and temperature) ensemble was carried out for 50 ps, during which the system was heated from 100 to 300 K. Subsequent MD simulations in the NPT (constant number of particles, pressure, and temperature) ensemble were used for 150 ps to adjust the solvent density. Finally, the force constant of the harmonic restraints on solute

atom positions was gradually reduced to zero during 100 ps of NVT MD simulations. Subsequently, we performed 1 μs as unrestrained simulation; the first 200 ns were discarded and the following 800 ns were used for analysis with the programs ptraj/cpptraj (69), with conformations extracted every 20 ps. The production MD simulations were performed with the GPU version of the program pmemd (70).

Analysis of the trajectories. For the analysis of the trajectories, ptraj/cpptraj (69) of the AmberTools suite of programs (62) was applied. For investigating structural deviations along the MD trajectories, the root-mean-square deviation (RMSD) of all C_α atoms was computed after minimizing the mass-weighted RMSD of the C_α atoms of the βA and propeller domains with respect to the starting structure. In addition, to investigate the structural changes of a domain, the C_α atom RMSD of each domain was computed after superimposing the respective domain. To evaluate the level of compactness of the structure, the radius of gyration (R_{og}) was calculated with respect to the complete ectodomain. To examine atomic mobility, root-mean-square fluctuations (RMSF) were computed for the backbone atoms of the PSI domain. An analysis of the secondary structure of the PSI domain was carried out to monitor variations in the content of the two helices bordering the AB loop. Structural changes in the ectodomain were characterized, as reported previously (18,27). The kinking of the helix α1 was measured by the point triple (center of mass of C_α atoms of Lys112 and Ile118, center of mass of C_α atoms of Gln119 and Lys125, and center of mass of C_α atoms of Leu126 and Leu132). The unbending of the structure was evaluated using the angle formed by the centers of mass of the propeller, βA, and PSI domains, and the splaying of the two legs was evaluated using the angle formed by the centers of mass of the CALF-2, thigh, and β-tail domains. Changes in the β_3 genu region were first quantified by computing the distance between the C_α atom of residue 33 with the C_α atom of Ser469 (EGF-1 domain), and the C_α atom of Gln481 (EGF-2 domain). To identify a network of interactions keeping the inter-domain interface stable, a maximal distance of 3.5 Å and a minimal angle of 120° were used as exclusion criteria to identify hydrogen bond formation.

The Constraint Network Analysis (CNA) software package was used to provide a link between structure and rigidity/flexibility of the HPA-1 isoforms (71). To derive information of the effect of Pro33 on a local level, we first generated an ensemble of 400 equally distributed structures from the 200 - 1000 ns intervals of each MD simulation, considering only the hybrid, PSI, and EGF block domains. Thermal unfolding simulations of the Leu33 and Pro33 isoforms were then carried out with CNA to identify differences in the structural stability within the β_3 genu region, following established protocols (71). For each isoform, we generated three different stability maps and three different neighbour stability maps; from them we calculated the mean values used to build a final stability map and neighbour stability map for Leu33 and Pro33. Finally, a difference stability map was calculated as rc_{ij} (Leu33 isoform) - rc_{ij} (Pro33 isoform).

Statistical analysis. Results from three independent MD simulations are expressed as arithmetic means ± SEM (standard error of the mean) calculated over the time. The overall SEM for each simulated system was calculated according to the law of error propagation (eq. 1):

$$\mathrm{MSE}_{total} = \sqrt{\mathrm{MSE}_1^2 + \mathrm{MSE}_2^2 + \mathrm{MSE}_3^2} \quad \text{eq. 1}$$

where the subscripts 1, 2, 3 indicate the three trajectories. Differences between mean values are considered statistically significant if $p < 0.001$ according a Student's t-test for parametric tests and Wilcox test for non-parametric tests. The statistical analysis was performed using the R software (72).

The FRET efficiency results obtained performing the FRET-AB experiments are expressed as means ± SEM; for statistical analysis the unpaired t-test was applied, using GraphPad Prism version 6.00 for Windows, GraphPad Software, La Jolla, CA, USA, www.graphpad.com.

Figure preparation. The crystal structure of the $\alpha_{IIb}\beta_3$ integrin (PDB ID: 3FCS) was used to represent the protein, together with conformations extracted from the MD trajectories. Pymol was used to generate molecular figures (73), and graphs were prepared using Gnuplot (74).

Live-cell imaging of $\alpha_{IIb}\beta_3$-transfected HEK 293 cells expressing either isoform, Leu33 or Pro33.
Live-cell imaging was performed to examine the cellular distribution of $\alpha_{IIb}\beta_3$-transfected HEK 293 cells expressing either isoform, Leu33 or Pro33. 24 h after transfection, $3.7x10^4$ cells in complete culture medium were allowed to settle for more 24 h in individual chambers in a µ-slide 4 well ibiTreat chamber slide (Ibidi, Martinsried, Germany), previously coated with 50 µg/ml of fibrinogen from human plasma (Sigma-Aldrich, St. Louis, MO, USA) in PBS without Ca^{2+} and Mg^{2+} for 1 h at 37 °C. Live-cell imaging was performed with an Axiovert S100 inverted fluorescence microscope (Zeiss, Jena, Germany), equipped with a 12.0 Monochrome w/o IR-18 monochromatic camera (Diagnostic Instruments, Inc, Sterling Heights, MI, USA) and a LEJ EBQ 100 isolated lamp (Leistungselektronik Jena GmbH, Jena, Germany). Images were obtained with a 63 x oil immersion objective lens using 5000 ms exposure time for mVenus, 100 ms for mCherry, and 300 ms for Brightfield. Image acquisition was performed with the Metamorph Software (v. 7.7.7.0). Background subtraction and image processing were obtained using Adobe Photoshop CS3 (Adobe, San Jose, CA, USA) software.

Flow cytometry
Transfected cells at 70-80% confluence were harvested 24, 48, and 72 h after transfection. Subsequently, cells were pelleted by centrifugation at 400 g for 7 min and suspended again in 100 µl of DPBS (Dulbecco's phosphate-buffered saline). Staining with allophycocyanin (APC)-conjugated mouse anti-human CD41 monoclonal antibody (clone MEM-06; Exbio, Praha, Czech Republic; 0.15 µg/ml) was performed for 30 min at RT, protected from light. After staining, cells were washed once in DPBS and analyzed on a FACS Canto II flow cytometer (BD Biosciences, San Jose, CA, USA), equipped with 488 nm and 633 nm lasers for excitation, and the FITC, PE, and APC filters for detection of mVenus, mCherry, and APC, respectively. The collected data were analyzed with the FACSDiva software V. 6.1.3 (BD Biosciences, San Jose, CA, USA). PAC1 was obtained from BD Biosciences (Heidelberg, Germany) and Alexa647 fibrinogen from Thermo Fisher Scientific (Dreieich, Germany).

Förster Resonance Energy Transfer (FRET) measurements using acceptor-photobleaching (APB)
24 h after transfection, cells were harvested and seeded in µ-slide 8 well ibiTreat chamber slide (Ibidi, Martinsried, Germany). Subsequently, 24 h later (48 h after transfection) and before measuring FRET efficiency, the culture medium was substituted by identical medium but this time containing phenol red free Fluorobrite™ DMEM (Thermo Fisher, formerly Life Technologies, Waltham, MA, USA).
Living cells were examined with a LSM 780 (Zeiss, Jena, Germany) inverted microscope, equipped with a C-Apochromat 40x/1.20 W Corr (from Correction ring) M27 water immersion objective lens, an AxioCam camera, and a HPX 120C lamp. FRET acceptor photobleaching experiments including image acquisition, definition of regions of interest for bleaching, and data readout were performed using the LSM Software package ZEN 2012 (Zeiss, Oberkochen, Germany). The chamber slide containing the living cells was mounted on a heating frame within a large incubation chamber (PeCon, Erbach, Germany) set to 37 ºC. mVenus was excited with the 488 nm line of an argon multi-line laser, and detected between 513-558 nm using a GaAsP detector, while mCherry was excited at 561 nm using a DPSS laser and detected between 599-696 nm. The beam splitter was MBS 488/561/633. In total, a time series of 20 frames (128x128 pixel, pixel size 0.33 µm) at a pixel time of 2 µs/pixel was acquired for each FRET experiment. The entire measurement including bleaching of mCherry was finished within 3.5 s. After the 5th frame, an area corresponding to half of a cell, with a constant dimension of 42x42 pixels (region of interest), was bleached by 30 iterations of the mCherry excitation wavelength (561 nm) using 100% laser power. After bleaching, 15 additional frames were recorded. The mean intensity of mVenus fluorescence at the cell membrane within the bleached area was extracted and analyzed according to the following equation (eq. 2):

$$\text{FRET efficiency} = \frac{(I_{\text{after}} - I_{before})}{I_{\text{after}}} \times 100 \quad \text{eq. 2}$$

whereby I_{before} (intensity of mVenus before bleaching) and I_{after} (intensity of mVenus after

bleaching) correspond to the mean intensity values of mVenus fluorescence of five images before and after bleaching within the bleached area at the cell membrane (33,34).

Acknowledgements
This project was funded in part by a grant to RES and VRS from the Deutsche Forschungsgemeinschaft (Sonderforschungsbereich 612, project ID : B2). We are grateful for computational support and infrastructure provided by the "Zentrum für Informations- und Medientechnologie" (ZIM) at the Heinrich Heine University Düsseldorf and the computing time provided by the John von Neumann Institute for Computing (NIC) to HG on the supercomputers JUROPA and JURECA at Jülich Supercomputing Center (JSC) (project IDs: 6710, 8348, 10307; user ID: HDD11). We thank Dr. Rainer B. Zotz and Beate Maruhn-Dembowski for genotyping of HPA-1 of $\alpha_{IIb}\beta_3$ and α_2C807T of $\alpha_2\beta_1$. The assistance of Bianca Maaßen-Weingart and Jan Peveling-Oberhag in the platelet experiments is also gratefully acknowledged.

Conflict of interest
None declared

Author contributions
HG and RES conceived and supervised the study; GP performed computational study; GP and HG analyzed computational data; JPVP and VRS performed experiments; JPVP, VRS, and RES analyzed experimental data; AB performed platelet thrombus volumetry; GP, JPVP, VRS, RES, and HG wrote the manuscript.

[1]The abbreviations used are:

APB	acceptor photobleaching
APC	allophycocyanin
CAD	coronary artery disease
CNA	Constraint Network Analysis
Fg	Fibrinogen
FRET	Förster resonance energy transfer
GP	glycoprotein
HPA-1	human platelet antigen-1 (HPA-1)
MD	molecular dynamics
NPT	constant number of particles, pressure, and temperature
NVT	constant number of particles, volume, and temperature
PSI	plexin-semaphorin-integrin
RAC	root-mean-square average correlation
RMSD	root-mean-square deviation
RMSF	root-mean-square fluctuations
ROI	region of interest
R_{og}	radius of gyration
TMD	transmembrane domain
VWF	von Willebrand factor

References

1. Hynes, R. O. (2002) Integrins: bidirectional, allosteric signaling machines. *Cell* **110**, 673-687
2. Coppolino, M. G., Dedhar, S. (2000) Bi-directional signal transduction by integrin receptors. *J. Biochem. Cell Biol.* **32**, 171-188
3. Mould, A. P. (1996) Getting integrins into shape: recent insights into how integrin activity is regulated by conformational changes. *J. Cell Sci.* **109**, 2613-2618
4. Arnaout, M. A. (2003) Integrin structure: new twists and turns in dynamic cell adhesion. *Immunol. Rev.* **186**, 125-140
5. Arnaout, M. A., Goodman, S. L., and Xiong, J. P. (2007) Structure and mechanics of integrin-based cell adhesion. *Curr. Opin. Cell. Biol.* **19**, 495-507
6. Luo, B. H., Carman, C. V., and Springer, T. A. (2007) Structural basis of integrin regulation and signaling. *Annu. Rev. Immunol.* **25**, 619-647
7. Askari, J. A., Buckley, P. A., Mould, A. P., and Humphries, M. J. (2009) Linking integrin conformation to function. *J. Cell Sci.* **122**, 165-170
8. Bennett, J. S., Berger, B. W., and Billings, P. C. (2009) The structure and function of platelet integrins. *J. Thromb. Haemost.* **7 Suppl 1**, 200-205
9. Zhu, J. H., Luo, B. H., Xiao, T., Zhang, C. Z., Nishida, N., and Springer, T. A. (2008) Structure of a complete integrin ectodomain in a physiologic resting state and activation and deactivation by applied forces. *Mol. Cell.* **32**, 849-861
10. Springer, T. A., and Dustin, M. L. (2012) Integrin inside-out signaling and the immunological synapse. *Curr. Opin. Cell. Biol.* **24**, 107-115
11. Bledzka, K., Smyth, S. S., and Plow, E. F. (2013) Integrin alpha(IIb)beta(3): from discovery to efficacious therapeutic target. *Circ. Res.* **112**, 1189-1200
12. Luo, B. H., and Springer, T. A. (2006) Integrin structures and conformational signaling. *Curr. Opin. Cell. Biol.* **18**, 579-586
13. Arnaout, M. A., Mahalingam, B., and Xiong, J. P. (2005) Integrin structure, allostery, and bidirectional signaling. *Annu. Rev. Cell Dev. Biol.* **21**, 381-410
14. Xiong, J. P., Stehle, T., Diefenbach, B., Zhang, R., Dunker, R., Scott, D. L., Joachimiak, A., Goodman, S. L., and Arnaout, M. A. (2001) Crystal structure of the extracellular segment of integrin alpha(V)beta(3) *Science* **294**, 339-345
15. Xie, C., Zhu, J., Chen, X., Mi, L., Nishida, N., and Springer, T. A. (2010) Structure of an integrin with an alpha(I) domain, complement receptor type 4. *The EMBO J.* **29**, 666-679
16. Takagi, J., Petre, B. M., Walz, T., and Springer, T. A. (2002) Global conformational rearrangements in integrin extracellular domains in outside-in and inside-out signaling. *Cell* **110**, 599-511
17. Beglova, N., Blacklow, S. C., Takagi, J., and Springer, T. A. (2002) Cysteine-rich module structure reveals a fulcrum for integrin rearrangement upon activation. *Nat. Struct. Biol.* **9**, 282-287
18. Reinehr, R., Gohlke, H., Sommerfeld, A., vom Dahl, S., and Häussinger, D. (2010) Activation of integrins by urea in perfused rat liver. *J. Biol. Chem.* **285**, 29348-29356
19. Xiong, J. P., Stehle, T., Goodman, S. L., and Arnaout, M. A. (2004) A novel adaptation of the integrin PSI domain revealed from its crystal structure. *J. Biol. Chem.* **279**, 40252-40254
20. Zang, Q., and Springer, T. A. (2001) Amino acid residues in the PSI domain and cysteine-rich repeats of the integrin beta(2) subunit that restrain activation of the integrin alpha(X)beta(2). *J. Biol. Chem.* **276**, 6922-6929
21. Xiao, T., Takagi, J., Coller, B. S., Wang, J. H., and Springer, T. A. (2004) Structural basis for allostery in integrins and binding to fibrinogen-mimetic therapeutics. *Nature* **432**, 59-67
22. Zotz, R. B., Winkelmann, B. R., Muller, C., Boehm, B. O., Marz, W., and Scharf, R. E. (2005) Association of polymorphisms of platelet membrane integrins alpha(IIb)beta(3) (HPA-1b/Pl) and alpha(2)beta(1) (alpha807TT) with premature myocardial infarction. *J. Thromb. Haemost.* **3**, 1522-1529
23. Weiss, E. J., Bray, P. F., Tayback, M., Schulman, S. P., Kickler, T. S., Becker, L. C., Weiss, J. L., Gerstenblith, G., and Goldschmidt-Clermont, P. J. (1996) A polymorphism of a platelet

glycoprotein receptor as an inherited risk factor for coronary thrombosis. *N. Engl. J. Med.* **334**, 1090-1094

24. Zotz, R. B., Winkelmann, B. R., Nauck, M., Giers, G., Maruhn-Debowski, B., Marz, W., and Scharf, R. E. (1998) Polymorphism of platelet membrane glycoprotein IIIa: Human platelet antigen 1b (HPA-1b/PIA2) is an inherited risk factor for premature myocardial infarction in coronary artery disease. *J. Thromb. Haemost.* **79**, 731-735
25. Zotz, R. B., Klein, M., Dauben, H. P., Moser, C., Gams, E., and Scharf, R. E. (2000) Prospective analysis after coronary-artery bypass grafting: platelet GP IIIa polymorphism (HPA-1b/PIA2) is a risk factor for bypass occlusion, myocardial infarction, and death. *J. Thromb. Haemost.* **83**, 404-407
26. Loncar, R., Stoldt, V., Hellmig, S., Zotz, R. B., Mihalj, M., and Scharf, R. E. (2007) HPA-1 polymorphism of alpha(IIb)beta(3) modulates platelet adhesion onto immobilized fibrinogen in an in-vitro flow system. *Thromb. J.*, 10.1186/1477-9560-1185-1182
27. Gohlke, H., Schmitz, B., Sommerfeld, A., Reinehr, R., and Häussinger, D. (2013) alpha(5)beta(1)-integrins are sensors for tauroursodeoxycholic acid in hepatocytes. *Hepatology* **57**, 1117-1129
28. Aurich, V., Beck, A. (2002) ECCET: Ein System zur 3D-Visualisierung von Volumendaten mit Echtzeitnavigation. in *Bildverarbeitung für die Medizin 2002*. (Meiler, M., Saupe, D., Kruggel, F., Handels, H., Lehmann, T. M. ed.), Springer Berlin, Heidelberg. pp 389-392
29. Scharf, R. E., Hasse, M., Reiff E., Gyenes, M., Stoldt, V.R. (2009) CD40 ligand (CD40L) increases thrombus stability and outside-in signaling through integrin alpha(IIb)beta(3). *J. Thromb. Haemost.* **7 Suppl 2**, 920-929
30. Galindo-Murillo, R., Roe, D. R., and Cheatham, T. E., 3rd. (2015) Convergence and reproducibility in molecular dynamics simulations of the DNA duplex d(GCACGAACGAACGAACGC). *Biochim. Biophys. Acta* **1850**, 1041-1058
31. Donner, L., Falker, K., Gremer, L., Klinker, S., Pagani, G., Ljungberg, L. U., Lothmann, K., Rizzi, F., Schaller, M., Gohlke, H., Willbold, D., Grenegard, M., and Elvers, M. (2016) Platelets contribute to amyloid-beta aggregation in cerebral vessels through integrin alpha(IIb)beta(3)-induced outside-in signaling and clusterin release. *Sci. Signal.* **9**, ra52
32. El Khattouti, A., Stoldt, R.V., Scharf, R.E. (2010) The HPA-1b (Pro33) isoform of platelet integrin alpha(IIb)beta(3) is a prothrombotic variant: characterization by fluorescence resonance energy transfer. *Blood* **116**, 2028
33. Bleckmann, A., Weidtkamp-Peters, S., Seidel, C. A. M., and Simon, R. (2010) Stem Cell Signaling in Arabidopsis Requires CRN to Localize CLV2 to the Plasma Membrane. *Plant Physiol.* **152**, 166-176
34. Karpova, T. S., Baumann, C. T., He, L., Wu, X., Grammer, A., Lipsky, P., Hager, G. L., and McNally, J. G. (2003) Fluorescence resonance energy transfer from cyan to yellow fluorescent protein detected by acceptor photobleaching using confocal microscopy and a single laser. *J. Microsc.* **209**, 56-70
35. Shi, M. L., Foo, S. Y., Tan, S. M., Mitchell, E. P., Law, S. K. A., and Lescar, J. (2007) A structural hypothesis for the transition between bent and extended conformations of the leukocyte beta(2) integrins. *J. Biol. Chem.* **282**, 30198-30206
36. Pfleger, C., Radestock, S., Schmidt, E., and Gohlke, H. (2013) Global and local indices for characterizing biomolecular flexibility and rigidity. *J. Comp. Chem.* **34**, 220-233
37. Jacobs, D. J., and Thorpe, M. F. (1995) Generic rigidity percolation: the pebble game. *Phys. Rev. Lett.* **75**, 4051-4054
38. Hermans, M. A., Pfleger, C., Nutschel, C., Hanke, C. A., Gohlke, H. (2017) Rigidity theory for biomolecules: concepts, software, and applications. *WIREs Comput. Mol. Sci.* **7**, 10.1002/wcms.1311
39. Thorpe, M., Jacobs, D., and Djordjevic, B. (1996) Generic rigidity percolation. *J. Phys. Condens. Matter* **11**, 407-424
40. Radestock, S., and Gohlke, H. (2008) Constraint network analysis: exploiting the link between protein rigidity and thermostability. *Eng. Life Science* **8**, 507-522

41. Pfleger, C., Radestock, S., Schmidt, E., and Gohlke, H. (2013) Global and local indices for characterizing biomolecular flexibility and rigidity. *J. Comput. Chem.* **34**, 220-233
42. Whiteley, W. (2005) Counting out to the flexibility of molecules. *Phys. Biol.* **2**, S116-S126
43. Stoldt, V. R., Peveling, J., Loncar, R., Beck, A., Aurich, V., and Scharf, R. E. (2005) Evaluation of platelet thrombus formation under flow. *Blood* **106**, 70B-71B
44. Savage, B., Ruggeri, Z. M. . (2013) The basis for platelet adhesion. in *Hemostasis and Thrombosis. Basic Priciples and Clinical Practice* (Marder, V. J., Aird, W., Bennett, J. S., Schulman, S., White, G. C. ed.), 6 Ed., Lippincott, Philadelphia. pp 400-409
45. Watson, S. P., Farndale, R. W., Moroi, M., Jung, S. M. (2013) Platelet collagen receptors. in *Haemostasis and Thrombosis. Basic Priciples and Clinical Practice* (Marder, V. J., Aird, W., Bennett, J. S., Schulman, S., White, G. C. ed.), 6 Ed., Lippincott, Philadelphia. pp 420-430
46. Kritzik, M., Savage, B., Nugent, D. J., Santoso, S., Ruggeri, Z. M., and Kunicki, T. J. (1998) Nucleotide polymorphisms in the alpha(2) gene define multiple alleles that are associated with differences in platelet alpha(2)beta(1) density. *Blood* **92**, 2382-2388
47. Vijayan, K. V., Liu, Y., Sun, W., Ito, M., and Bray, P. F. (2005) The Pro33 isoform of integrin beta(3) enhances outside-in signaling in human platelets by regulating the activation of serine/threonine phosphatases. *J. Biol. Chem.* **280**, 21756-21762
48. Puklin-Faucher, E., Gao, M., Schulten, K., and Vogel, V. (2006) How the headpiece hinge angle is opened: New insights into the dynamics of integrin activation. *J. Cell. Biol.* **175**, 349-360
49. Chen, W., Lou, J., Hsin, J., Schulten, K., Harvey, S. C., and Zhu, C. (2011) Molecular dynamics simulations of forced unbending of integrin alpha(V)beta(3). *PLOS Comput. Biol.* **7**, e1001086
50. Campbell, I. D., and Humphries, M. J. (2011) Integrin structure, activation, and interactions. *Cold Spring Harb. Perspect. Biol.* **3**, a004994
51. Xiong, J. P., Stehle, T., Goodman, S. L., and Arnaout, M. A. (2003) New insights into the structural basis of integrin activation. *Blood* **102**, 1155-1159
52. Puklin-Faucher, E., and Vogel, V. (2009) Integrin activation dynamics between the RGD-binding site and the headpiece hinge *J. Biol. Chem.* **284**, 36557-36568
53. Puklin-Faucher, E., and Sheetz, M. P. (2009) The mechanical integrin cycle. *J. Cell Sci.* **122**, 179-186
54. Vijayan, K. V., Goldschmidt-Clermont, P. J., Roos, C., and Bray, P. F. (2000) The Pl(A2) polymorphism of integrin beta(3) enhances outside-in signaling and adhesive functions. *J. Clin. Invest.* **105**, 793-802
55. Abraham, D. G., Nutt, E. M., Bednar, R. A., Bednar, B., Gould, R. J., and Duong, L. T. (1997) Arginine-glycine-aspartic acid mimics can identify a transitional activation state of recombinant alpha(IIb)beta(3) in human embryonic kidney 293 cells. *Mol. Pharm.* **52**, 227-236
56. Li, J., Su, Y., Xia, W., Qin, Y., Humphries, M. J., Vestweber, D., Cabanas, C., Lu, C., and Springer, T. A. (2017) Conformational equilibria and intrinsic affinities define integrin activation. *EMBO J.*, 629-645
57. Jallu, V., Poulain, P., Fuchs, P. F., Kaplan, C., and de Brevern, A. G. (2012) Modeling and molecular dynamics of HPA-1a and -1b polymorphisms: effects on the structure of the beta(3) subunit of the alpha(IIb)beta(3) integrin. *PloS One* **7**, e47304
58. Bennett, J. S. (2005) Structure and function of the platelet integrin alpha(IIb)beta(3). *J. Clin. Invest.* **115**, 3363-3369
59. Fiser, A., and Sali, A. (2003) ModLoop: automated modeling of loops in protein structures. *Bioinformatics* **19**, 2500-2501
60. Webb, B., and Sali, A. (2014) Comparative protein structure modeling using MODELLER. *Curr. Protoc. Bioinformatics* **47**, 1-32
61. Guex, N., and Peitsch, M. C. (1997) SWISS-MODEL and the Swiss-PdbViewer: an environment for comparative protein modeling. *Electrophoresis* **18**, 2714-2723

62. al., C. D. e. (2005) The Amber biomolecular simulation programs. *J. Comp. Chem.* **26**, 1668-1688
63. Cornell, W. D., Cieplak, P., Bayly, C. I., Gould, I. R., Merz, K. M., Ferguson, D. M., Spellmeyer, D. C., Fox, T., Caldwell, J. W., and Kollman, P. A. (1995) A 2nd generation force-field for the simulation of proteins, nucleic-acids, and organic-molecules. *J. Am. Chem. Soc.* **117**, 5179-5197
64. Hornak, V., Abel, R., Okur, A., Strockbine, B., Roitberg, A., and Simmerling, C. (2006) Comparison of multiple Amber force fields and development of improved protein backbone parameters. *Proteins* **65**, 712-725
65. Aqvist, J. (1992) Modeling of ion ligand interactions in solutions and biomolecules. *J. Mol. Struct.* **88**, 135-152
66. Jorgensen, W. L., Chandrasekhar, J., Madura, J. D., Impey, R. W., and Klein, M. L. (1983) Comparison of simple potential functions for simulating liquid water. *J. Chem. Phys.* **79**, 926-935
67. Cheatham, T. E., Miller, J. L., Fox, T., Darden, T. A., and Kollman, P. A. (1995) Molecular-Dynamics simulations on solvated biomolecular systems - the particle Mesh Ewald method leads to stable trajectories of DNA, RNA, and proteins. *J. Am. Chem. Soc.* **117**, 4193-4194
68. Ryckaert, J. P., Ciccotti, G., and Berendsen, H. J. C. (1977) Numerical-Integration of cartesian equations of motion of a system with constraints-Molecular-Dynamics of N-Alkanes. *J. Comp. Phys.* **23**, 327-341
69. Roe, D. R., and Cheatham, T. E. (2013) PTRAJ and CPPTRAJ: software for processing and analysis of molecular dynamics trajectory data. *J. Chem. Theory Comput.* **9**, 3084-3095
70. Salomon-Ferrer, R., Gotz, A. W., Poole, D., Le Grand, S., and Walker, R. C. (2013) Routine microsecond molecular dynamics simulations with AMBER on GPUs. 2. Explicit solvent particle Mesh Ewald. *J. Chem. Theory Comput.* **9**, 3878-3888
71. Pfleger, C., Rathi, P. C., Klein, D. L., Radestock, S., and Gohlke, H. (2013) Constraint Network Analysis (CNA): a python software package for efficiently linking biomacromolecular structure, flexibility, (thermo-)stability, and function. *J. Chem. Inf. Mod.* **53**, 1007-1015
72. Team, R. D. C. (2010) R: a language and environment for statistical computing.
73. Schrodinger, L. (2010) The PyMOL molecular graphics system.
74. Williams T, K. C. (2011) Gnuplot 4.5: an interactive plotting program.

Fig. 1

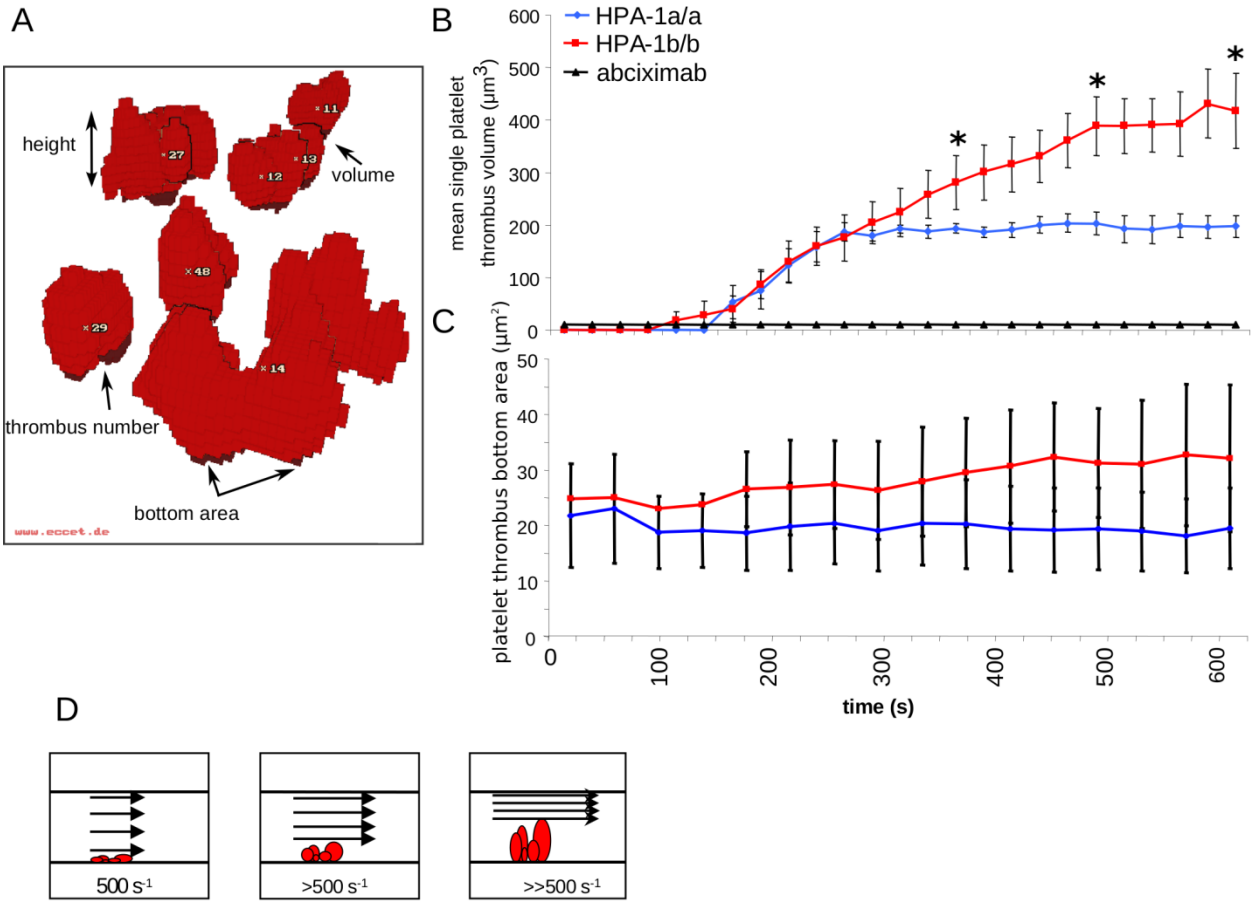

Fig 1. Dynamics and volumetric of platelet thrombus formation under flow-dynamic conditions.
A rectangular flow chamber coated with collagen type I (3 mg/ml) at the lower surface was perfused with mepacrine-labeled citrated whole blood for 10 min at an initial wall-near shear rate of 500 s^{-1}, simulating arterial flow conditions. Fluorescence signals were detected by confocal laser scanning microscopy, and digital imaging was processed, as described in Experimental Procedures. Volumetry of forming platelet thrombi was assessed by real time 3D visualization.
(A) Depicted is a reconstruction of formed platelet thrombi obtained from a stack of 30 images by confocal laser scanning microscopy and subsequent data processing by ECCET. **(B, C)** Initial platelet thrombus formation and subsequent thrombus growth were recorded in 25 s intervals for each single thrombus. Addition of abciximab (4 µg/ml), an inhibitory antibody to $\alpha_{IIb}\beta_3$, abrogated any platelet thrombus formation. Panel B shows the mean single platelet thrombus volume, panel C the corresponding thrombus bottom area. **(D)** The cartoon illustrates the narrowing of the flow path within the perfusion chamber, with a resulting increase in shear rates upon apical thrombus growth.
Homozygous Leu33 (HPA-1a) platelets (blue diamonds, $n = 8$) and homozygous Pro33 (HPA-1b) platelets (red squares, $n = 8$), control in the presence of abciximab (black rectangles , $n = 2$). Error bars indicate mean ± SEM, stars indicate $p < 0.01$.

Fig. 2

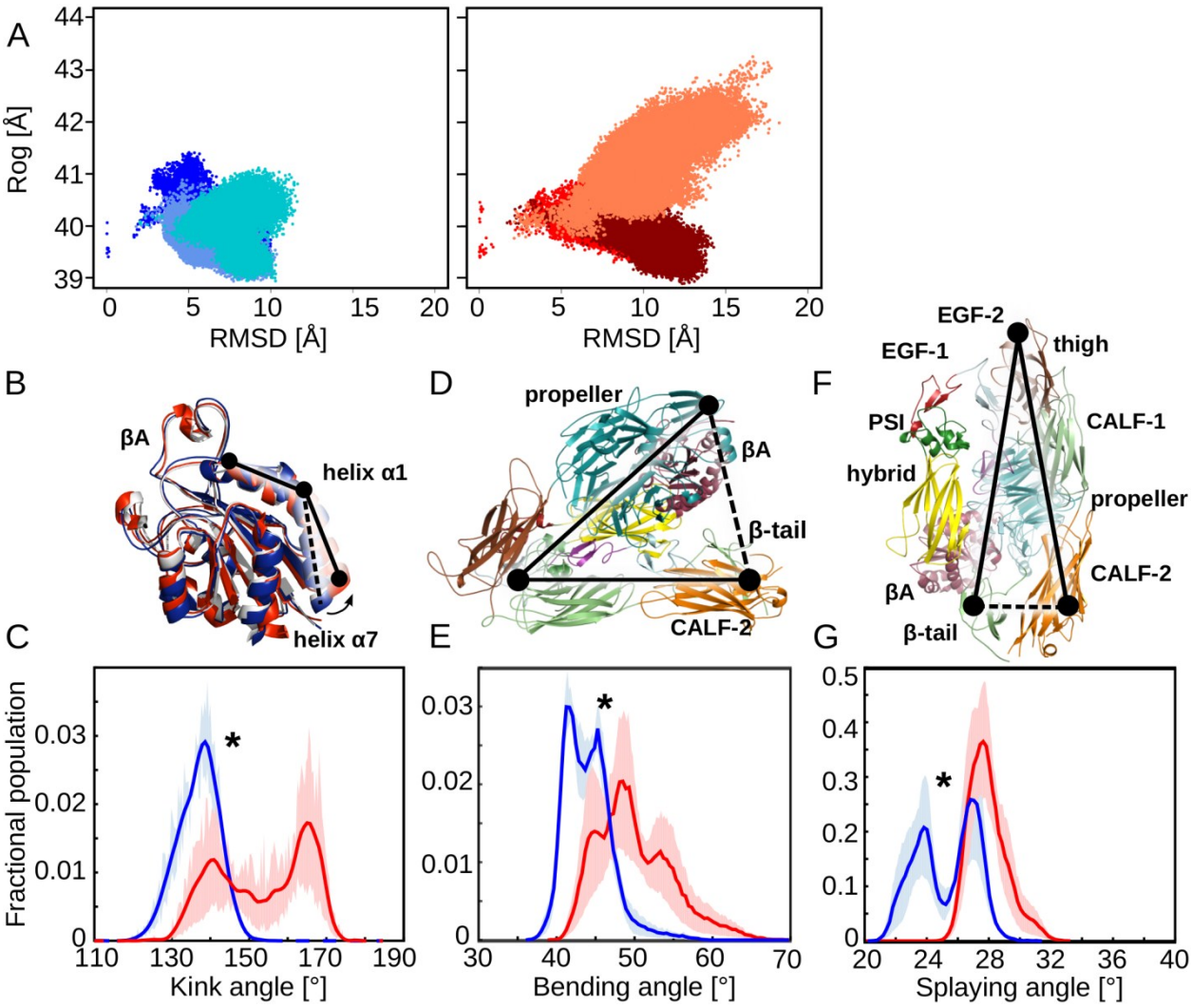

Fig 2. Conformational changes of the Leu33 and Pro33 isoforms of $\alpha_{IIb}\beta_3$ during MD simulations. **(A)** Two-dimensional (2D) histogram of the RMSD of C_α atoms of the entire ectodomain after mass-weighted fitting on the propeller and βA domains of the starting structure *versus* R_{og} for the ectodomains. Bluish colors represent the three MD simulations of the Leu33 isoform and redish colors those of the Pro33 variant. **(B, D, F)** Definition of the kink (B), bending (D), and splaying angles (F). The black solid lines connect the point triples: kinking of the helix α1 (center of mass (COM) of C_α atoms of K112-I118; COM of C_α atoms of Q119-K125; COM of C_α atoms of L126 and L132) (B), bending of $\alpha_{IIb}\beta_3$ integrin ectodomain (COM of the propeller and βA domains; COM of the PSI domain; COM of the CALF-2 and β-tail domains) (D), and splaying of the integrin legs (COM of C_α atoms of L788 and G796 in the CALF-2 domain; COM of the C_α atoms of C602 and C608 in the thigh domain; COM of C_α atoms of E1557 and V1561 in the β-tail domain) (F); the $\alpha_{IIb}\beta_3$ ectodomain starting structure (PDB ID 3FCS) is depicted in cartoon drawing, and the domains are labeled. In panel (B), a superimposition of the βA domains of the Leu33 isoform (blue) and Pro33 variant (red) onto the starting structure (white) is shown. **(C, E, G)** Fractional population of the kink angle (C), bending angle (E), and splaying angle (G) computed over the last 800 ns of three MD simulations each; solid lines represent the mean and transparent, filled curves show ± SEM; * indicates a significant difference between the mean values ($p < 0.001$). Color code as in panel (A).

Fig. 3

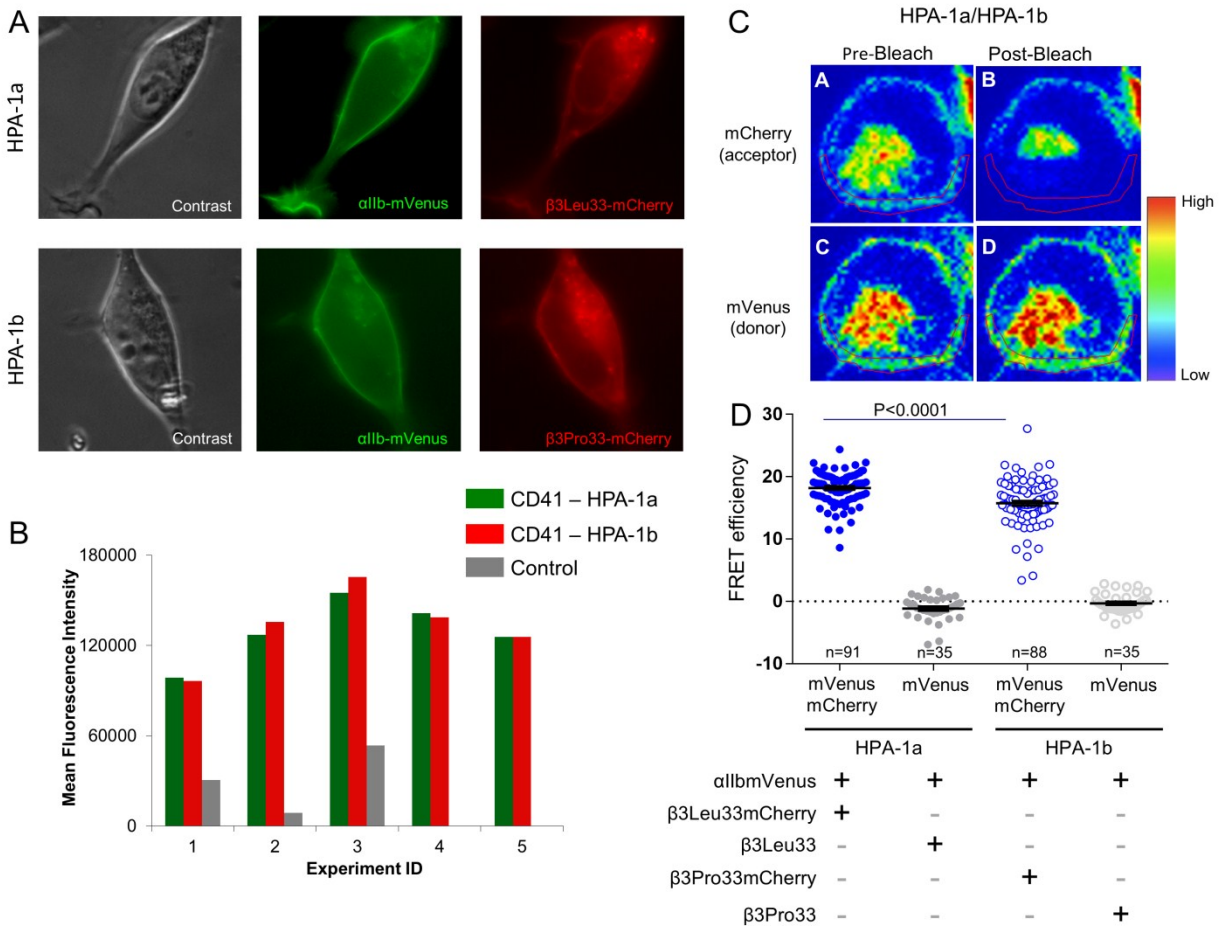

Fig 3. Transient expression of the complete $\alpha_{IIb}\beta_3$ receptor in HEK293 cells. (A) Phase contrast and fluorescence microscopy images of a representative HEK293 cell transfected with α_{IIb}mVenus and β_3Leu33mCherry plasmids (upper panel) and a representative HEK293 cell transfected with α_{IIb}mVenus and β_3Pro33mCherry plasmids (lower panel). **(B)** Flow cytometric analyses of $\alpha_{IIb}\beta_3$ (CD41), expressing either isoform, Leu33 (HPA-1a) or Pro33 (HPA-1b), performed 48 h after transfection in 5 independent experiments. Of note, the transfectants displayed less than 10% difference in $\alpha_{IIb}\beta_3$ expression of either isoform, Leu33 (HPA-1a) or Pro33 (HPA-1b). Values represent mean fluorescence intensity after staining of the transfectants with allophycocyanin (APC)-conjugated CD41 antibody, a complex-specific anti-$\alpha_{IIb}\beta_3$ antibody. **(C)** FRET-acceptor photobleaching (APB) measurements in a representative HEK293 cell transfected with α_{IIb}mVenus and β_3Leu33mCherry plasmids. **(D)** Results of FRET efficiency of fused individual Leu33 (HPA-1a) or Pro33 (HPA-1b) cells and respective donor controls. To determine the efficiency of energy transfer, the fluorescence of mVenus was measured in a defined region of the membrane (red circled) before and after photobleaching of mCherry at 561 nm (33,34). Details are given in **Experimental Procedures.** The error bars indicate mean ± SEM.

Fig. 4

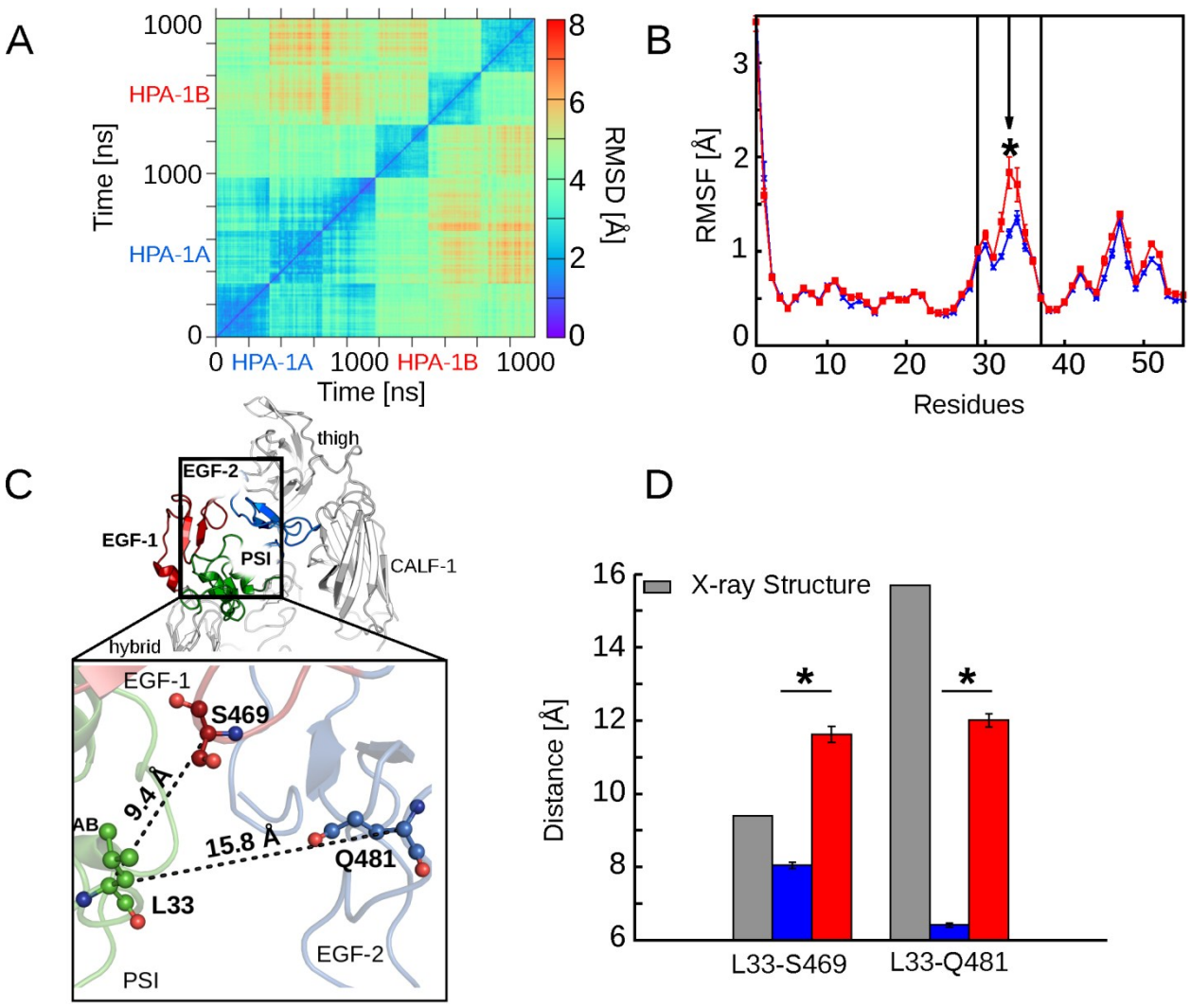

Fig 4. Short- and mid-range structural and dynamics changes induced by the Leu→Pro exchange. (A) Two dimensional (2D) RMSD plot calculated for the C_α atoms of the EGF-1, EGF-2, and EGF-3 domains after superimposing onto the respective domains. All trajectories accounting for an aggregate simulation time of 2 x 3 µs were considered together in the analysis, excluding the first 200 ns of each trajectory and extracting frames at intervals of 100 ns. **(B)** Residue-wise mean backbone RMSF of the PSI domain after a mass-weighted fitting onto the starting structure. Error bars denote SEM. Blue and red bars represent the Leu33 and Pro33 isoforms, respectively; two black lines delineate the AB loop (residues Glu29-Pro37), and the arrow highlights residue 33. The star indicates a significant difference between Leu and Pro at residue 33 ($p < 0.05$). **(C)** $\alpha_{IIb}\beta_3$ is shown in cartoon representation and colored in light grey (with the exception of the PSI domain (green), EGF-1 domain (firebrick), and EGF-2 domain (marine)). Domains are labeled. The blow-up shows the location of the Leu→Pro exchange in the PSI domain within the genu interface of the β_3 subunit. Black dashed lines indicate distances computed in panel (D), with the distance values of the starting structure reported next to them. Residues Leu33 (PSI domain), Ser469 (EGF-1 domain), and Gln481 (EGF-2 domain) are depicted in ball-and-sticks representation. **(D)** Mean distances between the C_α atoms of Leu33/Pro33 as well as Ser469 (EGF-1) and Gln481 (EGF-2) calculated for the Leu33 isoform (blue boxes) and the Pro33 variant (red boxes) and measured in the crystal structure (PDB ID 3FCS, grey boxes). SEM < 0.1 Å in all cases. Error bars indicate mean ± SEM, stars denote a significant difference ($p < 0.0001$) between the two isoforms of $\alpha_{IIb}\beta_3$.

Fig. 5

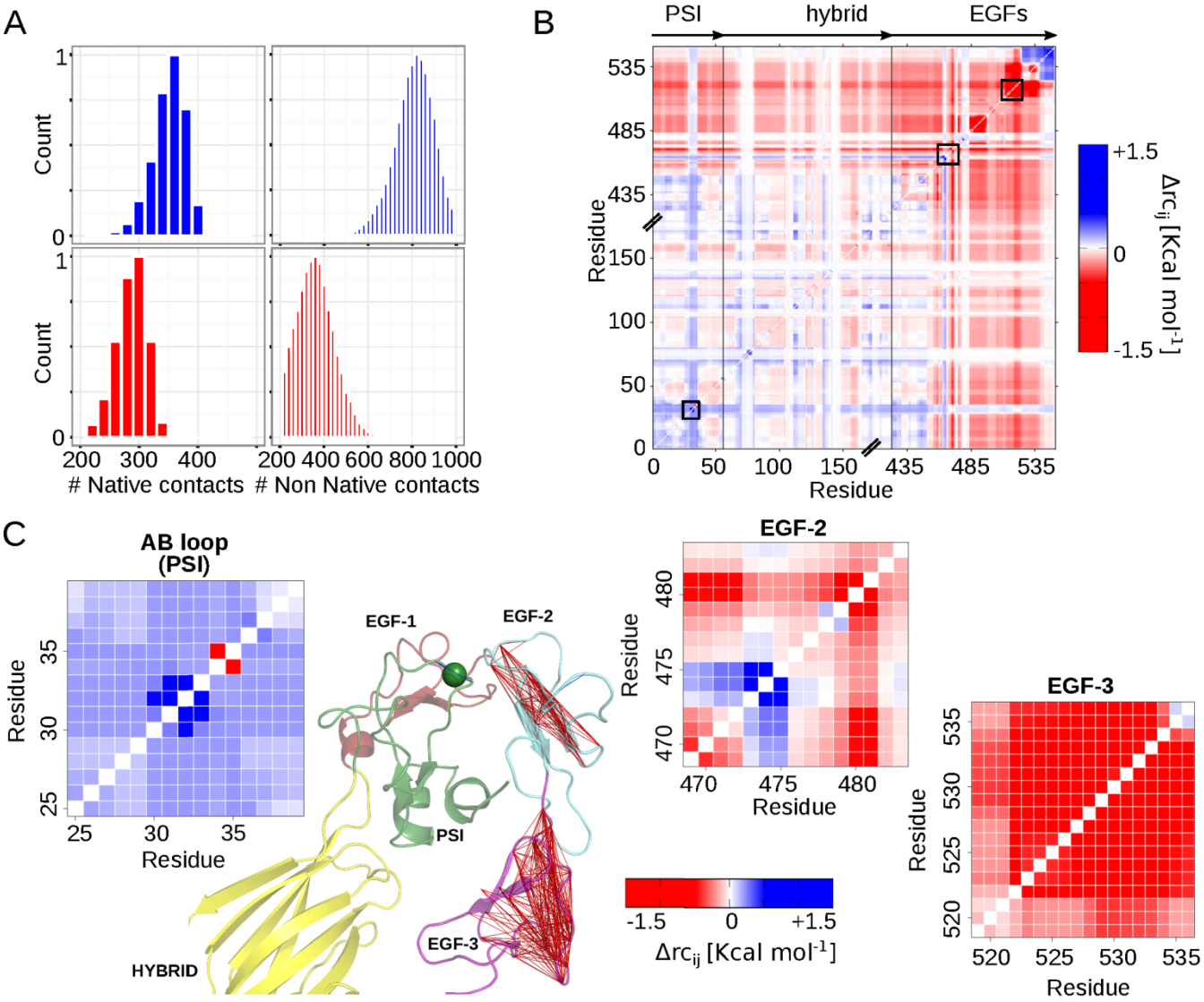

Fig 5. Changes within the PSI/EGF domains interface and in the structural stability between the Leu33 and Pro33 isoforms (A) Histograms showing the relative mean number of native contacts (left) and non-native contacts (right) formed between the AB loop (PSI domain) and all those side-chains located within a distance range of 7 Å. Mean values were computed over three MD simulations of the Leu33 isoform (blue histograms) and Pro33 variant (red histograms). **(B)** Difference stability map generated by CNA and averaged over three MD simulations showing the difference in structural stability between both isoforms, focusing on the β_3 genu region. The color gradient indicates residues with lower structural stability in the Leu33 (blue) or Pro33 isoform (red). **(C)** Blow-ups of three areas highlighted within the difference stability map by black boxes (panel B) and corresponding to the AB loop (PSI domain), residues Ser469 to Asp484 (loop connecting the EGF-1 domain to the EGF-2 domain), and residues Gly519 to Cys536 (EGF-3 domain), exemplifying changes in structural stability due to the Leu→Pro exchange. The results for the latter two regions are also displayed on the structure of the hybrid (yellow), PSI (green), EGF-1 (firebrick) / EGF-2 (light blue) / EGF-3 (purple) domains of $\alpha_{IIb}\beta_3$ (green sphere: C_α atom of residue 33) in terms of lines connecting residues whose mutual stability has decreased in the Pro33 isoform (Δrc_{ij} > -1.5 kcal mol^{-1})

Supporting Information

Supplemental Methods

Blood collection
Blood was collected through a 21-gauge needle from 15 healthy, medication-free volunteers into vacutainer tubes (BD, Heidelberg, Germany) containing sodium citrate (0.38% wt/vol). The volunteers were recruited by the Düsseldorf University Blood Donation Center. Written informed consent was obtained from the volunteers according to the Helsinki Declaration. The Ethics Committee of the Faculty of Medicine, Heinrich Heine University Düsseldorf, approved the study.

***Determination of HPA-1 alleles* of $\alpha_{IIb}\beta_3$ and α_2 C807T genotypes of $\alpha_2\beta_1$**
Prior to blood collection for this study, genotyping of HPA-1 and α_2C807T had been performed. Genomic DNA was extracted from whole blood using the QIAmp blood kit (Qiagen, Hilden, Germany). Upon amplification by polymerase chain reaction, genotypes were determined by allele-specific restriction enzyme analysis (1). The results of genotyping were confirmed by a second analysis using the LightCycler™ system (Roche Diagnostics, Mannheim, Germany) (2) and the results of both procedures were in 100% concordance.

Donor population
Homozygous carriers of either allele, Leu33 (HPA-1a) or Pro33 (HPA-1b), which did not carry the $\alpha_2$807CT or $\alpha_2$807TT genotype of $\alpha_2\beta_1$, were selected for the subsequent experiments. Group A (HPA-1a/1a) consisted of 8 individuals (5 males, 3 females, mean age: 38.8 yrs., range: 21 to 58 yrs.); group B consisted of 7 individuals (4 males, 3 females, mean age: 45.3 yrs., range: 35 to 54 yrs.).

Compounds
Abciximab 4µg/ml (c7E3, ReoPro, Centocor, Inc/Eli Lilly, Indianapolis, IN, USA) is a murine-human chimeric monoclonal antibody fragment directed against human $\alpha_{IIb}\beta_3$. A complex-specific anti-$\alpha_{IIb}\beta_3$ antibody, anti-CD41 (clone MEM-06, Exbio, Praha, Czech Republic) was used for flow cytometric analysis of transfected HEK293 cells. For calibration of the flow cytometer and quantitation of $\alpha_{IIb}\beta_3$ expression, fluorescent microspheres (F-36905, Molecular Probes, Eugene, OR, USA) were used.

Design and construction of plasmids
Two plasmids were generated first by cloning the cDNA of the α_{IIb} human integrin gene (ITGA2B), a gift from Dr. S. Shattil (University of California, San Diego, CA, USA), and the cDNA of the β_3 human integrin gene (ITGB3), a gift from Dr. J. Jones (Northwestern University Medical School, Chicago, IL, USA), downstream the cytomegalovirus promoter in the pcDNA3.1(-) plasmid (Thermo Fisher, formerly Invitrogen, Waltham, MA, USA). A third plasmid, containing the Pro-for-Leu substitution in the β_3 subunit was generated by site-directed mutagenesis, as reported by Kunkel (3). Subsequently, the coding sequence of mVenus (plasmid # 27794), a gift from S. Vogel (Addgene, Cambridge, MA, USA) was cloned downstream the α_{IIb} coding sequence, and the coding sequence of mCherry (Clontech Laboratories, Takara Bio, Mountain View, CA, USA) was cloned downstream the β_3Leu33 and β_3Pro33 coding sequences in the respective plasmids. In initial fusion constructs, the

length of the linker between the C-terminus of each subunit and the N-terminus of the corresponding fluorescent protein (mVenus or mCherry) was varied (4), and combinations of these constructs were tested in transiently transfected HEK293 cell by acceptor-photobleaching to determine optimal basal FRET efficiency. Accordingly, the construct containing a linker of 39 amino acids between α_{IIb} (C-terminus) and mVenus (N-terminus), and a linker of 6 amino acids between β_3Leu33 or β_3Pro33 (C-terminus) and mCherry (N-terminus), was chosen.
Importantly, mVenus and mCherry coding sequences were cloned in frame with the integrin subunits coding sequences with removal of the original stop codon of the integrin subunits (4) for expression as fusion proteins. The sequences of the three resulting plasmids were confirmed by Sanger sequencing (Biological Medical Research Center, Heinrich Heine University Düsseldorf), using the primers listed in **Tables S1** and **S2**.

Cell line culture and transfection
HEK293 cells were purchased from the Leibniz Institute DSMZ - German Collection of Microorganisms and Cell Cultures (DSMZ, Braunschweig, Germany) and cultured according to the recommended conditions (DMEM supplemented with 10% of fetal bovine serum (FBS) and 1% penicillin-streptomycin (PCN-STR). DMEM, FBS, and PCN-STR were obtained from Thermo Fischer Scientific (Waltham, MA, USA). To achieve expression of the complete $\alpha_{IIb}\beta_3$ receptor complex of either isoform, Leu33 (HPA-1a) or Pro33 (HPA-1b), in HEK293 cells, a double transient transfection was performed with the plasmids α_{IIb}mVenus and β_3Leu33mCherry or β_3Pro33mCherry, respectively. HEK293 cells transfected with an empty vector DNA were used as controls in the flow cytometry analyses, and cells double transfected with αIIbmVenus and β_3Leu33 or β_3Pro33 plasmids (without mCherry) served as controls in FRET-APB experiments. The transfection protocol was performed using the Effectene® Transfection Reagent (Qiagen, Hilden, Germany). 24 h prior to transfection, $1.6x10^5$ cells were seeded on a 6-well plate (Greiner Bio-one, Frickenhausen, Germany) in culture medium. On the next day, 0.4 µg of integrin α_{IIb} encoding plasmid and 0.4 µg of each β_3 encoding plasmids were diluted in EC (Enhancer and DNA condensation) buffer (total final volume of 100 µl), 3.2 µl of transfection enhancer was added and the mixture incubated at RT for 5 min. Subsequently, 10 µl of Effectene® was added and the mixture incubated at RT for 10 min. Finally, 200 µl of cell culture medium was added, and the mixture was carefully pipetted into the wells containing the cells. 24 h after transfection, the medium was replaced by standard cell culture medium (DMEM supplemented with 10% FBS and 1% PCN-STR).
Image acquisition was achieved by using the Metamorph Software (v. 7.7.7.0), and image processing was performed with Adobe Photoshop CS3 (Adobe, USA) software.

FRET acceptor-photobleaching (APB) analyses
mVenus fluorescence intensity measured in the ROI varied between 11 and 134 (mean ± SEM, 37.85±1.992) for cells transfected with α_{IIb}mVenus and β_3Leu33mCherry plasmids and between 7 and 93 (35.27 ± 2.048) for cells transfected with αIIbmVenus and β3Pro33mCherry plasmids, respectively; mCherry fluorescence intensity varied between 12 and 120 (54.37 ± 2.284) for cells transfected with α_{IIb}mVenus and β_3Leu33mCherry plasmids and between 12 and 99 (44.90 ± 2.159) for cells transfected with α_{IIb}mVenus and β_3Pro33mCherry plasmids. Transfected cells were randomly chosen for analysis.

Supplemental Tables

Table S1: Primers for αIIbmVenus.

T7minus1	AATACGACTCACTATAGGG
Seq-p101-I	TGGGACAAGCGTTACTGTG
Seq-p101-II	GACCGGGATGGCTACAATG
Seq-p101-III	TCGAGATGAGGCAGACTTC
Seq-p101-IV	CAGCAGAAGAAGGTGAGAG
Seq-p101-mVenus	GGCAACTAGAAGGCACAGTC
RPC	ACAGCTATGACCATGATTACG
Seq-p101-Hyg-fw	ACAGCTATGACCATGATTACG
pEGFP-RP	AACAGCTCCTCGCCCTTG

Table S2: Primers for β3mCherry.

pEGFP-FP	TTTAGTGAACCGTCAGATC
Seq-p106-I	CTTGCCCATGTTTGGCTAC
Seq-p106-II	GGCCTCAAGTCTTGTATGG
Seq-p106-III	TGGCAGCTGTGTCTGTATC
pEGFP_C2-RP	TTTAAAGCAAGTAAAACCTC
Seq-p106-Zeo	GAACAAACGACCCAACAC

Table S3: RMSD of $\alpha_{IIb}\beta_3$ domains after domain-wise alignment.[a]

		Leu33 (HPA-1a) isoform			Pro33 (HPA-1b) isoform		
	Domain	Sim I	Sim II	Sim III	Sim I	Sim II	Sim III
Sub α_{IIb}	Propeller	1.89	1.83	1.75	2.13	1.94	1.93
	Thigh	2.15	1.85	1.90	1.78	1.82	1.82
	CALF-1	2.18	2.07	1.87	1.99	1.82	1.85
	CALF-2	1.75	2.61	1.85	2.87	2.18	2.09
Sub β_3	βA	1.75	1.43	1.69	1.50	1.67	2.05
	Hybrid	2.70	2.46	2.34	2.48	2.44	2.56
	PSI	1.62	1.59	1.60	1.71	1.72	1.69
	EGFs	2.59	2.58	2.48	3.21	4.22	3.88
	β-tail	4.55	5.42	4.88	4.26	4.67	4.49

[a] Mean values, in Å, of the of C_α atom RMSD of $\alpha_{IIb}\beta_3$ domains with respect to the starting structure after a mass-weighted alignment onto the respective domain.

Table S4: RMSD of the $\alpha_{IIb}\beta_3$ integrin domains after alignment of the head region.[a]

		Leu33 (HPA-1a) isoform			Pro33 (HPA-1b) isoform		
	Domain	Sim I	Sim II	Sim III	Sim I	Sim II	Sim III
Sub α_{IIb}	Propeller	2.93	2.43	2.26	2.64	2.44	2.36
	Thigh	5.84	5.18	6.50	9.88	10.69	8.27
	CALF-1	8.13	5.75	8.15	10.34	12.64	11.91
	CALF-2	9.35	9.30	11.0	13.02	15.68	21.31
Sub β_3	βA	4.35	2.78	2.94	2.58	2.43	3.18
	Hybrid	7.10	7.54	6.59	5.72	8.32	6.60
	PSI	14.2	14.1	11.27	9.12	18.99	6.54
	EGFs	10.4	11.1	10.3	9.40	15.22	8.47
	β-tail	14.6	7.81	16.5	7.85	19.26	18.48

[a] Mean values, in Å, of the C_α atom RMSD of $\alpha_{IIb}\beta_3$ domains with respect to the starting structure after a mass-weighted alignment onto the propeller and βA domains.

Table S5: R_{og} of $\alpha_{IIb}\beta_3$ domains.[a]

		Leu33 (HPA-1a) isoform			Pro33 (HPA-1b) isoform		
	Domain	Sim I	Sim II	Sim III	Sim I	Sim II	Sim III
$\alpha_{IIb}\beta_3$	all	39.7	39.6	39.7	40.0	39.6	41.3
	PSI	10.3	10.2	10.3	10.2	10.3	10.2
	EGFs	19.1	19.6	18.8	19.0	20.1	19.4
	PSI+EGFs	15.6	15.5	15.3	15.8	16.0	15.7

[a] Mean values, in Å, of the C_α atom R_{og} of $\alpha_{IIb}\beta_3$ integrin domains.

Table S6: Kink, bending, and splaying angles.

	Leu33 (HPA-1a) isoform			Pro33 (HPA-1b) isoform			
	SimI	SimII	SimIII	SimI	SimII	SimIII	p[d]
Kink angle	136°	137°	139°	140°	153°	166°	-[e]
	137°[a]			153°[a]			***
	136°[b]		-[c]	147°[b]		-[c]	***
Bending angle	45°	43°	43°	49°	46°	55°	-[e]
	44°[a]			50°[a]			***
	-[c]	43°[b]		47°[b]		-[c]	***
Splaying angle	23°	27°	28°	27°	28°	29°	-[e]
	25°[a]			28°[a]			***
	25°[b]		-[c]	27°[b]		-[c]	***

[a] Mean value calculated across three MD simulations.
[b] Mean value calculated across two MD simulations.
[c] Simulations showing the highest mean values were not considered in the statistics.
[d] ***: $p < 0.001$ (according to the *t*-test for parametric testing and the Wilcox test for non-parametric testing with respect to the difference in the mean values).
[e] Not significant.

Supplemental Figures

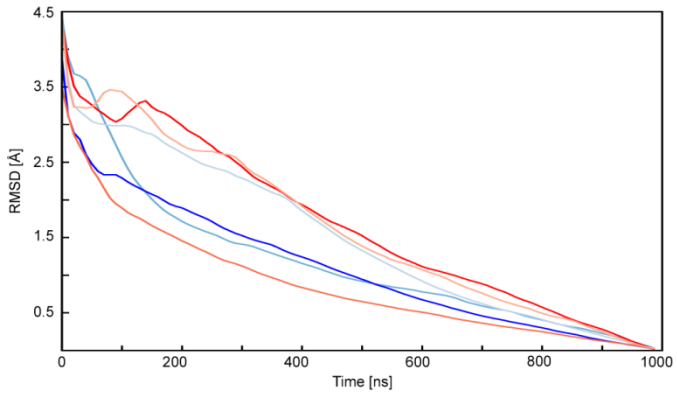

Fig. S1: RMSD average correlation.
RMSD average correlation (RAC) computed for the three independent MD simulations of $\alpha_{IIb}\beta_3$ expressing Leu33 (HPA-1a) (colored in three different shades of blue) or Pro33 (HPA-1b) (colored in three different shades of red) isoforms, respectively, as described in ref. (5). The structures were mass-weighted fitted on the C_α atoms of the head part (propeller domain

and βA domain), excluding the first 200 ns from the trajectories, applying an offset of 250 frames, and using as reference the running average calculated over each time interval.

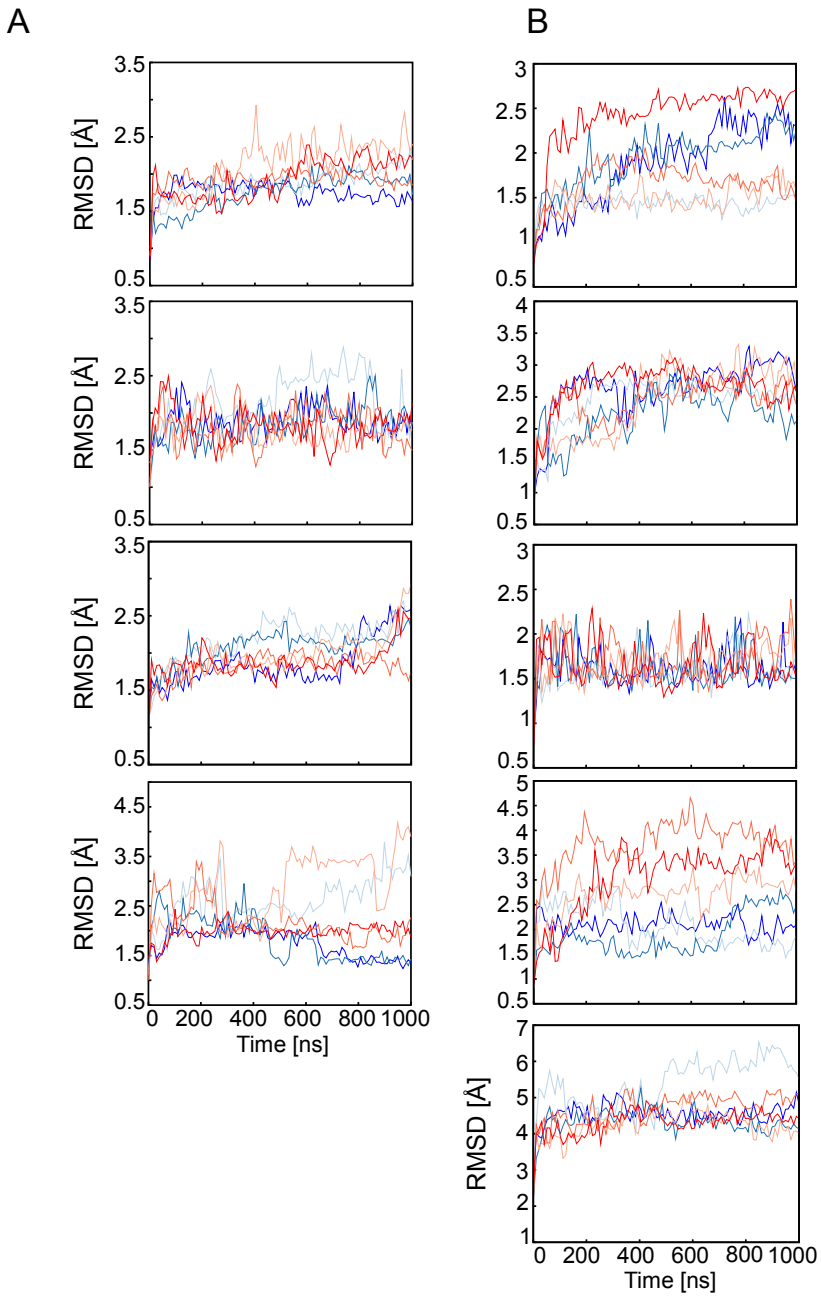

Fig. S2: Internal changes of $\alpha_{IIb}\beta_3$ domains: RMSD profiles.
RMSD of the C_α atoms of each domain of $\alpha_{IIb}\beta_3$ as a function of time with respect to the starting structure after a mass-weighted superimposition on the respective domain. From top to bottom, **(A)** the RMSD of the propeller domain, thigh domain, CALF-1, and CALF-2 domains is depicted, as is **(B)** the RMSD of the βA domain, hybrid domain, PSI domain, EGF block, and β-tail domains. Three different shades of blue and three different shades of red are used to represent the Leu33 and Pro33 isoforms, respectively.

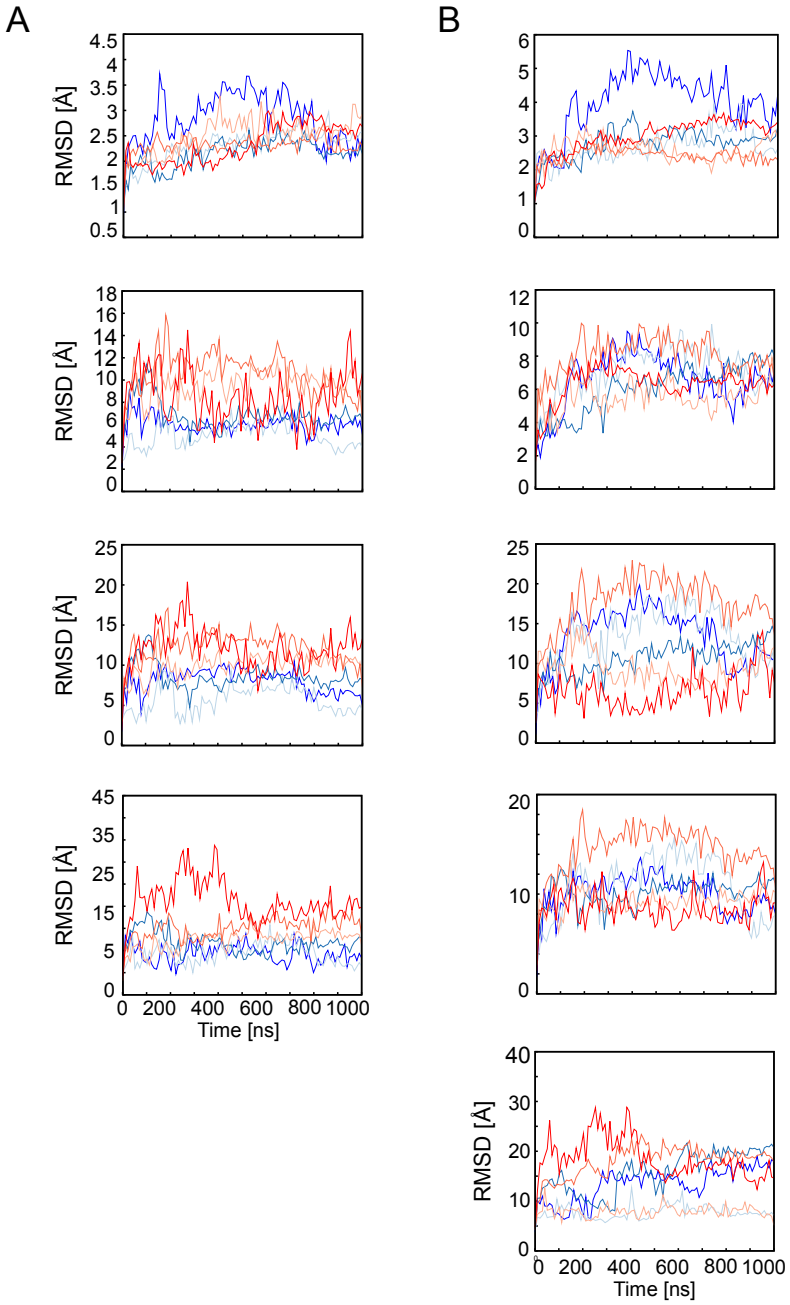

Fig. S3: Global changes of $\alpha_{IIb}\beta_3$ domains: RMSD profiles.
RMSD of the Cα atoms of each domain of $\alpha_{IIb}\beta_3$ as a function of time with respect to the starting structure after a mass-weighted superimposition on the head part (propeller domain and βA domain). From top to bottom, **(A)** the RMSD of the propeller domain, thigh domain, CALF-1, and CALF-2 domains is shown, as is **(B)** the RMSD of the βA domain, hybrid domain, PSI domain, EGF block, and β-tail domain. Color code as in Fig. S2.

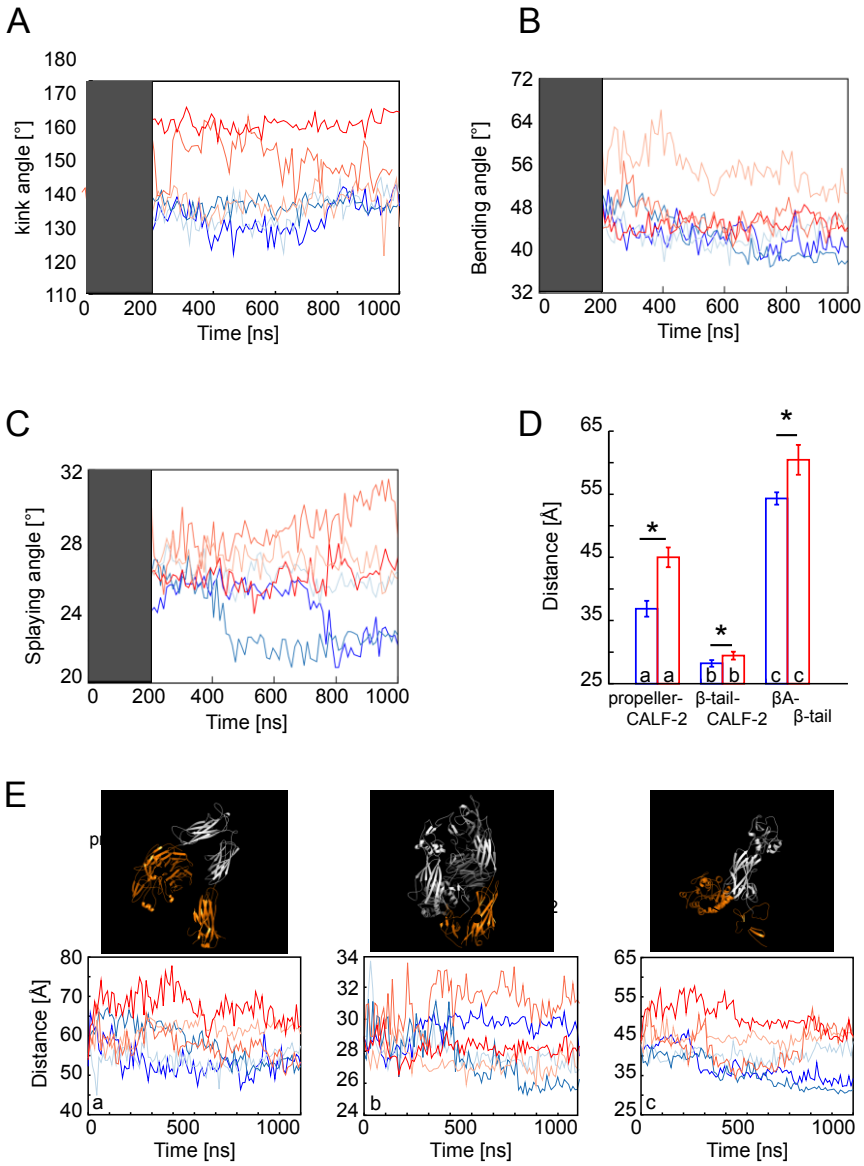

Fig. S4: Time series of geometric parameters.
(A, B, C) Time evolution of the kink angle, bending angle, and splaying angle defined as in the Methods section. Blue and red lines are used for the Leu33 (HPA-1a) isoform and Pro33 (HPA-1b) isoform, respectively. **(D)** Histogram indicating the mean of the distance between the head (propeller and βA domains) and the terminal domains (CALF-2 and β-tail domains) for the α- and β-subunits, respectively, calculated across three MD simulations. **(E)** Time evolution of the distances indicated in panel D. Above each panel, the initial structure of the respective MD simulations is depicted in cartoon representation. Domains involved in the measurements are labeled and highlighted in orange; the black line indicates the calculated distance between the COM of the domains (shown in black circles). Lines in color code as in panels (A)-(C).

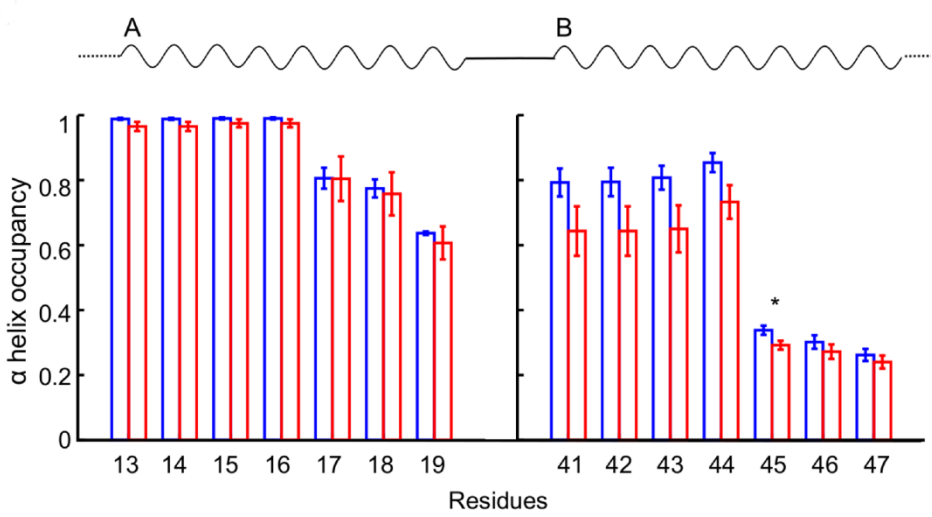

Fig. S5: Secondary structure analysis.
Normalized distribution of the helix content of **(A)** residues Cys13 to Met19 and **(B)** residues Leu40 to Asp47. Mean values calculated over three MD simulations are given, with error bars indicating SEM. The star indicates $p = 0.1$ for the difference. Blue and red colors represent the Leu33 and Pro33 isoforms, respectively.

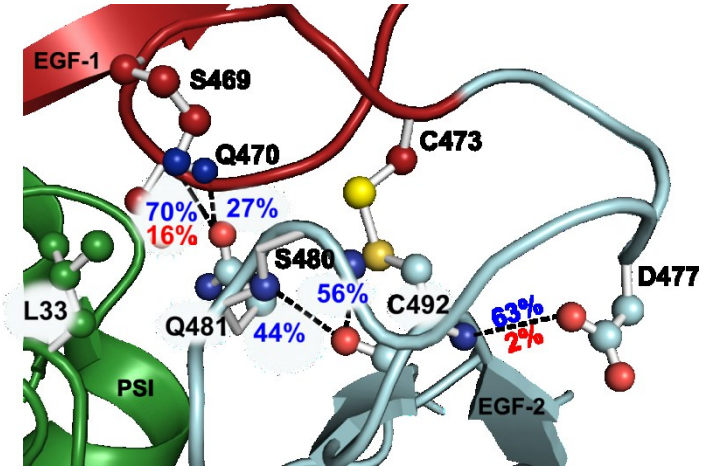

Fig. S6: Hydrogen bond network.
Mean occupancy of hydrogen bonds during three MD simulations each for the Leu33 (HPA-1a) and Pro33 (HPA-1b) isoform shown as labels next to the hydrogen bond marked by black dashed lines in the closest-to-average structure calculated from one simulation of the Leu33 (HPA-1a) isoform; occupancy values < 1% are not reported. For the sake of clarity, only the PSI (green), EGF-1 (firebrick), and EGF-2 (marine) domains of $\alpha_{IIb}\beta_3$ are shown. Residues Leu33 (PSI domain), Ser469-Gln470-Cys473 (EGF-1 domain), and Asp477-Ser480-Gln481-Cys492 (EGF-2 domain) are depicted in ball-and-sticks representation.

Supplemental References

1. Unkelbach, K., Kalb, R., Santoso, S., Kroll, H., Mueller-Eckhardt, C., and Kiefel, V. (1995) Genomic RFLP typing of human platelet alloantigens Zw(PlA), Ko, Bak and Br (HPA-1, 2, 3, 5). *Br. J. Haematol.* **89**, 169-176
2. Nauck, M. S., Gierens, H., Nauck, M. A., Marz, W., and Wieland, H. (1999) Rapid genotyping of human platelet antigen 1 (HPA-1) with fluorophore-labelled hybridization probes on the LightCycler. *Br. J. Haematol.* **105**, 803-810
3. Kunkel, T. A. (1985) Rapid and efficient site-specific mutagenesis without phenotypic selection. *Proc. Natl. Acad. Sci. U. S. A.* **82**, 488-492
4. Kim, M., Carman, C. V., and Springer, T. A. (2003) Bidirectional transmembrane signaling by cytoplasmic domain separation in integrins. *Science* **301**, 1720-1725
5. Galindo-Murillo, R., Roe, D. R., and Cheatham, T. E., 3rd. (2015) Convergence and reproducibility in molecular dynamics simulations of the DNA duplex d(GCACGAACGAACGAACGC). *Biochim. Biophys. Acta* **1850**, 1041-1058

ACKNOWLEDGEMENTS

I started my PhD project in the beginning of 2012 and since that time I got the opportunity to get in contact and to get to know several people that by different reasons helped me in this journey.

I would like to thank **Prof. Dr.** Rüdiger **Scharf** for giving me the opportunity to join its research group and for involving me on such an interesting project. In our weakly meetings I learned a lot with his extensive experience and vast knowledge. I am also very thankful for giving me the possibility to have a stable contractual situation.

I would like to thank also Dr. **Volker** Stoldt, the lab leader, for being always available for discussion and for willing to contribute with constructive ideas. Dr. Volker Stoldt gave me constantly the support to develop my own ideas and to establish collaborations with other research groups.

I would like to express my gratitude to **Prof. Dr.** William **Martin**, for the wise advices and for spending his time reviewing my project and reading my doctoral thesis.

I would like to express my gratitude to **Prof. Dr.** Nikolas H. **Stöcklein** for his availability to assume the position of supervisor when necessary.

I want to thank specially to Dr. **Melanie** Eberhard for receiving me and integrate me so well in the group as well as for the enormous daily support, professionally and privately. I thank also the rest of my lab colleagues, Dr. **Marianne** Gyennes, Dr. **Khon** Huynh, Dr. Huong Nguyen (**Helen**), and Frau **Elisabeth** Kirchhoff for the helping me in different moments of my work and for being such nice colleagues to me.

I could not forget Dr. **Christian** Mielke for being so generous to me. He promptly and effectively helped me solving problems with the transfection of HEK293 cells and he helped me to make important decisions concerning my work. Naturally I am also very thankful to the rest of his research group namely, Dr. **Faiza** Khalfalah**, Elke** Berg, Dr. **Stefan** Sobek and **Birgit** Hanzen for teaching me techniques.

With Dr. **Stefanie** Weidtkamp-Peters I learned the FRET-APB technique and she gave me the possibility to do the measurements in the Center of Advanced Imaging and for that I am very thankful too.

Prof. Dr. Andreas **Janshoff** accepted our collaboration proposal and allowed me to perform the AFM measurements on his department at the University of Göttingen. I address a

special note to **Susanne** Karsch, for being tireless and entirely dedicated supporting me in the AFM experiments during the two weeks that I spent in Göttingen. To both I express my enormous gratitude.

To **Prof. Dr.** Holger **Gohlke** and **Giulia** Pagani I am thankful for the collaborative work. It was very exciting to learn how their MD simulations and my FRET-APB results could be a perfect mutual complement. I am sure that the work developed already will bring us good fruits and I hope that we can continue working together.

I would like to thank (again) **Prof. Dr.** Nikolas H. **Stöcklein** for letting me use the Bioflux System and Frau **Maria** Wecker for her availability and patience teaching me how to use the instrument.

I am very grateful to **Prof. Dr.** Margitta **Elvers** for the use of the microscope and of the flow chamber. To **Meike** Klier, Frau **Martina** Spelleken and **Lily** Donner I thank all the technical support.

I acknowledge Dipl. Ing. **Katharina** Rabba for countless hours spent on the FACS, trying to achieve pure populations of transfected cells.

I thank Dr. **Diana** Kleinschrodt and Frau **Iris** Fey for the help given in the cloning strategy.

I also thank **Prof. Dr.** med. **Eickhoff** for his support concerning the statistical part of this work.

I thank also Frau **Uta** Vandercapelle, Frau **Gunda** Grosse, Frau **Maria** Völkl, Frau **Britta** Protz, Frau **Hannelore** Hamachers and Frau **Tatjana** Fuchsberger for all the small big helps and their daily sympathy.

Besides the work directly related with the doctoral project I had the chance to meet people that decisively encouraged me pursuing my objectives and those I would like to thank now. One of them was Dr. **Carmen** Zirngibl, my Mentor in the SelmaMeyerMentoring Programm. Due to her optimistic personality, she gave me an extraordinary support and increased my self-confidence and I am extremely grateful for that. As project leader in the SelmaMeyerMentoring Programm, Frau **Monika** Demming-Pälmer gave me the possibility to know my rights as a woman and mother. I am very thankful for that. The next words of big gratitude go to **Dr.** Anja **Vervoorts**. I got to know her in the context of the SelmaMeyerMentoring Program. She had a decisive role concerning my contractual situation, allowing me to finish my doctoral project.

And because the accomplishment of this doctoral project would not be possible for me without a strong familiar background I thank from all my heart to my husband **Rui**, for his love, friendship, his scientific counseling and permanent support in the good and bad times of the last years. I thank my son **Francisco** for its strong power. He pushed me to switch off from work immediately when I went home. Next I would like to mention my parents**, Zé** and **Clara**, to whom I express my tremendous gratitude for being always with me despite the distance, helping me to make difficult decisions, and giving me unconditional support since the beginning. I don´t forget my parents-in-law **Ilda** and **Luis** for the interest shown in my academic career and to them I say "thank you". To the rest of our family in Portugal I thank for the comfort conversations on the phone, for receiving us so well when we are there which turns the farewell more difficult but keep us warm in the return.

It is not by chance that I choose this position to mention **Beate**. Working colleagues from different departments since 2012, we got to know us better and we became friends, despite we never worked together. In the times of less motivation she didn´t let me to give up. I am very thankful to her for that and for the tremendous support concerning my family.

To my friends in Germany (**Nassra, Carolin, Catherine and Bärbel**) and in Portugal (**Carina, Andreia, Sara, Manuela, Diana, Sónia, Elsa e Mónica**) I am thankful for the interest in my professional and private life. The long and good years of social life with you gave me strength to achieve one more academic objective.

I declare under oath that I have compiled my dissertation independently and without any undue assistance by third parties under consideration of the "Principles for the Safeguarding of Good Scientific Practice" at Heinrich Heine University Düsseldorf. No other person´s work has been used without due acknowledgement. My dissertation has not been submitted in the same or similar format to any other institution. I have not previously failed a doctoral examination procedure.

Düsseldorf, 1st December 2017

Joana Patrícia Ventura Pereira